THE UNIVERSITY
of EDINBURGH

A Novel Component of the Fission Yeast Memory-Based Polarity Landmark

Hayley Johnson

Doctor of Philosophy
University of Edinburgh
November 2018

Acknowledgements

Firstly I would like to thank my supervisor Professor Ken Sawin for the opportunity to work in his lab and for his advice and guidance throughout many discussions throughout my PhD, and for pushing me to work hard and think critically. During this project I have grown both academically and personally. Thank you to the rest of the members of the Sawin lab Sanju Ashraf, Xun Bao, Su Ling Leong, Delyan Mutavchiev, Ana Rodriquez, Ye Dee Tay and Harish Thakur for their support both inside and outside of the lab. I would also like to thank David Kelly for his guidance, patience and humour regarding all things microscopy-based and Christos Spanos for his accommodating contribution to mass spectrometry experiments and data analysis. I would like to thank David Barass and Bella for their technical advice and protocols for the RT-Q-PCR experiments.

I would like to thank the Wellcome Trust for the opportunity and the financial support to be able to pursue this PhD and for enabling me to present my work and communicate science both to the international scientific community and to the general public.

Thank you to my parents for teaching me to keep working hard and to be kind especially when times are tough. I would like to thank my sister Hannah and my Grandma for always believing in me. To Dunika, for being so annoying that he made even the most challenging aspects of my PhD seem like a comparable light relief. I would like to thank my friends both in Edinburgh and all over the world, especially Sarah, Katie, Sara, Lucy and Niki for always being there for me. I would also like to thank my fellow students Bella, Elana, Greg and Sadhbh for being such wonderful friends from day one of my PhD.

Declaration

I declare that this thesis has been composed solely by myself and that it has not been submitted, in whole or in part, in any previous application for a degree. Except where states otherwise by reference or acknowledgement, the work presented is entirely my own.

Hayley Johnson

14 November 2018

Abstract

Polarised cells have spatial differences in their shape, structure or function. Polarisation is essential for many cellular processes, including directional growth. This occurs at specific sites within the cell determined by polarity cues. Fission yeast are an excellent model to study how polarity cues are generated and maintained. Fission yeast are rod-shaped cells that grow exclusively from their tips, co-ordinated by two independent internal polarity cues, the Tea1-Tea4 system and the Rax1-Rax2 system. The Tea1-Tea4 polarity cue is highly dynamic and is based on the cell's existing geometry. Tea1 and Tea4 are delivered to the cell tips on the plus ends of microtubules that run along the length of the cell. The Rax1-Rax2 system is a stable cue and is based on sites of previous growth. Rax1 and Rax2 are delivered to the cell tips through the secretory pathway during active growth. Once delivered, Rax1 and Rax2 are stably retained at the cell tips and are able to recruit growth machinery back to a previously growing cell tip in the next cell cycle. By this mechanism cell is able to 'remember' a site of previous cell growth and reinitiate growth from this site.

In order to correctly function as a polarity landmark for growth at the cell tips, both Rax1 and Rax2 need to localise correctly. In this work I have shown that large C-terminal tags on Rax2 impair its function, despite Rax2 correctly localising to the cell tips. Additionally, I have shown that Rax1 is required for Rax2 trafficking out of the ER, and that the cytoplasmic 26 amino acids of Rax2 are also required for Rax2 trafficking. I have identified interactors of Rax2-His-Tev-Biotin using cross-linking, purification and mass spectrometry. Known polarity proteins Bgs1, Bgs3, Rga1 and Rga3 were found to interact with Rax2. Additionally, a previously uncharacterised protein, Lrx1, interacts with Rax2 and is important for the correct localisation of Rax1-Rax2 to the cell tips, and thus the correct functioning of the Rax1-Rax2 memory-based polarity cue.

Lay summary

The human body is arranged asymmetrically. Organs are sited at specific places within the body and if any organ is wrongly placed this can lead to disease. Cells are also asymmetrical. They require that the proteins and structures within them are correctly located to function normally, just as we need our organs to be in the right place. This generated asymmetry is called polarisation. As a model to study cell polarisation, fission yeast are used.

Fission yeast are rod shaped cells, and to maintain this rod shape they grow exclusively from their cell tips, and not from their cell sides. When they reach a certain length, they divide in the middle to create two equally sized daughter cells, which then once again start growing from their cell tips.

There are two groups of proteins that localise at the tips to promote growth. One group contains the proteins Tea1 and Tea4 and the other group contains the proteins Rax1 and Rax2. In my work I have focused on the latter proteins, i.e. Rax1 and Rax2.

Rax1 and Rax2 work together and act as a 'memory' for the cell growth. As the yeast cell grows, Rax1 and Rax2 accumulate at the cell tips and are retained there so that, following cell division into two daughter cells, the new cells know that they should start growing where Rax1 and Rax2 are.

In my project I identified another protein, which I have called Lrx1, which is involved in growth memory. Lrx1 is involved in ensuring that Rax1 and Rax2 accumulate the cell tips, and don't accumulate elsewhere in the cell. This is very important for their function to promote growth at the cell tips.

Table of contents

Abbreviations

ADEL	ER retention sequence
ADP	Adenosine diphosphate
BSA	Bovine serum albumin
CAH	Citrine-Avitag-His
CAPS	N-cyclohexyl-3-aminopropanesulfonic acid
CHAPs	3-[(3-cholamidopropyl)dimethylammonio]-1-propanesulfonate
CLAAPE	chymostatin, leupeptin, antipain, pepstatin, E64
CRIB	Cdc42-Rhointeracting binding domain
DAMP	Damage associated molecular pattern
DMSO	Dimethyl sulfoxide
DNA	Deoxyribonucleic acid
dNTP	deoxyribonucleotide triphosphate
DSS	Disuccinimidyl suberate
DTT	Dithiothreitol
EDTA	Ethylenediaminetetraacetic acid
EMCCD	Electron multiplying charge-coupled device
EMM	Edinburgh Minimal Media
ER	Endoplasmic reticulum
g	grams
GAP	GTPase-activating protein
GDI	Guanine nucleotide dissociation inhibitor
GDP	Guanine diphosphate
GEF	Guanine nucleotide exchange factor
GFP	Green fluorescent protein
GTP	Guanine triphosphate
HBH	His-Biotin-His
HTB	His-Tev-Biotin
ID	Internal deletion
IMAC	Immobilised metal affinity chromatography
KB	Kilobase
Kd	Dissociation constant
kDa	Kilo Daltons
L	Litres
LB	Lysogeny broth
LFQ	Label-free quantification
LSB	Laemmli sample buffer
MEF	Membrane-enriched fraction
MHz	Megahertz
NETO	New-end take off
NF-κβ	Nuclear factor kappa-light-chain-enhancer of activated B cells
Ni-NTA	Nickle-nitrilotriacetic acid
nm	Nanometers

nmt	No message thiamine
OD	Optical density
PAMP	Pathogen associated molecular pattern
PCI	Phenol:Chloroform:Isoamyl Alcohol
PCR	Polymerase chain reaction
PMSF	phenylmethylsulfonyl fluoride
PNGase F	Peptide -*N*-Glycosidase F
RNA	Ribonucleic acid
rpm	Revolutions per minute
RT-Q-PCR	Reverse transcriptase-quantitative polymerase chain reaction
Sc	Saccharomyces cerevisiae
SDS	Sodium dodecyl sulfate
SRM	Sterol-rich membrane
TBS	Tris-buffered saline
TCA	Trichloroacetic acid
TEV	Tobacco etch virus
TM	Transmembrane
TMD	Transmembrane domain
UTR	Untranslated region
WCE	Whole-cell extract
YE5S	Yeast extract 5 supplements
Δ	Deletion
µl	Microlitres
µm	Micrometers

List of figures

Chapter One: Introduction

1.1 What is cell polarity?

Cell polarity is a spatial difference in shape, structure or function within a cell (Nelson 2003). Essentially all cells are polarised to some extent, because cell polarity plays an important role in cell function. Examples of highly polarised cells range from simple single celled organisms such as yeast to complex higher eukaryotic cells such as neurons (Figure 1.1).

1.1.1 Polarisation is important for cell function

Cells whose polarity is tightly linked to their function include neurons, hair cells and intestinal epithelia. Neurons have a long axon at one end of the cell and a cluster of shorter dendrites at the other end, this allows neural networks to propagate signals effectively and unidirectionally through the central nervous system (Figure 1.1B) (Nance and Zallen 2011) (Takano, Xu et al. 2015). Hair cells are the sensory cells located in the mammalian cochlea. At their apical surface they have long actin-based villi, called stereocilia, with mechanotransducer channels at the tips (Jia, Dallos et al. 2007). Sound vibrations lead to the activation of these channels, which produce a series of action potentials. At the synaptic (basal) surface, the action potential leads to the release of neurotransmitters to the afferent nerve that contacts the hair cell (Figure 1.1D) (Jia, Dallos et al. 2007). Intestinal epithelia have a highly polarised apical-basal polarity. One of the functions of these cells is to transport glucose from the intestinal lumen into the bloodstream. At the apical membrane, glucose is absorbed into the epithelial cell from the intestinal lumen. The epithelial cells contain a high concentration of glucose, and therefore glucose must be actively transported into the cells through sodium-glucose symport channels (Wood and Trayhurn 2003). At the basal membrane, glucose is passively transported down its concentration gradient into the capillaries that lie beneath the basement membrane (Figure 1.1C)((Wood and Trayhurn 2003). The two different types of glucose transport channels must be localised to the correct surface of the cell for efficient transport of glucose from the intestinal lumen to the bloodstream.

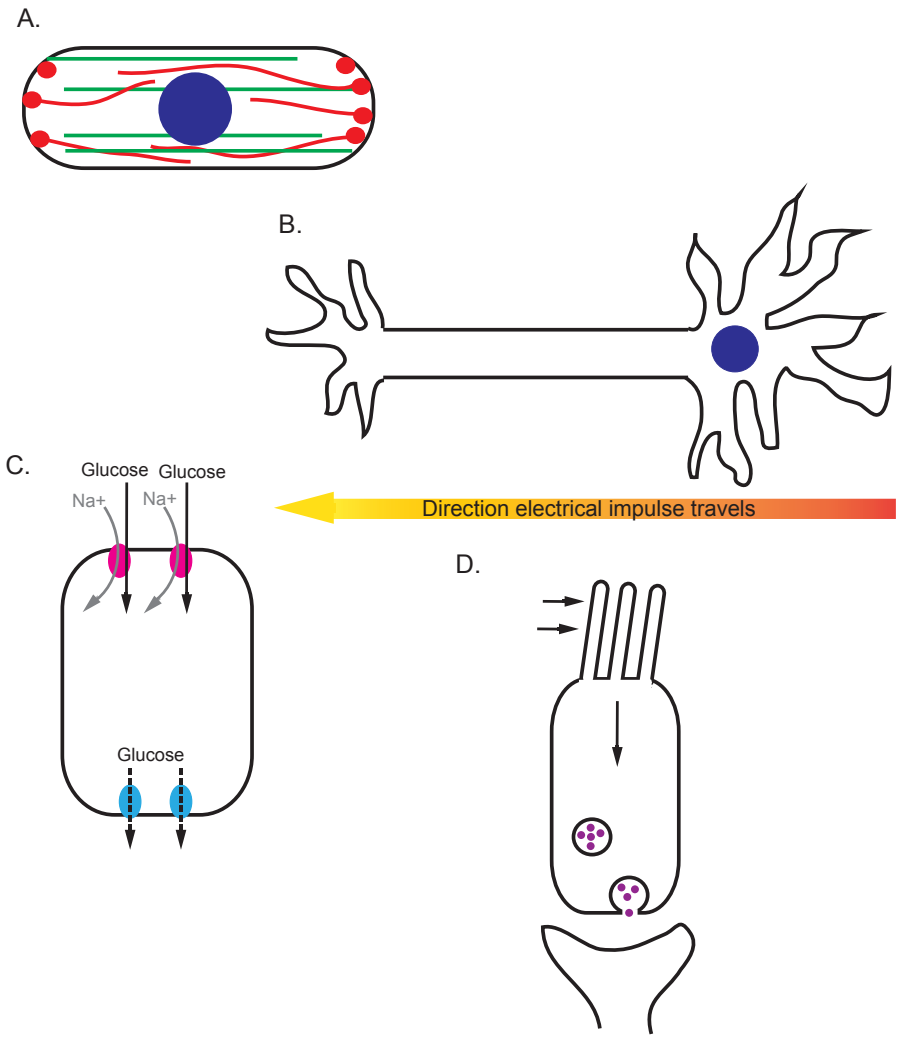

Figure 1.1: Essentially all cells are polarised, ranging from yeast single cells to cells that make up tissues in multicellular organisms. A. Fission yeast have a polarised cytoskeletons: microtubules in green and actin in red run along the length of the cell, nucleus is blue. B. Neurons are divided into functional regions of axons and dendrites. C. Intestinal epithelial cells have active Na+- Glucose transporter (pink) on their apical surface and passive glucose transporters (blue) on their basal surface. D. Hair cells have mechanosensitive cilia on their apical surface and release neurotransmitters (purple) from their basal surface to an efferent nerve below. Adapted from Fettiplace and Kim, 2014.

1.1.2 The mechanisms for cell polarisation are highly conserved

Despite the huge diversity in cell shape, size and functions, the mechanisms for how eukaryotic cells interpret a cue to generate asymmetry are quite similar. There are three essential components for polarised growth:

1. A cue that defines the site of polarised growth
2. Activation of a RhoGTPase
3. An organised cytoskeleton (Figure 1.2)

I will briefly introduce the role of the cytoskeleton in cell polarity and how the RhoGTPase Cdc42 is activated. The main focus of this thesis is the role of polarity cues in cell polarisation, and I will explore polarity landmark proteins in fission yeast in depth.

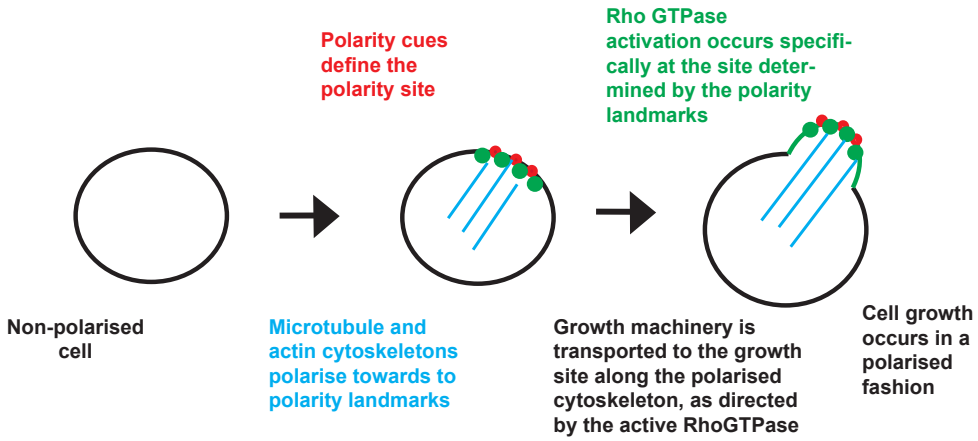

Figure 1.2: There are three essential components for polarisation of all cells. Cell growth in budding yeast is used as an example for polarisation. Polarised growth occurs at a site determined by a polarity cue, in this case a polarity landmark protein. The cytoskeleton polarises towards this site. A RhoGTPase is specifically activated at this defined site in the cell. The active RhoGTPase reinforces cell polarisation towards the polarity cue, and for cell growth directs targeted transport of growth machinery (such as proteins involved in cell wall and plasma membrane growth) towards the polarity cue along the microtubule and actin cytoskeletons.

1.2 Cdc42 is a master regulator of polarised growth of eukaryotic cells

The Rho-family GTPase Cdc42 is a universal regulator of cell polarity in eukaryotes. Cdc42 is among the most highly conserved GTPases, for example, yeast and human Cdc42 are 80 % identical (Chiou, Balasubramanian et al. 2017). Like all Rho GTPases, Cdc42 cycles between a GTP-bound (active) and GDP-bound (inactive) state. This cycling between a GTP- and GDP- bound state enables Cdc42 to act as a molecular switch to modulate a wide range of signalling pathways (Etienne-Manneville 2004). Cdc42-GTP is able to co-ordinate various cellular activities. These include polarisation of the actin and microtubule cytoskeletons, as well as targeted delivery of vesicles and exocytic machinery for the expansion of the plasma membrane (and delivery of cell wall components for plant and yeast cells) (Etienne-Manneville 2004).

Cdc42-GTP levels are positively regulated by guanine nucleotide exchange factors (GEFs) and negatively by GTPase-activating proteins (GAPs) and guanine nucleotide dissociation inhibitors (GDIs). GAPs, GEFs and GDIs ensure that Cdc42 activation is both spatially and temporally controlled (Etienne-Manneville 2004). The GEFs and GAPs involved in Cdc42 regulation in fission yeast are described in greater detail in section 1.5.5. Alongside GAPs and GEFs, a combination of both positive and negative feedback loops for Cdc42 activation are required to ensure that sufficient levels of Cdc42-GTP are generated in a timely fashion at precise locations to drive cell polarisation in a controlled manner (Wu and Lew 2013, Woods and Lew 2017).

1.3 Cell polarity is directed by various cues

Polarity cues lead to the Cdc42 activation at specific sites within the cell. Polarity cues are important for cell growth, daughter fate determination, cell shape, migration and adhesion (Thompson 2013). Here, I will briefly introduce how polarity-landmark proteins, cell-cell contacts, extracellular cues and tissue damage can be involved in the polarisation of a range of cells.

1.3.1 Polarity landmark proteins

The use of polarity landmark proteins in establishing polarity is highly prevalent in both multicellular organisms and single cells. Both budding and fission yeast are valuable model organisms for studying polarity landmark proteins as cues for polarised growth. This will be elaborated on in detail in sections 1.5, 1.7 and 1.8. In multicellular organisms, the polarity-landmark PAR (partitioning defective) proteins play an essential role in cell polarisation for daughter cell fate determination and are highly conserved from worms to mammals (Goldstein and Macara 2007). The PAR proteins regulate cell polarisation in a wide range of different cell types and have been most highly studied in the *C.elegans* embryo. In the *C.elegans* embryo, the PAR proteins segregate into anterior and posterior domains. PAR-3 and PAR-6 become enriched at the anterior cortex and PAR-1 and PAR-2 become enriched at the posterior cortex (Nance and Zallen 2011). This leads to an asymmetric distribution of various developmental determinants, for example, the cortical proteins LET-99 and GPR1/2 (Nance and Zallen 2011). LET-99 and GPR1/2 regulate mitotic spindle positioning and ensure that the first embryonic cleavage is unequal. Differential inheritance of these determinants in the daughter cells results in specific cell fates along the anterior-posterior axis as the embryo develops (Nance and Zallen 2011).

1.3.2 Cell-cell contact

Cell-cell contact is essential for the correct organisation of tissues in multicellular organisms. Within tissues, cells need to be organised with respect to each other. The cell-cell contact between cells of a tissue is a cue for their polarisation. For example, epithelial cells polarise into distinct apical and baso-lateral surfaces upon cell-cell contact (Etienne-Manneville 2004) (Rojas, Ruiz et al. 2001). In epithelial cells, polarisation is initiated when

adhesion proteins, including nectin and E-cadherin, adhere to the neighbouring cell. This adhesion induces Cdc42 activation and its association both with PAR proteins and the apical Crumbs complex, to organise cellular polarity in coordination with the neighbouring cells (Baum and Georgiou 2011).

1.3.3 Extracellular cues

Extracellular cues can lead to cell polarisation and migration during development and in adult cells. A key example of this is the polarisation and migration of immune cells towards extracellular cues such as pathogen-associated molecular patterns (PAMPs) released by invading organisms, or damage associated molecular patterns (DAMPs) released from dead or damaged cells (Nourshargh and Alon 2014). This migration is called chemotaxis; the chemotactic immune cells migrate towards the highest concentration of a variety of soluble PAMPs or DAMPs. This directed migration is achieved by localised activation of Cdc42 (Etienne-Manneville 2004). The locally activated Cdc42 polarises the actin cytoskeleton to allow cells to protrude at the front (the end closest to the infection or wound site) and retract at the back and consequently move forwards (Yang, Collins et al. 2016).

1.3.4 Tissue damage

In multicellular organisms, scratches, burns or oxygen starvation lead to cell death, which needs to be repaired. The new cells that replace the dead cells often come from specific niches within the damaged tissue or from specialised sites such as the bone marrow (Palumbo, Galvez et al. 2007). The repair cells need to migrate towards the wound site. Factors such as NF-κB are released from the damaged tissue and leads to the polarisation and migration of the repair cells to the wound site (Palumbo, Galvez et al. 2007). These factors lead to polarised activation of Cdc42, which polarises the actin cytoskeleton towards the front of the cell, as in chemotaxis, and aligns microtubules in the direction of migration (Etienne-Manneville 2004). Additionally, the centrosome and Golgi reorient to be in front of the nucleus (Sadok and Marshall 2014)

1.3.5 Spontaneous polarisation

Spontaneous polarisation is cell polarisation in the absence of any spatial cues, and is a phenomenon that occurs in both unicellular and multicellular organisms (Wedlich-Soldner and Li 2003). Cells that are able to polarise spontaneously include the zygotes of fucid algae, neutrophils, leukocytes and germination of fission yeast spores.

Normally, the zygotes of fucid algae polarise towards a source of light, which stimulates asymmetric cell division that produces rhizoid and thallus cell types. However, in the absence of a light source, the zygotes polarise spontaneously and are still able to correctly specify the rhizoid and thallus cell types (Wedlich-Soldner and Li 2003).

Chemotactic cells, such as neutrophils and leukocytes normally polarise towards the highest concentration of a soluble chemoattractant. If chemotactic cells are exposed to a uniform concentration of a chemoattractant they polarise spontaneously. This suggests that the presence of a chemoattractant, even without a concentration gradient, is able to intrinsically activate a cell's ability to break asymmetry (Wedlich-Soldner and Li 2003).

Finally, fission yeast spend the majority of their lifetime in a polarised rod shape. However, fission yeast spores initially grow in a near-isotropic fashion. This is due to small spontaneous active Cdc42-GTP clusters forming randomly, disassembling and reforming at another random site (Bonazzi, Julien et al. 2014). Growth from the spontaneous active Cdc42-GTP cluster is limited by the spore's rigid outer cell wall. Rupturing of the cell wall results in stabilisation Cdc42-GTP at a single site and polarised germination of the spore, co-ordinated by Cdc42-GTP, to generate a rod shaped cell (Wu and Lew 2013) (Bonazzi, Julien et al. 2014).

1.4 The cytoskeleton plays a crucial role in symmetry breaking and maintenance of cell polarity

Actin and microtubules are obvious candidates as contributors to cell polarity due to their intrinsically polarised and highly dynamic nature (Li and Gundersen 2008). Subtle polarity cues including external factors, fertilisation or polarity proteins localised at a specific site can be amplified into large-scale cellular responses through the autocatalytic assembly, disassembly or reorganisation of the cytoskeleton (Mullins 2010).

Actin and microtubules have distinctive characteristics that allow them to contribute to cell polarity in different ways. The symmetry breaking process is driven by the actin cytoskeleton, which reorganises rapidly in response to polarity signals. Two key actin structures that play a key role in cell polarisation actin cables and actin patches. Actin cables play a role in the establishment of a polarised distribution of regulatory molecules through targeting of exocytic vesicles, directed transport of specific cargoes and organelles (Li and Gundersen 2008) (Nelson 2003). Whereas actin patches are endocytic structures concentrated areas of membrane expansion (Li and Gundersen 2008).

Microtubules are rigid structures, rendering them ideal for enhancement and maintenance of cell polarisation. Microtubules form polarised arrays that both maintain cell shape and act as hubs for long-range intracellular trafficking (Li and Gundersen 2008) (Nelson 2003).

The actin and microtubule cytoskeletons act independently to contribute to cell polarity, however their functions are bridged together to both enhance and further contribute to a robust polarisation system (Nelson 2003). For example, in fission yeast the polarity proteins Tea1 and Tea4, discussed in section 1.6.4, link microtubules and actin (Martin, McDonald et al. 2005).

1.5 Fission yeast grow in a highly polarised manner

Fission yeast are an excellent model to study polarised growth. They are genetically tractable, have a simple geometry, a highly regulated polarised growth pattern, and a polarisation mechanism that is conserved with higher eukaryotic cells (Martin and Arkowitz 2014). Fission yeast cells are rod shaped and grow exclusively from their cell tips. Once the cells reach a certain cell size they divide by medial fission (Snell and Nurse 1993) (Martin and Arkowitz 2014). During interphase, the growth machinery localises to the cell tips. The growth machinery includes proteins involved in expansion of the cell wall (such as ß-glucan synthases Bgs1-4) and plasma membrane (such as exocyst components Sec6, Sec10 and Exo70) and actin nucleation (For3) (Feierbach and Chang 2001, Cortes, Ishiguro et al. 2002, Wang, Tang et al. 2002, Martin, Garcia et al. 2003, Cortes, Carnero et al. 2005). The growth machinery is later redistributed to the cell septum for cell division into two equally sized daughter cells (Feierbach and Chang 2001, Cortes, Ishiguro et al. 2002, Wang, Tang et al. 2002, Martin, Garcia et al. 2003, Cortes, Carnero et al. 2005).

1.5.1 CRIB is a reporter of active Cdc42 and allows monitoring of cell growth patterns

In early experiments investigating the polarised growth of fission yeast, the growth patterns of fixed cells could be investigated using dyes such as calcofluor (which binds to the chitin of the yeast cell wall) or antibodies that recognise actin (which accumulates at the growing tip) (Mata and Nurse 1997). The Cdc42/Rac interacting binding domain (CRIB) reporter allows us to image growth patterns in live cells (Tatebe, Nakano et al. 2008). Substrates of Cdc42, such as p21-activated Kinases (PAKs), contain a CRIB domain that binds specifically to GTP-bound Cdc42. Fluorescently tagged CRIB is used as a reporter of active Cdc42-GTP (and thus active growth) (Tatebe, Nakano et al. 2008) (Figure 1.3). The CRIB reporter responds rapidly to changes in the localisation of Cdc42-GTP and permits real-time analysis of the growth pattern (Ozbudak, Becskei et al. 2005, Tatebe, Nakano et al. 2008). The CRIB reporter also enables us to understand how the growth pattern of the mother cell can influence the growth pattern of the daughter cell, through monitoring of growth patterns over multiple generations. Additionally,

fluorescently tagged components of the growth machinery such as mCherry-Bgs4 can be used to monitor growth sites (Cortes, Carnero et al. 2005).

1.5.2 Following cytokinesis, daughter cells initially grow in a monopolar and then in a bipolar fashion

Fission yeast cells grow in a highly cell cycle regulated manner (Mitchison and Nurse 1985). Following cytokinesis, the two daughter cells initially start growing from their old ends (the ends inherited from the mother) (Figure 1.3). Once the cells have reached a certain cell size and have reached the early G2 phase of the cell cycle, they additionally grow from their new ends (the ends formed during cytokinesis) (Figure 1.3). This process is called New-End Take Off (NETO) (Mitchison and Nurse 1985). In rich media (yeast extract with added supplements), NETO occurs around stage 0.34 of the cell cycle, while in minimal media (a synthetic media) NETO occurs at around stage 0.49 of the cell cycle (Mitchison and Nurse 1985). This suggests that nutrient availability contributes to the regulation of polarised growth. When the cells enter mitosis, the growth machinery is redistributed to the cell septum and cells stop growing from the tips. A cytokinetic ring is formed at the cell septum and the cells undergo medial fission to produce two equally sized daughter cells (Hayles and Nurse 2001). Although this growth pattern was identified over 30 years ago, it was only recently discovered why and how yeast grow consistently in this pattern (Described in section 1.6) (S.Ashraf, thesis).

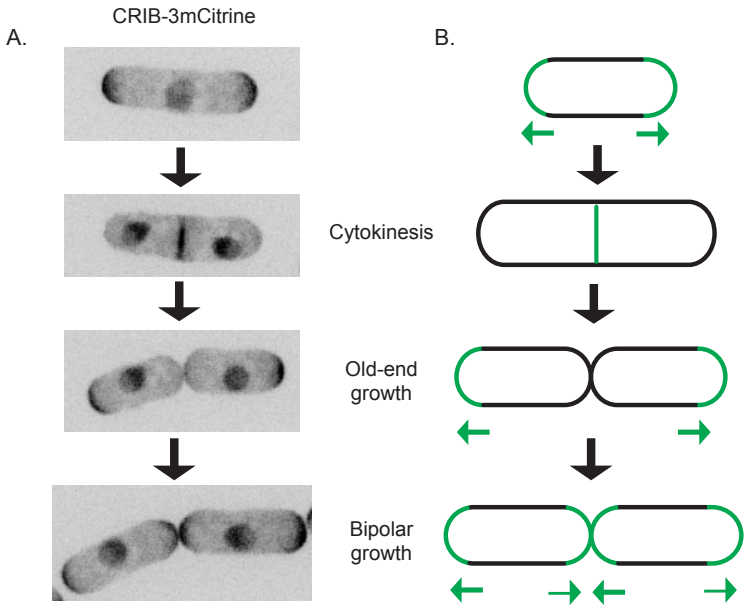

Figure 1.3: CRIB-3mCitrine is a growth marker for fission yeast polarised growth. A. Live-cell imaging of CRIB-3xmCitrine, snap shots from a 4 hour movie of a single cell dividing into two daughter cells. B. Cartoon of the growth pattern. Green celll tips indicate site of growth, green arrows represent direction of growth.

1.6 Polarity landmarks position growth to the cell tips

1.6.1 *tea1*∆ cells grow in a monopolar fashion, and can become bent and branched

The polarity landmark Tea1 (Tip Elongation Aberrant 1) was first identified in a screen to identify genes involved in fission yeast morphogenesis (Snell and Nurse 1994) (Verde, Mata et al. 1995). Tea1 is an 1147 amino-acid protein that has six kelch repeats at its N-terminus and mostly alpha-helical coiled-coils at its C-terminus (Mata and Nurse 1997). Tea1 is involved in correct positioning of the growth site; *tea1*∆ cells have defects in localising the sites of cell growth, mispositioning of the growth sites is more severe under stressed conditions such as increased temperature (Snell and Nurse 1994). At 25˚ C growth sites can become slightly offset from the tips, leading to bent cells. At 36 ˚C, cells form branches due to de novo growth site formation at the cell sides, and the prevalence of bent cells increases (Snell and Nurse 1994, Mata and Nurse 1997) Additionally, *tea1*∆ cells do not transition to bipolar growth. Instead, their growth is exclusively monopolar (Verde, Mata et al. 1995).

1.6.2 Tea1 localises to the cell tips is transported to the cell tips on the plus ends of microtubules

During interphase, Tea1 localises to both cell tips, whether they are growing or not, and during cytokinesis, Tea1 localises to the cell septum (Mata and Nurse 1997). Tea1 localisation to the cell tips is based on the existing geometry of the cell. Tea1 is highly dynamic; it is transported to the cell tips on the plus end of microtubules that are orientated along the length of the cell (Mata and Nurse 1997). Tea1 is trafficked to the cell tips in complex with the microtubule-associated proteins Mal3 (EB1 homolog), Tea2 (Kip2 homolog), and Tip1 (CLIP-170 homolog) (Figure 1.4) (Browning, Hayles et al. 2000, Brunner and Nurse 2000, Tatebe, Shimada et al. 2005). Mal3, Tea2 and Tip1 are required for the proper cytoplasmic organisation of microtubules, which is required for accurate delivery of Tea1 to the cell tips. Mal3 localises to the growing ends of microtubules, and is required for the binding of both Tea2 and Tip1 to the growing end of the microtubule (Busch and Brunner 2004, Busch, Hayles et al. 2004). In the absence of Mal3, Tea2 or Tip1, microtubules are much shorter and do not reach the cell tips (Brunner and

Nurse 2000, Busch and Brunner 2004, Busch, Hayles et al. 2004). This prevents efficient delivery of Tea1 to the cell tips and leads to bent and branched cells, as seen for *tea1*Δ. Additionally, Tea1 plays a role in the regulation of microtubule dynamics. In the absence of Tea1, microtubules curl around the cell tips, and overexpression of *tea1* leads to shorter microtubules (Mata and Nurse 1997).

1.6.3 Tea1 retention at the cell tips requires Mod5 and Tea3

Once trafficked to cell tips, Tea1 is released from microtubules and anchored there by the prenylated membrane protein Mod5 (Figure 1.4) (Snaith and Sawin 2003). The interaction between Mod5 and Tea1 is a highly dynamic, and they participate in a positive feedback loop for their spatial enrichment specifically at the cell tips (Snaith and Sawin 2003) (Snaith, Samejima et al. 2005) (Bicho, Kelly et al. 2010). In *mod5*Δ cells, Tea1 is delivered to the cell tips but fails to accumulate to normal levels because it is not anchored properly (Snaith and Sawin 2003). Additionally, in *tea1*Δ cells, Mod5 is present around the whole plasma membrane and is no longer restricted to the cell tips (Snaith and Sawin 2003). Once correctly localised and anchored at the cell tips, Tea1 participates in a variety of protein interactions to promote growth.

1.6.4 Tea4 acts with Tea1 to link the actin and microtubule cytoskeletons to regulate cell polarity

Tea4 is a polarity landmark protein with similar behaviour to Tea1. Tea4 is direct interactor of Tea1 and co-localises with Tea1 at the growing tips of microtubules and at the cell tips (Martin, McDonald et al. 2005). Additionally, *tea4*Δ cells exclusively grow in a monopolar fashion, which can become bent and branched as seen in *tea1*Δ cells (Tatebe, Shimada et al. 2005). Tea1 and Tea4 are co-dependent in their role as a polarity landmark, and are thought to act by working as a protein-protein interaction platform. At the cell tips, Tea4 directly binds to the actin-nucleating protein (formin) For3, and in turn For3 binds Bud6 and Cdc42 for the formation of actin cables (Figure 1.4) (Martin, McDonald et al. 2005, Martin, Rincon et al. 2007). In *for3*Δ cells the actin cables are absent and only disorganised actin patched are visible (Martin, McDonald et al. 2005). The actin cables formed by For3 are used as a track for Myo52 (class V myosin) transport of secretory

vesicles, which are generated from the Golgi or endosomal compartments, necessary for membrane expansion at the tips (Feierbach and Chang 2001, Motegi, Arai et al. 2001). In *tea4*Δ cells, For3, actin and Myo52 are still able to localise to the growing end, whereas microtubule based polarity proteins such as Tea1 and Tea3 accumulate at the non-growing cell tip (Martin, McDonald et al. 2005). This suggests that the role of Tea4 may be to act as a link between the microtubule base polarity proteins and actin cytoskeleton, which is required for bipolar growth.

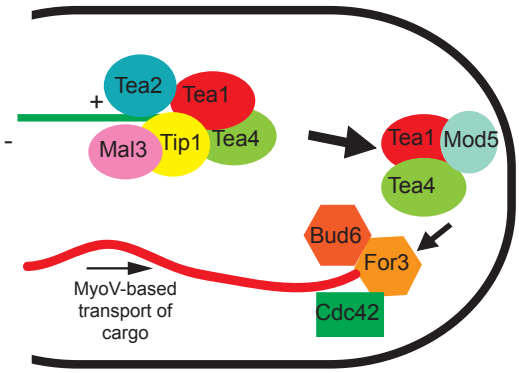

Figure 1.4: Tea1 and Tea4 act as a bridging link between the microtubule and actin cytoskeletons. Tea1 and Tea4 transport to the cell tips requires the microtubules binding proteins Mal3, Tea2 and Tip1. Once delivered, Tea1 (and Tea4) is anchored to the cell tips by Mod5. Tea4 then recruits the actin nucleating protein For3 which in turn recruits Bud6 and Cdc42 for the formation of actin cables. The actin cables are used as a track for Myo-V based transport of proteins and molecules required for cell growth.

1.6.5 Tea1 and Tea4 regulate the localisation of Cdc42 GEFs and GAPs

Cdc42 co-ordinates exocytosis and endocytosis at the cell tips for membrane incorporation for cell growth (Miller and Johnson 1994). Cdc42 is involved in localisation of the exocyst complex, which is required for tethering of exocytic vesicles to the cell tips. (Bendezu and Martin 2011) (Estravis, Rincon et al. 2011). Tea1 and Tea4 enrich for GEF-activated Cdc42 at the cell tips by preventing GAP localisation specifically at growth sites. There are two Cdc42 GEFs in fission yeast, Scd1 and Gef1. Scd1 is a "local" GEF that is localised to the cell tips (and is maintained at the tips through positive feedback), while Gef1 is a "global" GEF that is distributed throughout the cytoplasm (Figure 1.5) (Tay, Leda et al. 2018). *scd1*Δ and *gef1*Δ single deletions are viable, but a *scd1*Δ *gef1*Δ double deletion is not viable (Coll, Trillo et al. 2003, Hirota, Tanaka et al. 2003). Deletion of *scd1* leads to mostly round cells with undetectable levels of Cdc42-GTP at the cell tips (Chang, Barr et al. 1994) (Tatebe, Nakano et al. 2008). Gef1's main function is during septation. *gef1*Δ cells are significantly delayed, and mildly defective, in septum formation (Coll, Trillo et al. 2003) (Wei, Hercyk et al. 2016). Additionally, in *gef1*Δ cells, Cdc42-GTP recruitment to the septum is delayed and maintained ectopically following ring constriction (Wei, Hercyk et al. 2016). The GAP Rga4 is enriched the cell sides to prevent ectopic activation of Cdc42. *rga4*Δ cells are shorter and wider compared to wild-type (Cansado, Soto et al. 2010). The DYRK family kinase Pom1 is involved in restricting Rga4 to the cell sides by preventing Rga4 localisation at the cell tips (Figure 1.5) (Tatebe, Nakano et al. 2008). Pom1 localisation to the cell tips is dependent upon the Tea1 and Tea4 polarity landmarks, resulting in Rga4 antagonising Gef1 activity exclusively at the cell sides and channelling of the net activity of Gef1 to the cell tips (Figure 1.5) (Tay, Leda et al. 2018). Both GEF activity enrichment and Tea1-Tea4 dependent GAP exclusion at the cell tips ensure a robust system for polarised growth.

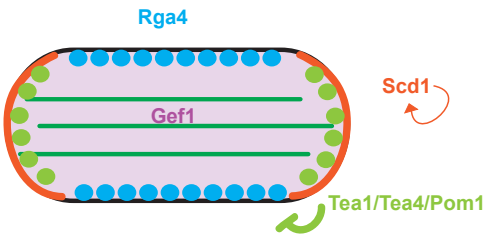

Figure 1.5: Tea1 and Tea4 landmarks are involved in restricting Cdc42 activation to the cell tips. Tea1 and Tea4 are localised to the cell tips in a mircotubule dependent manner. Tea1 and Tea4 recruit Pom1 to the cell tips. Tea1/Tea4/Pom1 restrict the activity of the GAP Rga4 to the cell sides (by preventing Rga4 localisation to the cell tips). The GEF Scd1 localises to the cell tips and is maintained at the cell tips through positive feedback. Gef1 activity is antagonised at the cell sides by Rga4. Gef1 activity is not antagonised at the cell tips. Cdc42 activity is resticted to the cell tips leading to polarised tip growth.Adapted from Tay et al. 2018.

1.7 Multiple polarity cues play a role in the polarised growth of fission yeast

As previously described, *tea1*Δ cells grow in an exclusively monopolar fashion. The daughter cell that inherits the previously growing tip from the mother cell grows from its old end, whereas the other daughter (that doesn't inherit a previously growing tip) grows from its new end (Figure 1.6B) (Verde, Mata et al. 1995) (Niccoli, Arellano et al. 2003). It has long been proposed that the old end is able to 'remember' previous cell growth, and that this memory is able to re-establish growth at a previously growing end independently of Tea1 (Niccoli, Arellano et al. 2003). Recent work in the Sawin lab has shown that the proteins Rax1 and Rax2 are required for 'memory' of previous cell growth (S.Ashraf, thesis). *rax1* and *rax2* are homologs of the budding yeast genes *rax1*^{Sc} and *rax2*^{Sc} (in this thesis, to avoid confusion between budding yeast and fission yeast genes, all budding yeast gene and protein names will include the superscript "Sc") (Chen, Hiroko et al. 2000, Fujita, Lord et al. 2004). In this section I will discuss how Rax1 and Rax2 influence the growth patterns of fission yeast. I discuss Rax1^{Sc} and Rax2^{Sc} in greater detail in section 1.7 and I explain the experiments that demonstrate that Rax1 and Rax2 are a 'growth-memory' polarity cue in budding yeast. I will describe the initial characterisation of Rax2 in fission yeast by Sanju Ashraf in Section 1.8, which I have continued in my PhD project.

1.7.1 *tea1*Δ *rax1*Δ and *tea1*Δ *rax2*Δ cells grow exclusively from their new ends

Double mutants of *tea1*Δ *rax1*Δ and *tea1*Δ *rax2*Δ are no longer able to initiate growth from their old ends; we refer to this growth pattern as "*Axial*" growth (Figure 1.6D). In the absence of polarity cues, the growth memory is lost. The default growth site of the daughter cells is exclusively from the new ends; the cells do not reinitiate growth at a previously growing tip. New end growth is directed by an unknown remnant of cytokinesis, whose capability to promote polarised growth is normally outcompeted by polarity landmarks present in the cell. Additionally, there is actin-based transport of cytokinesis remnants from the new ends to the old ends when the old end is growing (S.Ashraf, thesis). *tea1*Δ *rax1*Δ and *tea1*Δ *rax2*Δ cells are still able to grow in a

highly polarised fashion and, in physiological conditions, do not show any other morphological defects (S.Ashraf, thesis).

1.7.2 *rax1*∆ and *rax2*∆ cells grow in a premature bipolar fashion

After cytokinesis of a mother cell, wild-type daughter cells initially grow in a monopolar fashion (from their old ends) before transitioning to bipolar growth. However, *rax1*∆ and *rax2*∆ cells grow in a bipolar fashion immediately after cytokinesis (Figure 1.6C) (S.Ashraf, thesis). This is because the Tea cue is distributed to both cell tips equally through its constant transport to the cell tips on the plus ends of microtubules (Figure 1.6C). Therefore (in the absence of additional independent polarity cues, i.e. Rax1 and Rax2) both cell tips are equally competent to drive cell growth, resulting in immediate growth from both cell tips. Rax1 and Rax2 are required to bias initial growth to the old end by strengthening the polarity cue localised at the old end.

1.7.3 The independent Tea1 and Rax1-Rax2 cues lead to the initial monopolar then bipolar growth pattern of wild-type cells

The growth phenotypes described above have enabled us to now understand the wild-type fission yeast growth pattern. The daughter cells arising from wild-type mothers each inherit a previously growing old end. At the old ends of the daughter cells, there is both the “Tea” cue and the “Rax” cue (while at the new ends there is only the Tea cue). The combination of two independent polarity cues at the old ends causes them to more competent to initiate growth than the new ends, and therefore the cells initially grow from their old ends, in a “winner take all” mechanism (Figure 1.6A). As the cell grows, the competition between the two ends decreases until both tips are equally competent to drive cell growth, resulting in bipolar growth. This may be due to the two ends competing for a cytoplasmic factor that is limiting at the beginning of the cell cycle but increases in abundance as the cell cycle progresses. When such as factor is limiting, it would be recruited to the stronger polarity cue, at the old end. But when the factor is no longer limiting, it would also be recruited to the weaker polarity cue at the new end. Alternatively, it could be proposed that there is a negative feedback mechanism preventing bipolar growth immediately following cytokinesis. Old end growth could generate a factor that inhibits growth elsewhere in the cell. When the cells are small, immediately following cytokinesis, growth is

inhibited at the new end. As the cell grows, the distance between the new end and the inhibitory factor increases and the influence of the growth inhibition on the new end is lessened. When the cell reaches a certain size, the inhibitory cue produced from the old is no longer able to reach the new end and the cell grows in a bipolar manner.

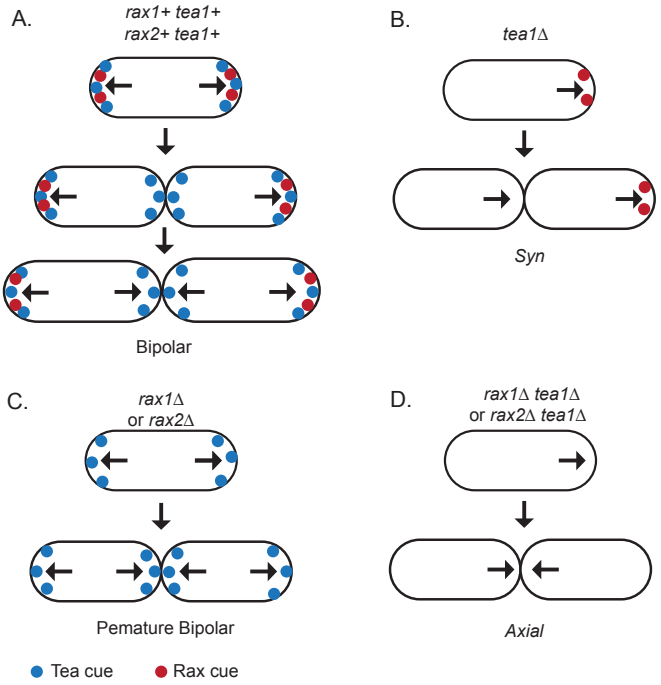

Figure 1.6: Tea1 and Rax1-Rax2 act independently to promote polarised growth at the cell tips. Cartoons of growth patterns in different genetic backgrounds. A. Wild-type, both Rax2 and Tea1 cues are at the old end of the daughter cells, and only Tea1 is at the new end. The combined Rax2 and Tea1 cue is stronger polarity cue resulting in intial growth at the old end. Once the cells reach a certain cell size, competition between the two cell ends is reduced and the new end is also competent to induce growth. B. *tea1*Δ, The daughter cell that inherits the previously growing cell tip is able to reinitate growth from this old end due to the stable Rax2 cue. The daughter that inherits a cell tip that was not growing in the mother grows from its new end. C. *rax2*Δ, Tea1 is equally distributed between the two tips. Both tips are equally competent to promote growth immediately after cell division. This results in premature bipolar growth. D. *rax2*Δ*tea1*Δ, in the absence of polarity landmarks the cells grow exclusively from the new cell tips.

1.8 Rax1^{Sc} and Rax2^{Sc} are polarity cues in budding yeast

1.8.1 The budding yeast bud site selection pattern

The budding yeast bud-site-selection pattern can be observed by staining birth and bud scars with the fluorescent dye Calcofluor. Bud scars are chitin-rich rings, which also contain the transmembrane proteins Rax1^{Sc} and Rax2^{Sc} (Cabib, Mol et al. 1993, Kang, Angerman et al. 2004). The chitin enrichment causes the bud scars to stain more brightly with calcofluor than the rest of the cell wall.

The bud site selection pattern is dependent on the cell mating type. Haploid (*a* and *α*) cells bud in an *Axial* budding pattern. In the *Axial* budding pattern, the mother cell will form a bud adjacent to the most recent bud scar and each subsequent bud will form adjacent to the preceding bud site (Figure 1.7) (the *Axial* budding pattern influenced the naming of the *Axial* fission yeast growth pattern, as the cells always grow from the pole of the previous division site) (Chant and Pringle 1995). Diploid cells (*a/α*) bud in a bipolar fashion. For example, the first bud of a daughter cell will form distally to the birth scar and the subsequent bud will form adjacent to the birth scar at the proximal pole (Figure 1.7). Even when budding in a bipolar fashion, the scars will form adjacent to a previous scar at that pole (provided there is a scar already at that pole). This suggests that there is a long-lived cue retained in the bud scar involved in directing bud site selection in subsequent cell cycles (Chant and Pringle 1995).

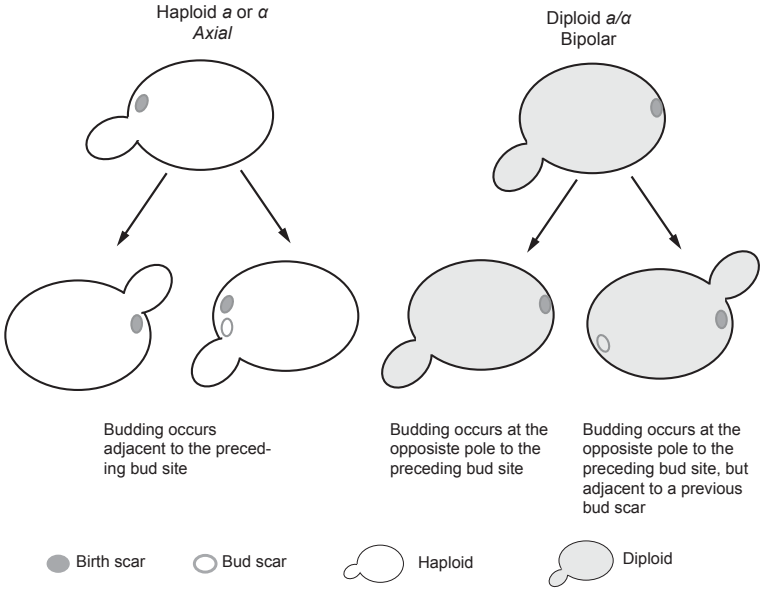

Figure 1.7: Budding yeast grow in an *Axial* pattern when haploid and in a bipolar pattern when diploid. Cartoon of *Axial* budding in haploid yeast and bipolar budding in diploid yeast.

Distinct groups of proteins act as landmarks for *Axial* vs. bipolar budding, or for budding in general. Landmarks involved in the *Axial* budding pattern are Bud3^{Sc}, Bud4^{Sc}, and Bud10^{Sc}. These are deposited at the mother-bud neck where they are distributed between the mother and daughter cells at the division site and disappear shortly after cytokinesis. (Chant 1999). Additionally, Axl1^{Sc} is an *Axial* specific component that localises to the bud sites and is only produced in haploid cells. Haploid *axl1*$^{Sc}\Delta$ cells grow in a bipolar fashion, whereas when Axl1^{Sc} is ectopically expressed in diploid cells, they shift to axial growth (Figure 1.8A) (Fujita, Oka et al. 1994) (Casamayor and Snyder 2002).

Proteins involved in the bipolar budding pattern include Bud8^{Sc} and Bud9^{Sc} (Harkins, Page et al. 2001). *bud8*$^{Sc}\Delta$/*bud8*$^{Sc}\Delta$ cells bud exclusively from their proximal pole (i.e. near the birth scar), whereas *bud9*$^{Sc}\Delta$/*bud9*$^{Sc}\Delta$ cells bud exclusively from the distal pole (Figure 1.8B) (Harkins, Page et al. 2001)

The third class of genes are those required for both axial and bipolar budding: *bud1*^{Sc}, *bud2*^{Sc} and *bud5*^{Sc}. Deletion of any of these genes results in the cells budding in an apparently random pattern (Chant 1999). Interestingly, in these mutants, even when the cells are budding in an apparently random pattern, budding never occurs in the same site twice (Meitinger, Khmelinskii et al. 2014). The inhibition of budding from a previous budding site is important to maintain the fitness of replicating cells. ‘Memory loss mutants’ which can bud from previous bud sites have nuclear segregation defects and a shorter lifespan (Meitinger, Khmelinskii et al. 2014).

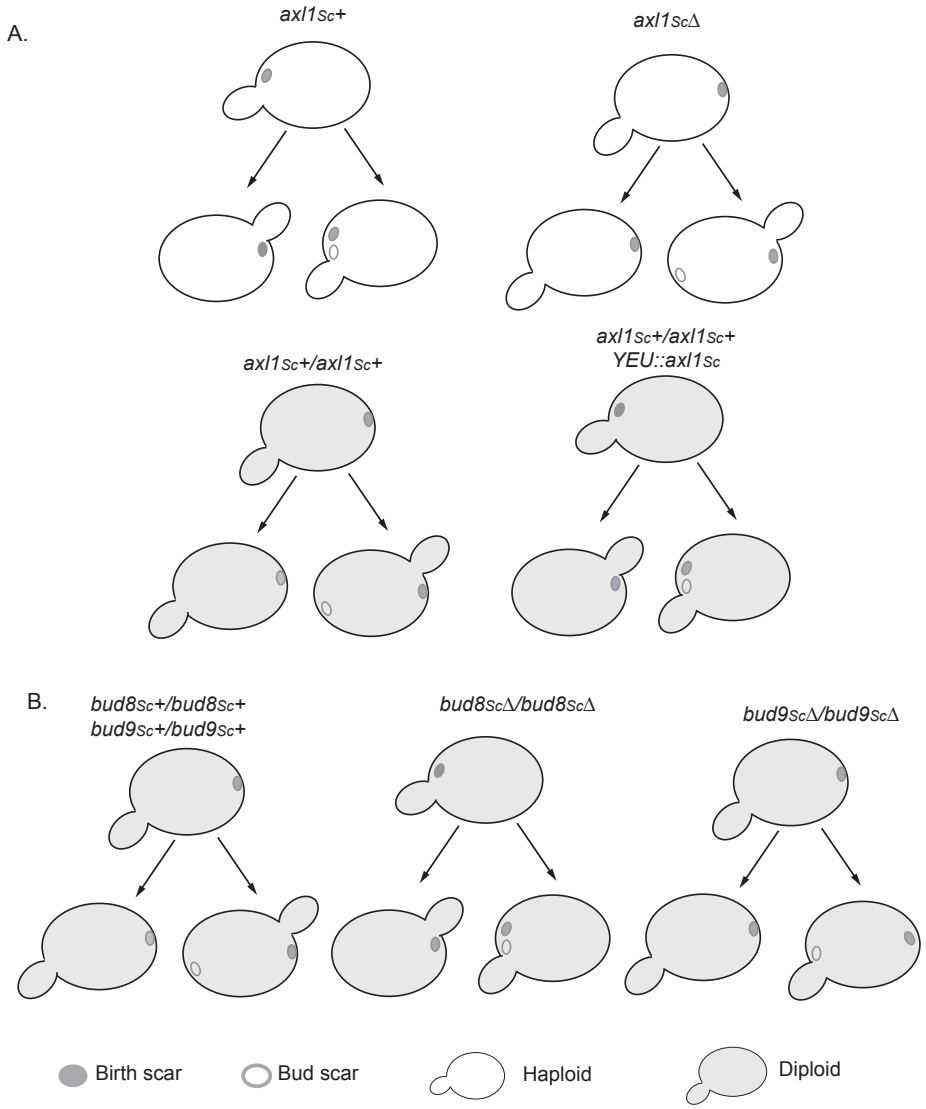

Figure 1.8: *axl1*$_{Sc}$Δ, *YEU::axl1*$_{Sc}$, *bud8*$_{Sc}$Δ/*bud8*$_{Sc}$Δ and *bud9*$_{Sc}$Δ*bud9*$_{Sc}$Δ cells have budding pattern defects. A. *axl1*$_{Sc}$Δ haploid cells bud in a bipolar manner, ectopic expression of *axl1*$_{Sc}$ in diploid cells under the YEU promoter leads to axial budding. B. *bud8*$_{Sc}$Δ/*bud8*$_{Sc}$Δ cells bud in an axial pattern at the pole proximal to the birth scar. *bud9*$_{Sc}$Δ/*bud9*$_{Sc}$Δ cells form all buds distal to the birth scar.

1.8.2 Rax1 and Rax2 were discovered in a screen of *axl1^{Sc}Δ* mutants

Rax1^{Sc} and Rax2^{Sc} are part of the 'growth-memory' cue localised at the bud scars (Meitinger, Khmelinskii et al. 2014). *rax1^{Sc}* and *rax2^{Sc}* were first identified in a screen for changes in bud site selection in an *axl1^{Sc}Δ* haploid strain. *axl1^{Sc}Δ* haploid cells grow in a bipolar pattern (instead of *Axial*), *rax1^{Sc}Δ axl1^{Sc}Δ* or *rax2^{Sc}Δ axl1^{Sc}Δ* double mutants revert back to the *Axial* budding pattern (rax, **R**evert to **AX**ial) ((Fujita, Oka et al. 1994). The budding pattern of wild type haploid cells is unaffected by *rax1^{Sc}Δ* or *rax2^{Sc}Δ* (Harkins, Page et al. 2001, Fujita, Lord et al. 2004). However, diploid *rax1^{Sc}Δ/rax1^{Sc}Δ* and *rax2^{Sc}Δ/rax2^{Sc}Δ* cells exhibit budding pattern defects (Chen, Hiroko et al. 2000). The first bud of new born cells is always correctly formed distally to the birth scar in *rax1^{Sc}Δ/rax1^{Sc}Δ* and *rax2^{Sc}Δ/rax2^{Sc}Δ* cells (Figure 1.9A). *rax1^{Sc}Δ/rax1^{Sc}Δ* and *rax2^{Sc}Δ/rax2^{Sc}Δ* cells choose subsequent bud sites at random (72 % of cells) (Figure 1.9A) (Chen, Hiroko et al. 2000). Rax1^{Sc} and Rax2^{Sc} are not required for positioning of the first bud site in new born diploid daughter cells but are required for the positioning of all subsequent buds.

1.8.3 Rax1^{Sc} and Rax2^{Sc} are a stable 'growth-memory' cue at bud sites

Rax1^{Sc} and Rax2^{Sc} localise to the bud sites in a co-dependent manner (Chen, Hiroko et al. 2000) (Kang, Angerman et al. 2004). Rax1^{Sc} and Rax2^{Sc} accumulate just before cytokinesis in the mother-bud neck and are inherited by both cells following cell division (Chen, Hiroko et al. 2000). Rax2^{Sc} is retained within the bud scar, and with subsequent cell divisions, characteristic rings of Rax2^{Sc} accumulate in number, along with the bud scars (Chen, Hiroko et al. 2000). To confirm that the localisation of Rax2^{Sc} in the buds scars is due to Rax2^{Sc} retention rather than new delivery of Rax2^{Sc}, Chen et al., 2000 investigated whether Rax2^{Sc} localisation is retained at the bud sites following shut-off of *rax1^{Sc}*. Rax2^{Sc} localisation to the bud sites depends on Rax1^{Sc} (Chen, Hiroko et al. 2000). Therefore, after shut-off of *rax1^{Sc}* expression, no new Rax2 can be delivered to the bud sites. After 18 hours of *rax1^{Sc}* shut-off, the birth scar retained Rax2^{Sc} but no new Rax2^{Sc} had been deposited to the new bud sites (Chen, Hiroko et al. 2000).

Rax2^{Sc} is retained in bud scars for multiple generations, this retention is required for to prevent budding from a previous bud sites (Chen, Hiroko et al. 2000) (Meitinger, Khmelinskii et al. 2014). Mutants that bud from the same

site multiple times have nuclear segregation defects and a shorter lifespan (Meitinger, Khmelinskii et al. 2014). Rax1^{Sc} and Rax2^{Sc} are involved in recruiting Cdc42^{Sc} antagonists Nba1^{Sc} and Nis1^{Sc} to the bud scars. At the bud scars, Nba1^{Sc} prevents Cdc42^{Sc} activation through inhibiting the interaction of Cdc24^{Sc} (Cdc42^{Sc} GEF) to GTP-bound Rsr1^{Sc} (Meitinger, Khmelinskii et al. 2014). The nuclear segregation defects are proposed to be due to narrowing of the bud-neck diameter due to the repeated re-use of the same polarity site (Meitinger, Khmelinskii et al. 2014).

1.8.4 How might Rax1^{Sc} and Rax2^{Sc} function in bud site selection?

Rax1^{Sc} and Rax2^{Sc} are primarily described as being cues for bud-site selection. The mechanism for how they guide the bipolar budding pattern is not yet fully understood. Rax1^{Sc} and Rax2^{Sc} are involved in recruiting the bipolar bud-site selection proteins Bud8^{Sc} to the distal pole and Bud9^{Sc} to the proximal pole (Figure 1.9B)(Kang, Angerman et al. 2004). Bud8^{Sc} is partially impaired in its localisation to the bud sites in the absence of Rax1^{Sc} and Rax2^{Sc} (Figure 1.9B) (Kang, Angerman et al. 2004). Additionally, Rax1^{Sc} and Rax2^{Sc} are largely impaired in bud site localisation in *bud8*^{Sc}Δ/*bud8*^{Sc}Δ cells (Figure 1.9B) (Kang, Angerman et al. 2004). This suggests some co-dependency for Rax1^{Sc} and Rax2^{Sc} localisation with Bud8^{Sc}. Differently, Rax1^{Sc} and Rax2^{Sc} localisation to the bud sites and bud necks is unaffected by *bud9*^{Sc}Δ/*bud9*^{Sc}Δ (Figure 1.9B). Bud9^{Sc} localisation to the initial bud of a new born daughter cell is not dependent on Rax1^{Sc} and Rax2^{Sc}, but Rax1^{Sc} and Rax2^{Sc} are required for Bud9^{Sc} localisation to all subsequent bud sites (Figure 1.9B) (Kang, Angerman et al. 2004). Once Bud8^{Sc}, Bud9^{Sc}, Rax1^{Sc} and Rax2^{Sc} are localised at the correct pole, Bud8^{Sc} or Bud9^{Sc} recruit the Cdc42^{Sc} activating module Rsr1^{Sc}/Bud5^{Sc}/Bud2^{Sc} through an indirect interaction with Bud5^{Sc} to promote growth at the chosen bud site (Krappmann, Taheri et al. 2007).

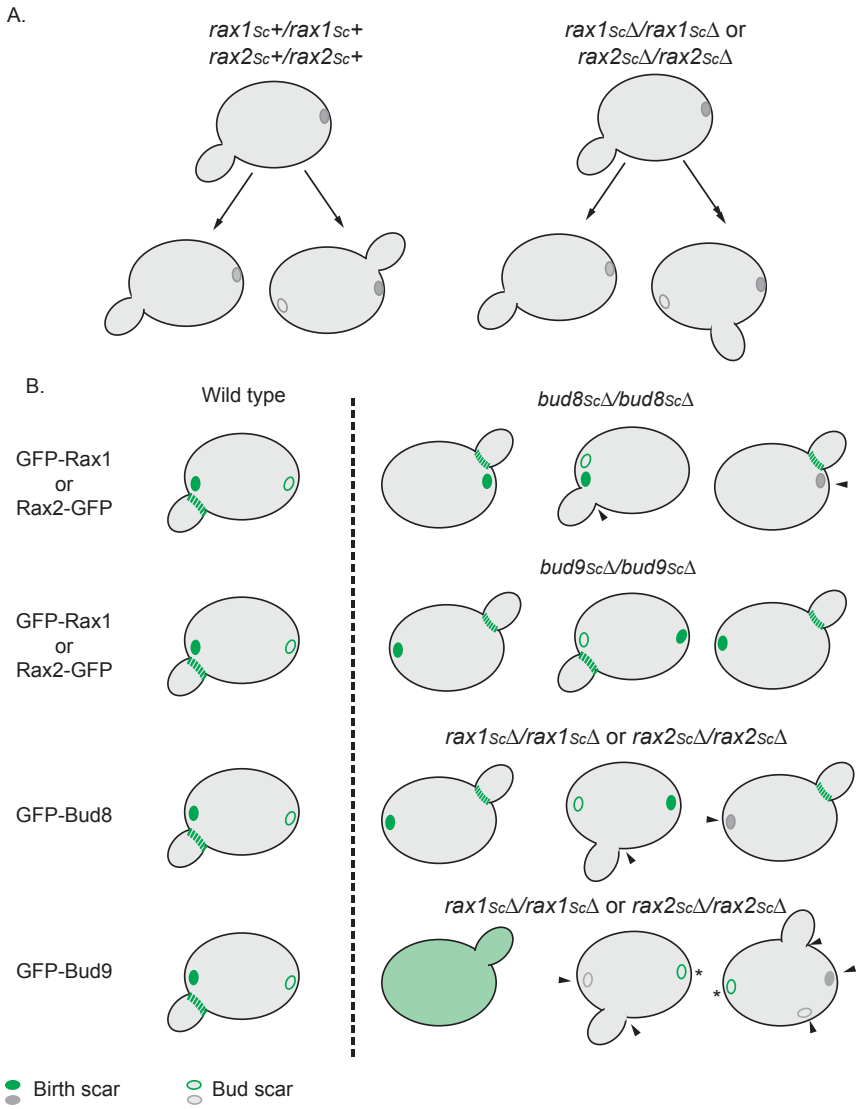

Figure 1.9: *rax1*$_{Sc}$Δ/*rax1*$_{Sc}$Δ and *rax2*$_{Sc}$Δ/*rax2*$_{Sc}$Δ cells exhibit budding pattern defects, localisation of bipolar budding pattern landmarks is partially co-dependent. A. *rax1*$_{Sc}$Δ/*rax1*$_{Sc}$Δ and *rax2*$_{Sc}$Δ/*rax2*$_{Sc}$Δ newborn cells correctly position their first bud distal to the birth scar, all subsequent bud sites are chosen randomly. B. Arrows point to sites of imparied bud site localisation. Rax1$_{Sc}$ and Rax2$_{Sc}$ have partial defects in localisation in *bud8*$_{Sc}$Δ/*bud8*$_{Sc}$Δ cells but do not have localisation defects in *bud9*$_{Sc}$Δ/*bud9*$_{Sc}$Δ cells. Bud8$_{Sc}$ has partial defects in bud site localisation in *rax1*$_{Sc}$Δ/*rax1*$_{Sc}$Δ and in *rax2*$_{Sc}$Δ/*rax2*$_{Sc}$Δ cells. Bud9$_{Sc}$ correctly localises to the first bud (marked by *) in *rax1*$_{Sc}$Δ/*rax1*$_{Sc}$Δ and in *rax2*$_{Sc}$Δ/*rax2*$_{Sc}$Δ cells but is completely impaired in localisation to subsequent bud sites and some cells and cytoplasmic signal is observed.

1.9 In fission yeast, Rax1 and Rax2 localise to the cell tips and act as a 'growth-memory' cue

As mentioned above, Rax1 and Rax2 have been identified in fission yeast as homologs of $Rax1^{Sc}$ and $Rax2^{Sc}$ (Chen, Hiroko et al. 2000, Choi, Lee et al. 2006). Additionally, in both fission and budding yeast, Rax1 and Rax2 play a role in positioning of the growth sites (Sections 1.6 and 1.7). Here I will describe the initial characterisation of Rax2 in fission yeast, demonstrating that Rax2 is stably localised at the cell tips and plays a role as a growth-memory polarity cue (S.Ashraf, thesis).

1.9.1 Rax1 and Rax2 are transmembrane proteins

Rax1 has three transmembrane domains separated by short cytoplasmic loops. The N-terminal tail is 236 amino acids long and the C-terminal tail is predicted to contain only five amino acids (Figure 1.10). The orientation of Rax1 in the membrane is uncertain as both orientations have been predicted by different transmembrane topology prediction programmes (Bernsel, Viklund et al. 2009)(Figure 1.10). Rax2 has a single transmembrane domain with a large extracellular domain of 1105 amino acids and a small C-terminal cytoplasmic tail of 26 amino acids (Figure 1.10).

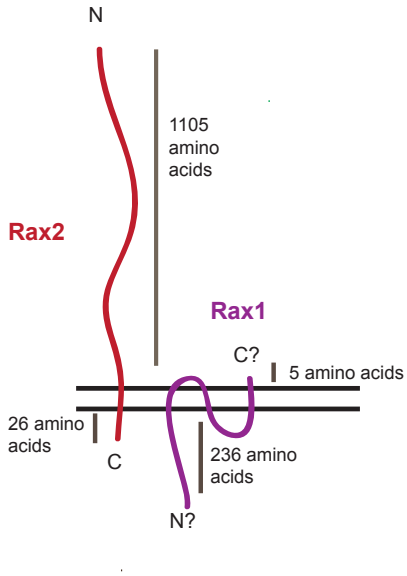

Figure 1.10: Rax1 and Rax2 are transmembrane proteins. Cartoon of the predicted topologies of Rax1 and Rax2. The orientation of the N- and C- termini of Rax1 are uncertain, as indicated by the question marks

1.9.2 Rax2 localises to the growing cell tips.

Rax2 localises to the cell tips of fission yeast, and, similar to $Rax2^{Sc}$, the correct localisation of Rax2 is dependent on Rax1 (S.Ashraf, thesis) (Kang, Angerman et al. 2004). So far, Rax1 has not been detected by live-cell imaging when tagged with fluorescent markers at its C-terminus, but it is hypothesised to also localise to cell tips (S.Ashraf, pers. Comm.). In monopolar-growing mutants, such as *tea1*Δ cells, Rax2-3mCitrine localises only to the actively growing cell tip (S.Ashraf, thesis). This suggests that Rax2 localisation to cell tips is dependent on active cell growth.

1.9.3 Rax2 is a stable cue at the cell tips

Unlike many other polarity proteins, which rapidly relocalise to the cell septum during cytokinesis, the majority of Rax2 is retained at the cell tips during cytokinesis, and only a weak Rax2 signal is detected at the septum (Figure 1.11) (S.Ashraf, thesis). This suggests that Rax2 may have slower dynamics than other polarity landmarks such as Tea1, and effectors of cell growth such as Bgs4 and Cdc42. Fluorescence recovery after photobleaching (FRAP) experiments indicate that Rax2-3mCitrine signal at the cell tips recovers within about 50 minutes after photobleaching of interphase cells (S.Ashraf, thesis). This is much slower than the highly dynamic proteins Cdc42-GTP and Bgs4, whose recovery following photobleaching takes 4.6 and 20 seconds respectively (Bendezu, Vincenzetti et al. 2015) (Estravis, Rincon et al. 2012). Interestingly, no recovery of Rax2 signal at the tips is seen in septating cells. This suggests that Rax2 is delivered to the cell tips during active growth and is relatively stable at cell tips once deposited.

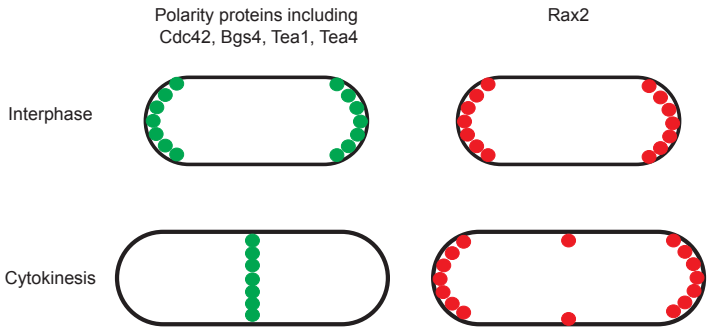

Figure 1.11: Polarity proteins localise to the cell tips during interphase. However, unlike most polarity proteins, Rax2 does not rapidly relocalise to the septum during cytokinesis. Cartoons showing protein localisation during interphase and cytokinesis.

1.9.4 Rax2 is trafficked to the growing cell tip through the secretory pathway

Rax2 is delivered to the cell tips through exocytosis during active growth. Growth machinery such as Bgs4 and Cdc42 are also delivered to the cell tips through exocytosis. In cells treated with Brefeldin A, an inhibitor of ER-to-Golgi transport, Rax2 signal at the cell tips does not recover following photobleaching (S.Ashraf, pers. Comm.). Once delivered to the cell tips Rax2 is stably retained.

1.9.5 Rax2 is stable following stresses such as perturbations to the cytoskeleton

Rax2 remains at cell tips after depolymerisation of the cytoskeleton. Unlike Tea1, whose localisation to the cell tips is completely dependent on a correctly organised microtubule cytoskeleton (Mata and Nurse 1997) Rax2 signal is unaffected 60 minutes following depolymerisation of microtubules with the drug Methyl Benzimidazol-2-yl Carbamate or the actin depolymerising drug Latrunculin A (S.Ashraf thesis). Apart from depolymerising actin, Latrunculin A also activates the Sty1 mediated stress signalling pathway, which leads to the relocalisation of Cdc42-GTP from the cell tips to ectopic sites (Mutavchiev, Leda et al. 2016). When 50 μm Latrunculin A is added and then washed from wild type cells, Cdc42-GTP first localises to ectopic sites and recovers to the cell tips after 70 minutes (S.Ashraf, thesis). *rax2*Δ cells recover from this treatment in a similar time frame to wild type cells. Whereas only 34 % of *tea1*Δ cells recover and this recovery takes 100 minutes. In *tea1*Δ*rax2*Δ cells, only 4 % of cells were able to recover Cdc42-GTP to the cell tips and re-establish polarity (S.Ashraf, thesis). The Rax2 growth memory cue works synergistically with the Tea1-Tea4 polarity cue to re-establish polarised growth following cell stress with the drug Latrunculin A.

1.10 Long lived proteins are important for a diverse range of functions

In human tissues, there are long-lived intracellular proteins that persist for months or even years, for example crystalline and collagen (Toyama, Savas et al. 2013). However, there are no repair mechanisms for long-lived proteins, and accumulation of damage in crystalline and collagen leads to cataract eye lenses and cartilage stiffening (Toyama, Savas et al. 2013).

Memory-based cues have been shown to play a role in polarisation of *Drosophila* sensory neurons (Pollarolo, Schulz et al. 2011). Cleavage of precursor neuronal cells generates cortical remnants, which are inherited by the neuron, and act as the initial landmark for polarisation (Pollarolo, Schulz et al. 2011). Neuronal polarisation is directed through cadherin-mediated signalling which is restricted to the apical pole of the neuron by the cortical remnants. The apical pole always corresponds to the site of the last mitotic cleavage (even when the cleavage plane is mispositioned in respect to the animal body axis) (Pollarolo, Schulz et al. 2011). At the apical pole, cell growth is promoted and there is further reinforcement of the cell polarity axis through microtubule reorganisation (Pollarolo, Schulz et al. 2011). This memory may be involved in co-ordination of the polarisation axis of neighbouring cells at early stages of neuronal development.

Directional memory plays an important role in migratory cells. This memory enables the robust migration of cells when there are fluctuations in chemoattractant concentrations, a transient loss of polarity or high saturating chemoattractant concentrations (Prentice-Mott, Meroz et al. 2016). Following induced depolarisation of chemotactic neutrophil-like cells, 80 % of cells repolarise to their original polarity within 10 minutes, without the need for readdition of chemoattractant to the environment. (Prentice-Mott, Meroz et al. 2016). The memory cue in these cells is the Ezrin, Radixin, Moesin (ERM) family member moesin. Moesin is a long-lived protein, and when it inhibited or mislocalised, this leads to loss of repolarisation of neutrophil-like cells (Prentice-Mott, Meroz et al. 2016). Unlike Rax2, moesin localisation is disrupted following depolymerisation of microtubules (Prentice-Mott, Meroz et al. 2016). This suggests that these cells require flexibility in directional memory to allow reorientation of migration when necessary.

Further characterisation of the Rax1 and Rax2 growth-memory landmarks will hopefully provide insights that will be relevant to understanding cell polarisation in higher eukaryotic cells.

1.11 Project aims

The aim of my PhD was to further characterise the Rax1-Rax2 growth - memory polarity cue. To this end I aimed to identify Rax2 interactors and investigate how they were functionally relevant to the growth-memory cue.

I first generated tagged strains of Rax1 and Rax2 that retained sufficient function to be physiologically relevant for studies involving live-cell imaging and purification of interacting proteins. I optimised live-cell imaging for both Rax1 and Rax2. Additionally, I characterised homemade antisera raised towards Rax1 and Rax2 (Chapter 3). I optimised purification of Rax2 from yeast and used cross-linking and mass spectrometry to identify interacting partners of Rax2 (Chapter 4). From a list of candidate Rax2 interactors, I chose to study one interactor in detail, and I showed that this protein, Lrx1, is important for localisation of Rax1 and Rax2 to cell tips (Chapter 5).

Chapter 2: Materials and Methods

2.1 Growing fission yeast cultures

Fission yeast cultures were grown in either rich yeast extract (YE5S) medium or in Edinburgh minimal medium (EMM). The recipes for these media are as below:

- YE5S: 0.5% (w/v) Difco yeast extract, 3.0% (w/v) glucose, 250 mg/L each of adenine, histidine, leucine, lysine and uracil.
- EMM: 14.7 mM potassium hydrogen phthalate, 15.5 mM Na_2PO_4, 2% glucose, 1X salt solution (50X stock salt solution: 52.5 g/l $MgCl_2.6H_2O$, 0.735 mg/l $CaCl_2.2H_2O$, 50 g/l KCl, 2 g/l Na_2SO_4); 1X vitamin mixture (1000X vitamin stock: 1 g/l pantothenic acid, 10 g/l nicotinic acid, 10 mg/l biotin); 1X minerals (10,000X mineral stock: 5 g/l boric acid, 4 g/l $MnS)_4$, 4 g/L $ZnSO_4.7H_2O$, 2 g/l $FeCl_2.6H_2O$, 0.4 g/Ll $CuSO_4.5H_2O$, 10 g/l citric acid); 2.2 g/l NH_4Cl or 3.75 g/l L-glutamic acid monosodium salt. 200 mg/L amino acid supplement added when required.

For growth on solid plates 2 % Difco Bacto agar was added. For drug selection, 100 µg/ml of G418 (Geneticin), nourseothricin (ClonNat) or hygromycin was added. Replica plating to YE5S + 5 mg/l Phloxin B was used to identify sick/dead or diploid cells. Sick/dead or diploid cells stain a dark pink colour, as they take up the Phloxin B dye more readily than living, haploid cells.

2.2 Genetic crosses

Fission yeast strains were mated on SPA plates (2 % Difco Bacto agar, 30 g/l glucose, 5 g/l KH_2PO_4, supplemented with amino acids and 1X vitamins as for EMM). The h+ and h- strains to be mated were patched onto SPA plates and mixed aided by adding 10 ul of distilled water. The plates were incubated at 25 °C for 3 x overnights or 28 °C for 2 x overnights to form asci. Asci were streaked onto a YE5S plate and incubated at 32 °C for 1 hour; this aids breaking down of the ascus wall and consequently makes

tetrad dissection easier. Tetrads were separated using a Singer micromanipulator. Plates were incubated at the suitable temperature for germination of the spores: 25 °C for temperature-sensitive strains, and 32 °C for non-temperature-sensitive strains. Once colonies were clearly visible, the plate was replica plated onto the relevant selection plates to identify colonies of the desired genotype.

If mating efficiency was found to be very low, and few asci were generated from the cross, spores were isolated by random spore analysis. A small patch of cells from the cross was dissolved in 300 µl of distilled water with 6 µl of helicase (Helix Pomatia juice, Life Technologies) added. Digestion of the ascus and vegetative cell walls occurred during incubation of the sample at 32 °C for 5 hours. The spores were separated through brief sonication, and were counted using a haemocytometer. Spores were plated onto three YE5S plates at a final density of ~150 spores per plate. Replica plating onto relevant selection plates was used to identify colonies of the desired phenotype as for tetrad dissection.

2.3 Generation of PCR based insertion sequences

The PCR method of C-terminal tagging, N-terminal tagging with an *nmt* promoter and deletion of fission yeast genes was used as described by Bähler *et al*, 1998**.** pFA6a plasmids containing the relevant tagging cassette were templates for PCR amplification using primers designed to have approximately 21 bases of sequence homology to the cassette and 80 bases of homology to the relevant genomic region. For C-terminal tagging, the cassette contained the tag of interest (for example mECitrine, 3xmCitrine, His-Tev-Biotin) followed by the resistance marker (G418, hygromycin, nourseothricin). For gene deletion, the cassette contained only the resistance maker. For *nmt* N-terminal tagging, the cassette contained the resistance marker, followed by the *nmt* promoter (typically *nmt41* or *nmt81*) and by the tag of interest.

PCR using Q5 polymerase

Component	Concentration
Q5 reaction buffer	1X
dNTPs (dATP, dTTP, dCTP, dGTP)	500 µM each
Forward primer	0.2 µM
Reverse Primer	0.2 µM
Template DNA	20 ng per 50 µl reaction
Q5 polymerase	2 units per 50 µl reaction

Cycling conditions:

1. 98°C 2 minutes
2. 98°C 20 seconds
3. 50-60°C* 20 seconds
4. 72°C 4 – 10 minutes**
5. Repeat steps 2-4 for 35 cycles
6. 72°C 10 minutes
7. 21°C hold

* Dependent upon annealing temperature of the primers

**Dependent upon the length of the PCR product

2.4 PCI clean up of PCR generated insertion sequences

Phenol/chloroform/isoamyl alcohol (PCI) extraction was used to purify the PCR-generated DNA. An equal volume of PCI was added to the DNA, vortexed and spun in a mircofuge at 13,000 rpm for 5 minutes. The upper phase was recovered and transferred to a fresh tube. Again, an equal volume of PCI was added and the sample was vortexed and spun as before. The upper phase was recovered transferred to a fresh tube, an equal volume of chloroform was added, and the sample was vortexed and spun as before. The upper phase was added to a fresh tube and 0.3 M of NaOAc pH 5.2 and 2 volumes of chilled 96 % ethanol were then added. The sample was spun at 13,000 rpm for 10 minutes at 4 °C. The supernatant was removed and the pellet was washed with chilled 70% ethanol, spun at 13,000 rpm for 5

minutes at 4 °C. The supernatant was discarded and the pellet was dried. The pellet was then resuspended in 50 µl TE buffer. DNA recovery was assessed by running 1 µl and 0.1 µl on a 1% agarose gel alongside a 1 kb DNA standard ladder (NEB) containing known masses of marker fragments.

2.5 Transformation of DNA insert into yeast cells

Cells were grown overnight in YE5S to an OD_{595} of 0.8. 20 ml of cells were spun at 4,000 rpm for 5 minutes. The supernatant was discarded and cells were washed with 20 ml of dH_2O and spun again. The supernatant was discarded and the cells were resuspended in 1 ml LiOAc in TE pH 7.5 and spun at 13,000 rpm for 1 minute in a microfuge. Cells were resuspended in LiOAc in TE to a final volume of 100 µl. At least 20 µg of PCI cleaned DNA was added and the sample was incubated at room temperature for 10 minutes. 260 µl of freshly prepared 40% polyethylene glycol 3350 in LiOAC in TE was added to the sample, mixed gently, and incubated at 32 °C for 30 minutes. 43 µl of DMSO was added, and the cells were heat shocked at 42 °C for 5 minutes. Cells were spun at 13,000 rpm for 1 minute and washed with 1 ml dH_2O and spun again. Cells were resuspended in 500 µl dH_2O and plated onto three YE5S plates and incubated at 32 °C overnight. The next day, the cells were replica plated onto YE5S plates containing the relevant antibiotic. These plates were incubated at 32 °C for two days and replica plated onto a selection plate. The second replica plate was incubated at 32 °C overnight. The next day individual colonies were streaked onto YE5S plates and incubated at 32 °C for 2 days so that individual cells could form independent colonies without antibiotic selection. The streaked plates were then replica plated onto selection plates to determine whether the DNA had been stably integrated.

2.6 Colony PCR to confirm correct integration of DNA insert into yeast

Colony PCR was carried out to confirm that the DNA inserts were integrated into the correct site in the genome (for gene deletions and tagging of proteins at the N- or C- terminus). In order to confirm gene deletions and

C-terminal tagging had occurred correctly, a forward primer was designed to have homology to the resistance gene for selection in the insert and a reverse primer was designed to have homology to the 3' untranslated region (UTR) of the gene of interest. For N-terminal tagging a forward primer was designed to have homology to the 5' UTR and a reverse primer to have homology to the resistance gene of the insert.

Cells grown on a YE5S plate for one day were used for DNA preparation. Cells, equivalent to approximately the size of a match stick tip, were collected from the plate using a sterile pipette tip and resuspended in 30 µl of 0.25% SDS in TE. Cells were boiled for 5 minutes and spun to pellet the cell debris. 1 µl of the supernatant was used as a DNA template for the colony PCR.

Colony PCR using Taq and Pwo polymerase

Component	Concentration
Buffer IV (750 mM Tris-HCl pH8.8, 200 mM Ammonium sulphate, 0.1 % Tween20)	1X
$MgCl_2$	3.5 mM
dNTPs (dATP, dTTP, dCTP, dGTP)	500 µM each
Forward primer	0.2 µM
Reverse Primer	0.2 µM
Template DNA	1 µl
Taq polymerase	0.2U/ µl
Pwo polymerase	0.0003 U/ µl

Cycling conditions:

1. 96 °C 2 minutes
2. 96 °C 20 seconds
3. 50-60 °C 20 seconds*
4. 72 °C 3-8 minutes**
5. Repeat steps 2-4 for 35 cycles
6. 72 °C 5 minutes

7. 20 °C hold

* Dependent upon annealing temperature of the primers

**Dependent upon the length of the PCR product

2.7 DNA sequencing

Sanger sequencing was carried out to confirm that certain inserts were integrated correctly into the genome or to confirm that plasmids constructed for transformations contained the correct sequence. Colony PCR was used as described in 2.6 to generate a fragment of DNA for sequencing from the yeast genome or purified plasmid was used as a template for sequencing.

BigDye sequencing reaction:

Component	Concentration
BigDye terminator mix	1 x
Primer	0.5 μM
DNA	80 – 120 ng

Cycling conditions:

1. 96 °C 30 seconds
2. 50 °C 15 seconds
3. 60 °C 5 minutes
4. 1-3 for 25 cycles
5. 20 °C hold

The sample was sequenced at Edinburgh Genomics using Sanger sequencing instruments ABI 3730 (Applied Biosystems) and analysed using Seqman softmare (DNASTAR Inc).

2.8 Growth of *E. coli*

Chemically competent *Escherichia coli* (*E. coli*) DH5α strain was used for transformation and cloning. Cells were grown at 37 °C in LB liquid medium (10 g/l Difco Bacto tryptone, 5 g/l Difco Bacto yeast extract, 5 g/l

NaCl, pH7.2) or on LB agar plates (LB medium with 2 % Difco Bacto agar). 100 µg/µl ampicillin was supplemented into the media for selection.

2.9 Transformation of *E. coli*

DH5α cells were thawed on ice, mixed with 50 ng of DNA from a ligation reaction or 5 ng of DNA from a purified plasmid and incubated on ice for a further 10 minutes. The cells were heat-shocked at 42 °C for 30 seconds and recovered in 1ml LB liquid media for 1 hour at 37 °C. The cells were plated onto an LB selection plate and incubated at 37 °C overnight for individual colonies to form.

2.10 Isolation of plasmid DNA from *E.coli*

A single colony that formed on the selection plate following transformation was isolated and grown in 5 ml LB liquid media supplemented with ampicillin at 37 °C overnight with shaking. The cells were pelleted by centrifugation at 13,000 rpm for 1 minute. The plasmid was isolated using the NucleoSpin Plasmid Kit (Macherey-Nagel). The cell pellet was resuspended in 250 µl of buffer A1, and then 250 µl of lysis buffer A2 was added, and contents were mixed thoroughly and incubated at room temperature for 5 minutes. 300 µl of neutralisation buffer A3 was added and mixed by gentle inversion until the blue mixture turned completely colourless. The sample was spun at 13,000 rpm for 10 minutes to pellet cell debris. The supernatant, containing the plasmid DNA, was transferred to a NucleoSpin plasmid column with a collection tube and spun at 13,000 rpm for 1 minute. The flow-through was discarded and 500 µl of buffer AW was added to the column, which was again spun at 13,000 rpm for 1 minute. The supernatant was discarded, 600 µl of wash buffer A4 was added and spun at 13,000 rpm for 1 minute. A final spin at 13,000 rpm for 2 minutes ensured that all of the buffer was removed from the column. The column was placed in a fresh 1.5 ml tube and 50 µl buffer AE was added to the column and incubated at room temperature for 5 minutes. The column was centrifuged at 13,000 rpm for 1 minute and the plasmid DNA was collected in the 1.5 ml tube. The DNA

concentration was quantified using the NanoDrop (Thermo Scientific) and stored at -20 °C.

2.11 Construction of Rax2 internal deletion vectors

Genomic DNA was prepared from KS 7867. Cells grown on a YE5S plate for one day were used for DNA preparation. Cells, equivalent to approximately the size of a match stick tip, were collected from the plate using a sterile pipette tip and resuspended in 30 µl of 0.25% SDS in TE. Cells were boiled for 5 minutes and spun to pellet the cell debris. 1 µl of the supernatant was used as a DNA template for the colony PCR. The entire Rax2 coding sequence plus the first 300 bps of 3mCitrine was amplified by Q5 polymerase (NEB) using oligos oKS 3327 and oKS 3328. A 1:3 molar ratio of insert to PJet 1.2 vector was incubated with 1X Quick Ligase buffer (NEB) and 1 µl Quick Ligase at room temperature for 30 minutes to create pKS 1585: pJet Rax2+first 300bps of 3xmCitrine The ligation product was transformed into DH5α cells as described in section 2.9 and isolated as described in section 2.10. The isolated plasmid pKS 1585 was sequenced as described in section 2.7 with oligos oKS 3406, oKS 3407, oKS 3408, oKS 3409, oKS 3410, oKS 3411, oKS 3412, oKS 3413 and oKS 3414 to confirm the sequence was correct.

Rax2 internal deletion plasmids were created by PCR of pKS 1585 using Q5 polymerase the oligos described in Table 2.1. Oligos were designed to amplify the plasmid outwards from each end of the internal deletion sites.

Table 2.1

Identifier	Vector	Forward	Reverse
pKS 1606	pJet Rax2Δ21-120 -3mCitrine	oKS 3423	oKS 3424
pKS 1607	pJet Rax2Δ121-220 -3mCitrine	oKS 3425	oKS 3426
pKS 1608	pJet Rax2Δ221-320 -3mCitrine	oKS 3427	oKS 3428
pKS 1609	pJet Rax2Δ421-520 -3mCitrine	oKS 3431	oKS 3432

The DNA was purified using Nucleospin Gel and PCR clean up (Macheray-Nagel). The linearised PCR generated fragments were incubated with T4 polynucleotide Kinase and 1x T4 Polynucleotide Kinase buffer at 37 ˚C for 45 minutes. 1 µl of T4 DNA ligase was added to the reaction and incubated at room temperature for 3 hours. The plasmids were transformed into DH5α cells as described in section 2.9 and isolated as described in section 2.10.

2.12 Construction of pFa6a 3mCitrine-HTB and pfa6a 3mCitrine-HBH vectors

3mCitrine-HTB-2XG(4)S and 3mCitrine-HBH-2XG(4)S sequences were synthesised by GeneArt (ThermoFisher). These sequences were amplified by Q5 polymerase with oligos oKS 3325 and oKS 3402 (for HTB) and oKS 3325 and oKS 3403 (for HBH). The PCR generated fragments were purified using Nucleospin Gel and PCR clean up (Macheray-Nagel). The inserts were cloned into pKS 1384, which was linearised using BamI and SmaI, using Gibson assembly. A 1:3 molar ratio of insert:vector was incubated with 1X Gibson Master Mix (NEB) at 50 ˚C for 1 hour. The ligation product was transformed into DH5α to create pKS 1586 pFA6a 3xmCitrine-HTB-HphMX6 and pKS 1605 pFa6a 3xmCitrine-HBH-HphMX6. The plasmids were isolated and sequenced using oligos oKS 2695, oKS 2708, oKS 2709, oKS 2710, oKS 2711, oKS 2712 and oKS 3325,

2.13 Construction of 1xmECitrine 2xG(4)S and 1xmCherry 2xG(4)S vectors

pKS 1381 was amplified by Q5 polymerase with oligos oKS 3417 and oKS 3418 to add a 2xG(4)S linker at the 3' end of 1xmECitrine, ligated into PJet 1.2 and transformed into DH5α as described in 2.11 to create pKS 1604.

pKS 1167 was amplified by Q5 polymerase with oligos oKS 3323 and oKS 3419 to add a 2xG(4)S linker at the 3' end of 1xmCherry, ligated into PJet 1.2 and transformed into DH5α as described in 2.11 to create pKS 1610.

2.14 Construction of pFa6a HBH-1xmECitrine-HphMX6 and pFa6a 1xmECitrine-HBH-HphMX6

HBH-1xmECitrine-HphMX6 and 1xmECitrine-HBH-HphMX6 sequences were synthesised by GeneArt (ThermoFisher). Both of these sequences contained a XmaI restriction site at the 5' and a AscI restriction site at 3' end. These sequences were amplified by Q5 polymerase with oligos oKS 3531 and oKS 3532. A 1:3 molar ratio of insert to PJet 1.2 vector was incubated with 1X Quick Ligase buffer (NEB) and 1 µl Quick Ligase at room temperature for 30 minutes to create pKS 1662 pJet HBH-1xmECitrine and pKS 1663 pJet 1xmECitrine-HBH. 200 ng of pKS 1662, pKS 1662 and pKS 1383 were restriction digested with XmaI (NEB) and AscI (NEB) at 37 ˚C for 2 hours. The digestion products were separated by electrophoresis at 100 V through a 1 % agarose gel with 0.5 µg/ml ethidium bromide. Digestion products were visualised using a UV transilluminator, and bands of interest were extracted from the gel using a sterile scalpel. The DNA was gel purified using the NucleoSpin Gel and PCR Clean-Up Kit (Macherey-Nagel). The HBH-1xmECitrine and 1xmECitrine-HBH inserts were ligated into the linearised pKS 1384 vector with T4 polymerase and transformed into DH5α as described above.

2.15 Construction of pFA6-1xmECitirine-avitag-6xHis-KanMX6

1xmECitirine-avitag-6xHis sequence was synthesised by GeneArt (ThermoFisher). Both of these sequences contained a PacI restriction site at the 5' and a AscI restriction site at 3' end. These sequences were amplified by Q5 polymerase with oligos oKS 3727 and oKS 3728. A 1:3 molar ratio of insert to PJet 1.2 vector was incubated with 1X Quick Ligase buffer (NEB) and 1 µl Quick Ligase at room temperature for 30 minutes to create pJet 1xmECitirine-avitag-6xHis. 200 ng pJet 1xmECitirine-avitag-6xHis and pKS 1382 were restriction digested with PacI (NEB) and AscI (NEB) 37 ˚C for 2 hours The digestion products were separated by electrophoresis at 100 V through a 1 % agarose gel with 0.5 µg/ml ethidium bromide. Digestion products were visualised using a UV transilluminator, and bands of interest were extracted from the gel using a sterile scalpel. The DNA was gel purified

using the NucleoSpin Gel and PCR Clean-Up Kit (Macherey-Nagel). The 1xmECitirine-avitag-6xHis insert was ligated into the linearised pKS 1382 vector with T4 polymerase and transformed into DH5α as described above.

2.16 Microscopy

Depending on the experiment, either the Spinning Disk Confocal or the Airyscan Microscope was used. All growth pattern analysis using the CRIB-3mCitrine reporter was carried out on the spinning disk confocal. For all other experiments the microscope used will be stated in the figure legends of the relevant images.

2.16.1 Spinning Disk Confocal Microscope

Spinning disk confocal microscopes contain a rotating disk with a pattern of holes designed to block out of focus light from both excitation and emission light paths. Spinning disk microscopes are most suitable for the time-lapse experiments I use to determine the growth patterns in different genetic backgrounds due to their high-speed, reduced photo-toxicity and reduced photo-bleaching compared to laser-scanning microscopes.

In this project I used a Spinning disk confocal microscope with a customised set-up. Multipoint imaging and autofocusing was enabled by Nikon TE2000 inverted microscope with a 100x/1.45 NA Plan Apo oil objective (Nikon) and an MS-2000 automated stage with CRISP autofocus (ASI). A Yokogawa CSU-10 spinning disk unit (Visitech) is placed between the microscope and the EMCCD camera. The spinning disk unit contains a collector disk with an array of microlenses and a pinhole disk in which each pinhole corresponds to an individual microlens. A dichroic mirror is placed in between the two disks and reflects emission light to be collected by the EMCCD camera. For all imaging carried out on the spinning disk the 514/594 dichroic mirror (Chroma Technology Corp., Vermont, USA) was used. Fluorescence signal was collected by an iXOn+ Du888 EMCCD camera (Andor Technology, UK). It has a pixel size of 1024 x 1024. The camera is chilled to -90 °C. An Optospin IV filter wheel (Cairn Research, UK) is controlled by Metamorph software to enable the appropriate filter set.

Illumination was carried out by a multi-line laser (Cairn Research, UK) with 488 nm, 514 nm, 561 nm and 594 nm laser lines, and was controlled by Metamorph software. Brightfield imaging was carried out using an OptoLED Lite (Cairn Research, UK). A temperature-controlled chamber (OKOlab, Italy) was used to maintain a temperature of 25 °C during imaging. Metamorph software was used to control the laser lines, filter wheels and all other imaging parameters (Molecular Devices, USA). Microscope settings for specific experiments are described in Table 2.2

Table 2.2

Fluorescent probe	Laser power	Exposure	Z-sections	Binning
CRIB-3mCitrine	5% 514 nm	50 ms	11 of 0.6 µm	2 x 2
Rax2-3mCitrine/ mECitrine	20% 514 nm	900 ms	3 of 0.3 µm	2 x 2
Rax2-mECitrine (rax1Δ experiments) and *nmt41:*mECitrine Rax1	50% 514 nm	900 ms	1	2 x 2
ADEL mCherry	20% 594 nm	300 ms	1	2 x 2

2.16.2 Airyscan microscope

The Airyscan module attaches to a confocal laser-scanning microscope and is comprised of an array of 32 GaAsP detectors in a hexagonal lattice. Each of the detectors is 0.2 Airy units in diameter, which gives a total detection area of 1.25 Airy units. This gives the module the increased resolution, produced from a 0.2 Airy unit pinhole with the increased sensitivity of a 1.25 Airy unit pinhole, providing a simultaneous increase in both resolution and signal.

Images are processed, which involves summing the images from all the detectors and reassigning the detected light with the central point and then Wiener filtering the resulting image. Resolution in the XY dimension is improved from ~240 nm to 140 nm and from ~550 nm to 400nm in the Z

dimension. Microscope settings for specific experiments are described in Table 2.3.

Table 2.3

Fluorescent probe	Laser power 514 nm	Z-sections	Averaging
Rax2-mECitrine	10 %	5 of 0.6 µm	None
mCherry-Bgs4	5 %	5 of 0.6 µm	None
mECitrine-Rax1 (and Rax2-mECitrine for comparison with Rax1)	15 %	3 of 0.6 µm	Four times

2.16.3 Image analysis

Analysis of raw images was carried out using Metamorph (Molecular devices), Airyscan (Zeiss) and ImageJ. CRIB-3mCitrine movies were processed by making a maximum projection of all of the Z planes. Still images of fluorescently tagged Rax1, Rax2 and Lrx1 were processed by making a sum projection of the Z planes. Tip fluorescence intensity was calculated by first drawing a freehand shape around the cell tip. This shape was copied both to a region of the image that did not contain a cell and to the cell cytoplasm. The average of the cytoplasmic signal and the 'no cell' signal was subtracted from the tip signal to provide the total tip intensity. The shapes being drawn freehand leads to some inaccuracies in the quantification, however this method of quantification was deemed suitable for the aims of this project.

2.17 Western blotting and protein purification

2.17.1 Preparation of protein extracts using TCA

TCA protein extracts were used to prepare Rax1 and *nmt41*:mECitrine-Rax1 samples for anti-Rax1 western blots. Cells were grown in EMM (+/-5 µM/ml thiamine) to an OD_{595} of ~ 0.8 and centrifuged at 4,000 rpm for 1 minute at 4 °C. The cell pellet was resuspended in ice-cold

STOP buffer (150 mM NaCl, 50 mM NaF, 10 mM EDTA, 1mM NaN_3). The sample was spun at 13,000 rpm for 15 seconds at 4 ˚C, the supernatant was discarded and the cell pellet was flash frozen in liquid nitrogen and stored at -80 °C. Ice cold 20 % TCA was added to the pellet and ~500 µl Zirconia acid washed glass beads. Samples underwent 3 rounds of ribolysation at speed 2.0 for 30 seconds with a 2 minute incubation on watery ice between rounds. The sample was spun at 13, 000 rpm for 5 minutes at 4 °C. The supernatant was discarded and the pellet was resuspended in sodium dodecyl sulphate containing 0.5% ß-mercaptoethanol and 300 mM Tris pH 8.0.

2.17.2 Preparation of protein extracts from frozen cell powder

All anti-Rax2 western blots presented in this thesis were generated from protein samples from frozen cell powder, as this improved the quality of detection of Rax2. Cells were grown in 4X YE5S and harvested at OD ~ 12 using a Beckman Avanti J-25 centrifuge with a JLA 8.1000 rotor. Cells were spun at 5,000 rpm at 4 ˚C for 15 minutes. Cells from each 1 l of culture were washed twice with 200 ml wash buffer (10 mM $NaPO_4$ pH 7.5, 0.5 mM EDTA). Each wash was followed by a spin at 5,000 rpm at 4 ˚C for 15 minutes. After the final wash, cells were weighed and resuspended in 0.3 ml of wash buffer per gram of cells. The cell resuspension was frozen as droplets in liquid nitrogen and stored at -80 ˚C. ~30 g of cells were ground using a Retsch RM100 electric mortar grinder (Retsch, Germany) pre-cooled (~ -190 ˚C) with liquid nitrogen for 40 minutes. Liquid nitrogen was topped up when necessary during grinding. The ground cell powder was transferred to 50 ml falcon tubes that were pre-cooled on dry ice, and stored at -80 ˚C. The appropriate amount of frozen cell powder was weighed out for the experiment. 2 ml of pre-cooled buffer (30 mM $NaPO_4$ pH 7.5, 85 mM NaCl, 2 mM Benzamidine, 0.2 mM PMSF, 1 x CLAAPE) was used per 1 g of cells. Cell powder was resuspended in the buffer by vortexing,

2.17.3 Generation of the Membrane-Enriched Fraction

Whole cell lysates were centrifuged at 2,400 x *g* for 5 minutes at 4 ˚C to pellet the cell debris. The supernatant was recovered and transferred to a fresh tube and spun at 13,000 x *g* for 15 minutes or 6,238 x *g* for 1 hour for

larger volumes. Supernatant was discarded and the pellet was resuspended in 5 x volume of LSB (or increased volume of LSB if cell pellet not completely resuspended).

2.17.4 PNGase F treatment

10X Glycoprotein Denaturing Buffer (400 mM DTT in 5 % SDS; NEB) was added to MEF protein samples to a final concentration of 1X. Samples were boiled at 100 ˚C for 10 minutes, spun briefly and left to cool to room temperature. 10X Glycobuffer 2 (500 mM $NaPO_4$ pH 7.5) and 10 % Nonidet P-40 were again added to the sample to a final concentration of 1X and 1 %. PNGase F was added at a concentration of 50 units per 100 µg of protein.

2.17.5 Mock PNGase F treatment

Membrane enriched fractions (MEFs) were resuspended in LSB with 40 mM DTT (Melford Biolaboratories Ltd) and 0.5 % SDS (National Diagnostics) and boiled at 100 ˚C for 10 minutes and spun briefly. Triton X-100 was added to the sample to a final concentration of 1 %, and sodium phosphate (pH 7.5) to a final concentration of 50 mM, and the fraction was then incubated at 36 ˚C for 2 hours.

2.17.6 SDS-PAGE, Coomassie staining and western blotting

Protein samples were prepared into 1X Laemmli sample buffer (2 % SDS, 10 % glycerol, 60 mM Tris-HCl pH 6.8, 0.05 % bromophenol blue, 0.1 M DTT), heated at 95 ˚C for 5 minutes and spun at 13,000 x *g* for 30 seconds. Different acrylamide concentrations in resolving gels were used for SDS-PAGE for specific experiments. Anti-Rax1 western blotting and Rax2-HTB mass spectrometry was carried out on samples that had been resolved using 12 % and 8 % home-made acrylamide resolving gels (respectively) with a 5 % stacking gel in 1 x Laemmli running buffer (25 mM Tris base, 192 mM glycine, 0.1% SDS, pH 8.3). For anti-Rax2 western blotting experiments, Rax2 protein samples were resolved on a 3 – 8 % tris-acetate resolving gel (Thermo Fisher Scientific) in NuPAGE Tris-acetate running buffer (Thermo Fisher Scientific).

For Coomassie staining after electrophoresis (Rax2-HTB mass spectrometry experiments), gels were transferred into a glass tray with

staining solution (25 % isopropanol, 10 % acetic acid, 0.05 % Brilliant Blue R-250) and heated in a microwave for 1 minute at the high setting. The glass tray was placed on a shaker for 2 hours to overnight. The staining solution was then discarded and replaced with a destaining solution (10% acetic acid). A paper towel was folded and placed in the tray to absorb extra stain from the gel. The gel was heated in a microwave for 1 minute at the high setting and then placed on a shaker until the protein bands were sufficiently distinguished (5 hours to overnight). When bands were sufficiently distinguished, the destaining solution was replaced with distilled water.

For western blotting, the protocol for protein transfer was different for anti-Rax1 western blots (in which proteins were separated on Tris-glycine gels) and anti-Rax2 western blots (in which proteins were separated on Tris-acetate gels).

For Anti-Rax1 western blots, proteins were transferred onto a nitrocellulose membrane through wet-transfer in CAPS buffer (10 mM CAPS, 10% methanol). Transfer was at 90 V for 90 minutes. For Anti-Rax2 western proteins were transferred to a nitrocellulose membrane through wet-transfer in Tris-Glycine transfer buffer (25 mM Tris, 192 mM glycine, 20% Methanol). Transfer was at 100 V for 60 minutes. Correct transfer of proteins for each method was confirmed through staining with Ponceau S (0.2% Ponceau S, 3% trichloroacetic acid, 3 % sulfosalicylic acid). Excess Ponceau S was washed off using 5 % acetic acid and scanned using a Epson V800 scanner. The membrane was washed with 1X TBS + 0.05 % Tween-20 (TBS-T) to remove the Ponceau S strain. The membrane was placed in a clean plastic tray and blocked with 2 % non-fat dried milk in TBS-T for one hour at room temperature on a shaker. The blocking solution was replaced with fresh blocking solution containing a 1:1,000 dilution of either anti-Rax1 (SA050) or anti-Rax2 (SA051) antiserum (homemade), raised in sheep. The membrane was incubated with the primary antibody overnight at 4 ˚C on a shaker. The next morning, the membrane was washed with TBS-T three times for fifteen minutes. The membrane was then incubated with a 1:10,000 dilution of GT-34, a secondary monoclonal mouse anti-sheep antibody, in blocking solution

for 1 hour at room temperature on a shaker. The membrane was washed with TBS-T three times for five minutes. This was followed by incubation with 1:5,000 dilution of anti-mouse IRDye800 fluorescent antibody (Licor Biosciences) in blocking solution for 1 hour at room temperature on a shaker. The membrane was washed with TBS-T three times for five minutes. Two final washes of the membrane were carried out using TBS without Tween-20. The membrane was scanned using a Licor Odyssey scanner, and ImageStudio software was used to visualise and quantify bands on the membrane. For quantification, a rectangle was drawn on the bands of interest, and the total fluorescence intensity within the rectangle region was determined. Background was subtracted by setting a rectangle of equal size to the band of interest to a region of the blot without a band.

2.17.7 Streptavidin binding assay

MEF protein samples from *rax2+*, *rax2-HTB* and *rax2-HBH* strains were prepared from frozen cell grindates and treated with PNGase F. Protein concentration was measured by the BCA assay. To each 200 ng protein sample, 0.1 M DTT and 0.01 % bromophenol blue was added, and heated at 95 ˚C for 5 minutes. The samples were spun at 13,000 rpm for 1 minute at room temperature and allowed to cool to room temperature. 2 µl of streptavidin (1 mg/ml) was added to the sample, mixed thoroughly and incubated at room temperature for 15 minutes. The samples were loaded onto a 3–8 % Tris-acetate precast gel followed by an anti-Rax2 Western blot.

2.18 Cross-linking and mass spectrometry

2.18.1 Cross-linking

60 g cell grindate was dissolved in 120 ml cross-linking buffer (30 mM $NaPO_4$, 85 mM NaCl, 1X CLAAPE (chymostatin, leupeptin, antipain, pepstatin, E64), 2 mM Benzamidine, 0.2 mM PMSF) through pipetting and vortexing. A 0.125 M stock solution of the cross-linker disuccinimidyl suberate (DSS) (in DMSO) was added to the cell suspension at a 2.5 mM final concentration. The cross-linking reaction took place in falcon tubes for 2 hours at room temperature, with rotation. Then, 300 mM Tris-HCl pH 8.8 was

added to the sample to quench the cross-linking reaction, at room temperature for 30 minutes.

2.18.2 Membrane enrichment and 'Mock PNGase F' treatment

After cross-linking and quenching, samples were centrifuged at 2,600 x *g* for 5 minutes to create a MEF. The supernatant was transferred to 50 ml centrifuge tubes and spun at 13,000 x *g* for 1 hour. The pellet was suspended in 5 x volume of LSB and heated for 5 minutes at 95 ˚C. 40 mM DTT and 0.5 % SDS was added to each sample and heated at 95 ˚C for 10 minutes. Triton X-100 was added to the sample to a final concentration of 1 % and sodium phosphate (pH 7.5) to a final concentration of 50 mM and incubated at 36 ˚C for 2 hours.

2.18.3 Bead binding and elution

For each sample, 60 µl of MyOne Streptavidin C1 Dynabead slurry (Invitrogen) was washed two times with LSB + 1 % TX-100, and beads were resuspended in 57 µl of LSB + 1 % TX-100. The washed bead slurry was added to the protein sample and incubated overnight at room temperature with rotation. The next morning, the beads were transferred to a fresh tube and washed twice with LSB + 1 % TX-100 and once with LSB before being resuspended into 20 µl LSB. The beads were heated at 95 ˚C for 5 minutes. The elution was transferred to a fresh tube and underwent PNGase F treatment (section 2.14.5). Following PNGase F treatment, 0.1 M DTT and 0.01% Bromophenol blue was added to the sample and heated at 95 ˚C for 5 minutes. The sample was separated using SDS-PAGE on an 8 % Tris-acetate gel (8 % acrylamide, 0.4 M Tris (pH 8.8), 1 % ammonium perisulphate, 1 % SDS, 3.5 µM Tetramethylethylenediamine). The gel was stained with Coomassie Blue and destained with 10 % acetic acid.

2.18.4 Gel extraction and trypsin digestion

The region above the Rax2-HTB band (or equivalent to where the Rax2-HTB band would be in the untagged Rax2 sample) was excised with a sterile scalpel. The gel for each sample was then further cut into 1 mm pieces. The gel pieces were transferred to a microfuge tube, and 150 µl 50 mM ammonioum bicarbonate (ABC) and 150 µl acetonitrile (ACN) were

added to the gel pieces and incubated at 37 ˚C with shaking. The ABC and ACN solution was replaced with fresh ABC and ACN until the coomassie stain had been washed away from the gel pieces (~3 washes). The ABC/ACN solution was discarded and 150 µl ACN was added to the tube and incubated for 5 minutes with shaking to shrink the gel pieces. ACN was removed, and the gel pieces were then incubated with 150 µl of 10 mM DTT in 50 mM ABC for 30 minutes at 37 ˚C with shaking, to reduce any disulfide bonds in the proteins. The solution was discarded and 150 µl ACN was added to the gel pieces for 5 minutes at 37 ˚C to shrink the gel pieces once again. The gel pieces were alkylated in 150 µl of 55 mM iodacetamide in 50 mM ABC for 20 minutes in the dark at room temperature. The solution was removed and the gel pieces were incubated in 150 µl ACN for 5 minutes at 37 ˚C once again. The solution was discarded and replaced with 150 µl Trypsin solution (13 ng/µl Trypsin, 10 mM ABC, 10 % ACN) and incubated on ice for 15 minutes. The gel pieces were transferred to 37 ˚C and incubated overnight. The next morning, 150 µl 0.1 % (v/v) trifluoroacetic acid (TFA) was added to the gel pieces, incubated at 37 ˚C for 15 minutes with shaking. The digestion solution was loaded onto a Stage Tip (Rappsilber, Ishihama et al. 2003).

2.18.5 Mass spectrometry analysis

LC-MS-analyses were performed on a Q Exactive mass spectrometer (Thermo Fisher Scientific) by Christos Spanos, (Rappsilber lab University of Edinburgh). The Q Exactive was coupled on-line to Dionex Ultimate 3000 RSLCnano Systems (Thermo Fisher Scientific) and the peptides were separated on a 50 cm EASY-Spray column (Thermo Fisher Scientific) that was assembled in an EASY-Spray source (Thermo Fisher Scientific).

The MaxQuant software platform version 1.5.2.8 (Cox and Mann 2008) was used to process raw files, and search was conducted against *Schizosaccharomyces pombe* complete/reference proteome set from PomBase (www.pombase.org; released in July, 2016; (McDowall, Harris et al. 2015) using the Andromeda search engine (Cox, Neuhauser et al. 2011). Label-free quantification analysis was performed using the MaxLFQ

algorithm as described in (Cox, Hein et al. 2014). Peptide and protein identifications were filtered to 1% FDR.

2.19 RT-Q-PCR

2.19.1 Cell synchronisation and RNA extraction

Strains in a *cdc25-22* mutant background were grown in YE5S at 25 ˚C to an OD_{595} of 0.8, and then synchronised using a temperature shift to 36 ˚C for 4 hours. The samples were cooled to the 25 ˚C permissive temperature and parallel samples were taken every 20 minutes for 1) formalin fixation (to count the septation index to confirm cell synchornisation) and 2) RNA extraction.

For formalin fixation, 900 µl of culture was added to 100 µl of 37 % formaldehyde and incubated on ice for 10 minutes. The cell suspension was washed twice with PBS and the cells were resuspended in 20 µl PBS and stored at 4 ˚C.

For RNA extraction, 10 ml of sample was added to 5 ml of methanol (precooled on dry ice) and mixed thoroughly. The sample was spun at 3,000 x *g* for 2 minutes at 4 ˚C. The supernatant was discarded and the cell pellet was resuspended in 1 ml of water, and the cells were centrifuged to repellet the cells. The supernatant was discarded and the pellet was stored at -80 ˚C. Cells were resuspended in 400 µl AE buffer (10 mM Tris-Cl; 0.5 mM EDTA; pH 9.0) with 200 µl acid-washed 0.5mm zirconium beads by vortexing vigorously and stored on ice. 40 µl of 10 % SDS was added and mixed gently. 80 µl phenol was added and vortexed for 10 seconds. The cells were lysed in a ribolyser set at the lowest power setting for 2 minutes, with 2 minute rests on ice between pulses. The lysed sample was put on dry ice until it solidified and spun at 13,000 x *g* for 5 minutes at room temperature. The upper phase was transferred to a fresh tube, and 600 µl of 5:1 Phenol: $CHCl_3$ was added, vortexed and spun at 13,000 x g. The upper phase was transferred to a fresh tube and 600 µl $CHCl_3$ was added, vortexed and spun at 13,000 x *g*. The upper phase was transferred to a fresh tube and the RNA was precipitated by adding 300 µl 10 M LiCl and mixing and placed at -20 ˚C overnight. The next day, the sample was spun at 13,000 x g for 5 minutes

and the supernatant was discarded. The pellet was washed with 70 % ethanol and the pellet was resuspended in 20 µl TE and stored at -20 ˚C.

2.19.2 Reverse transcriptase PCR

The RNA was quantified using a Nanodrop spectrophotometer. 10 µg of RNA, 10X Dnase I buffer (400mM Tris-HCl [pH 8.0 at 25°C], 100mM $MgSO_4$, 10mM $CaCl_2$) (Promega), 1 unit of Dnase I (Promega), 2 units of Ribolock RNase inhibitor (Thermoscientific) was added to a total reaction volume of 8 µl. The sample was incubated at 37 ˚C for 45 minutes and the Dnase I was inactivated by incubation at 75 ˚C for 10 minutes.

2.5 µl of 2.5 µM reverse primer mix (including all reverse primers used in the RT-Q-PCR) were added to the Dnase-treated RNA. The RNA was denatured at 70 ˚C for 5 minutes and returned to ice-water slurry. 5 µl of RNA was added to two fresh tubes (one positive and one negative control). 5 µl of 1^{st} strand synthesis mix (First strand synthesis buffer (Thermo Fisher Scientific), 750 µM dNTPs, 2 units RNase Inhibitor, 5 units Transcriptor (Sigma Aldrich) or water (in place of Transcriptor for negative control) was added to each RNA sample and incubated at 55 ˚C for 2 hours. The cDNA was diluted by adding 190 µl H_2O.

For each RT-Q-PCR, there were 3 positive replicates and one negative control for each primer pair. For each RNA sample, there were three RT-Q-PCRs carried out of housekeeping genes known to have a constant expression throughout the cell cycle (*cdc2, ade4 and rbp1*) for normalisation of RNA levels of the gene of interest to the total RNA levels in the sample. There were also two RT-Q-PCRs carried out of the known cell cycle regulated genes *gas1* and *chr1*, to confirm synchronisation of the RNA samples.

2 µl diluted cDNA was added to each well of a PCR plate, together with 5 µl of SyBr Green QPCR mix (Sigma Aldrich) and the relevant primer pair (0.6 µM final concentration).

The sample was amplified by PCR under the following conditions:

1. 94 ˚C 2 minutes
2. 94 ˚C 10 seconds
3. 60 ˚C 10 seconds
4. 72 ˚C 15 seconds
5. Cycle steps 2-4 40 times
6. 95 ˚C 10 seconds
7. 60 ˚C 10 seconds

2.19.3 Normalisation of RNA levels

For each RNA sample, *lrx1* RNA levels were averaged for the three positive replicates. The *lrx1* RNA levels were normalised to the total RNA input of the sample through comparison to the average RNA levels of the three non-cell cycle regulated genes (*cdc2, ade4, rpb1*) using the following formula:

Normalised *lrx1* RNA levels

$$=2^{\wedge} - \frac{1}{3}\sum_{1}^{3} lrx1 - \frac{1}{3}\left(\frac{1}{3}\sum_{1}^{3} cdc2 + \frac{1}{3}\sum_{1}^{3} ade4 + \frac{1}{3}\sum_{1}^{3} rpb1\right)$$

2.20 Plasmid list

Plasmid	Vector	Source
pKS 113	pFA6-natMX4	Sawin lab
pKS 705	pFA6a-natMX6-P41nmt1	Sawin lab
pKS 706	pFA6a-natMX6-P81nmt1	Sawin lab
pKS 1330	pFA6a-mEcitrine-KanMX6	Sawin lab
pKS 1332	pFA6a-KanMX6-P41nmt1-mEcitrine	Sawin lab
pKS 1333	pFA6a-KanMX6-P81nmt1-mEcitrine	Sawin lab
pKS 1382	pFA6-3xmCitrine-KanMX6	Sawin lab
pKS 1384	pFA6-3xmCitrine-hphMX6	Sawin lab
pKS 1412	pFA6a-rpl42-NatMX6	Hagan lab
pKS 1413	pFA6a-13Myc-NatMX6	Sawin lab
pKS 1585	pJet Rax2 + first 300bps of 3xmECitrine	This study
pKS 1586	pFA6a 3xmECitrine-HTB-HphMX6	This study
pKS 1594	pFA6a 3xmECitrine-HTB-NatMX6	This study
pKS 1604	pJet 1xmECitrine 2xG(4)S linker	This study
pKS 1605	pFa6a 3xmECitrine-HBH-HphMX6	This study
pKS 1606	pJet Rax2Δ21-120 -3mECitrine	This study
pKS 1607	pJet Rax2Δ121-220 -3mECitrine	This study
pKS 1608	pJet Rax2Δ221-320 -3mECitrine	This study
pKS 1609	pJet Rax2Δ421-520 -3mECitrine	This study
pKS 1610	pJet 1xmCherry 2xG(4)S linker	This study
pKS 1662	pJet HBH-1xmECitrine	This study
pKS 1663	pJet 1xmECitrine-HBH	This study
pKS 1664	pFa6a with HBH-1xmECitrine-HphMX6	This study
pKS 1665	pFa6a with 1xmECitrine-HBH-HphMX6	This study
pKS 1710	pFA6-1xmECitirine-avitag-6xHis-KanMX6	This study

2.21 Primer list

Identifier	Sequence
oKS 2828	AGATTATTCATTGGTTCTTTTCGGAGCATGTCGAAACGTTGCACGACT ATTCGAATTTTTTAAAAGAATTAAAGACCCAGCGGATCCCCGGGTTAA TTAA
oKS 2934	AGGACCGAAAGATTGAATCGTA
oKS 2829	CCTTCCACTGATCATATCAGTATTTAAACTTCAAAATTTGTATGTTTTA AGATAGCCTCCTTAGTACTGTGCATAATCATGAATTCGAGCTCGTTTA AAC
oKS 2868	CTTTATTCCAAATGCTGTTAGAACC
oKS 2979	CACGTTACGTTGTAATTATCAGTCTCGGGATAAGCATTGGAGTTATGT TTTTGATAATGTCGGGATCTATAGTTGTTGAGCGGATCCCCGGGTTA ATTAA
oKS 2980	TCGGGATAAGCATTGGAGTTATGTTTTTGATAATGTCGGGATCTATAG TTGTTGAGATTATTCATTGGTTCTTTTCGGAGCGGATCCCCGGGTTAA TTAA
oKS 2981	TGATAATGTCGGGATCTATAGTTGTTGAGATTATTCATTGGTTCTTTTC GGAGCATGTCGAAACGTTGCACGACTATTCGCGGATCCCCGGGTTA ATTAA
oKS 3036	TTATGTTTTTGATAATGTCGGGATCTATAGTTGTTGAGATTATTC
oKS 3037	GCATTGGAGTTATGTTTTTGATAATGTCGGGATCTATAGTTGTTG
oKS 3047	AAATGTTAGCGTGATTTATATTTTTTTTC
oKS 3287	AAACTTATGGCCGTTGACATCTCCGTCTAATTCGACCAATATAGGGA CGACTCCAGTGAACAATTCCTCGCCTTTTGAAACGAATTCGAGCTCG TTTAAAC
oKS 3319	GCGGCCGCTTACTCAAGTCCTGGTTTACTAG
oKS 3320	GCGGCCGCAAACTTATGGCCGTTGACATC
oKS 3321	AATCCGCTGTATTTTTTTTGATACACATTAAAATCGGATTAATTTAGGA ACTCTAGTACTTGTCTTGAGGTGGTTGTCTGAATGGTTTCAAAAGGC GAGGAAGA
oKS 3322	ATAAATGTAAAAGTTGTATAAACTCAACGGTGGAAGATTTTTTTTGGTT AAAACTTCTGAAACTCTCGGGGCGGAAGCCATAGATCCACCACCTCC AGAACCTC
oKS 3323	GTGTTAATTAATATGGTTTCAAAAGGCGAGGAA
oKS 3324	AGATCCACCACCTCCAGAACCTCCTCCACCTCGCGACTTGTATAACT CATCCATGCCACGGCGCGCCAGATCTCGTT
oKS 3325	TGGATGAGTTATACAAGGGTGG
oKS 3326	AGATCTGGCGCGCCTTAATT
oKS 3327	GCGGCCGCAAATTTGAAGCTTAATAATGATAG
oKS 3328	GCGGCCGCCTCGTGTCTTATAGTTACCATCG
oKS 3329	GCACCTTTGTACAATTCGTCC
oKS 3330	TCAAGGTAAGCTTACCATAGG
oKS 3331	GTATCCCAATAAGGCAAGAACAGG

oKS 3332	TAGACCTCTTATATGCTCTCG
oKS 3333	GGCGCGCCAGATCCACCACCTCCAGAACCTCCTCCACCTCGCGACT TGTATAACTCATCCATGCCAC
oKS 3347	AATTTTATTCATTCTATATCG
oKS 3348	TACTTTTACATTGCGATCGGG
oKS 3349	ATCTCCCTCAAACTTAACTTCG
oKS 3350	TCTGTTAACCAAGGTATCTCC
oKS 3402	TTTAGAAGTGGCGCGCCTTAAACGCCGATCTTGATTAGACC
oKS 3403	CGTTCATCATCACCACCATCATTAATGGCGCGCCACTTCTAAA
oKS 3404	GGCGCGCCACTTCTAAATAAGC
oKS 3405	ATTTGAAACTAAAGCGGAACCAATCCGCTGTATTTTTTTTGATACACA TTAAAATCGGATTAATTTAGGAACTCTAGTACTTGTCTTGAGGTGGTT GTCTGAATGGTTTCAAAAGGCGAGGAATTG
oKS 3406	ATGGCAATTTATTCCTCCTT
oKS 3407	ACATTTTTATAACGTTAAAGG
oKS 3408	AGACTTCTATTTCTCCAAAGG
oKS 3409	AATATGTGTCTCTTTATTCTGG
oKS 3410	CAATAAAGCTTAATTATATTGCG
oKS 3411	GAAGATATAGCCTATCCGTTTGC
oKS 3412	TGAAGTGCAGTCCATTTTGTGG
oKS 3413	CTATTGTGTCAATAAGTCTTGC
oKS 3414	GCCACCTATGGTAAGCTTACC
oKS 3415	GATGAACGCCGATCTTGATTAGACC
oKS 3416	ACAGATTCTCGCTGGCGGTTGTGGG
oKS 3417	ATGGTTTCAAAAGGCGAGGAATTG
oKS 3418	AGATCCACCACCTCCAGAACCTCCTCCACCTTTGTACAATTCGTCCAT GCC
oKS 3419	AGATCCACCACCTCCAGAACCTCCTCCACCTTTGTAAAGTTCGTCCA TACCGCCG
oKS 3420	GGTGGAGGAGGTTCTGGAGGTGGTGGATCTATGGTTTCAAAAGGCG AGG
oKS 3421	TATGCTACCACCACAGCTCGTTCAACCTATTTTAGATTGCAAGGAACA TCAAAGACAAGACGAGTTGCGTCTGTTTGAAGACGTCGAAACTTATC TTGGTGGAGGAGGTTCTGGAGGTGG
oKS 3422	ACCAATAATAAATCTCCCTGTGCAAGTTAAAGGATTGAGGTTGTGCTT AAATTTGTGGTTGAGAAAGCGATAGTAGGCGGGTTTGAGAAGGAAAT TGAGAGATCCACCACCTCCAGAACC
oKS 3423	TGGCCCGCAAATCGCAAAGC
oKS 3424	ACCTAAGAAGGAAACATCGG

oKS 3425	AAAGCTGTGGTTTTCCAGG
oKS 3426	TTGCTTGAACTGAATGGAC
oKS 3427	GCTGCTAGTAAGCTACGAGG
oKS 3428	CCTGGTTGTAGCTATCATCAAAG
oKS 3429	CATGTCCGGGTATCTTTTCG
oKS 3430	TGGAAACTCAATAATTGAGG
oKS 3431	ACAACAATATCTTCTTTGGTGG
oKS 3432	TAAAATCCAAGTTTCTCCATGC
oKS 3433	GTCCTTTCTGGCTTAATTG
oKS 3434	AAGAATCATCCACTATAACAC
oKS 3435	TGTAATTATCAGTCTCGGG
oKS 3436	GATTATCGAATCGTTGATTGG
oKS 3437	TTTAGAAGTGGCGCGCCATTAATGATGGTGGTGATGATGAACG
oKS 3453	AAATATTCAAAGTTTAACGCAGGAATCAACGGTTATCAGTAAAGAGCA AGTTAAAATGTTTACTCAAATTATTATCGAAAAATATTTCAATCCAGCA TCTGGTGGAGGAGGTTCTGGAGG
oKS 3454	TTCGACGTCTTCAAACAGACGCAACTCGTCTTGTCTTTGATGTTCCTT GCAATCTAAAATAGGTTGAACGAGCTGTGGTGGTAGCATAACTTCAT GTGGAGATCCACCACCTCCAGAACC
oKS 3455	TATCGAAAAATATTTCAATCCAGCATCTCCACATGAAGTTATGCTACC ACCACAGCTCGTTCAACCTATTTTAGATTGCAAGGAACATCAAAGACA AGACGGTGGAGGAGGTTCTGGAGG
oKS 3456	GAGGTTGTGCTTAAATTTGTGGTTGAGAAAGCGATAGTAGGCGGGTT TGAGAAGGAAATTGAGAAGATAAGTTTCGACGTCTTCAAACAGACGC AACTCAGATCCACCACCTCCAGAACC
oKS 3457	AAAATATTTCAATCCAGCATCTCCACATGAAGTTATGCTACCACCACA GCTCGTTCAACCTATTTTAGATTGCAAGGAACATCAAAGACAAGACG AGTTGGGTGGAGGAGGTTCTGGAGG
oKS 3458	AGGATTGAGGTTGTGCTTAAATTTGTGGTTGAGAAAGCGATAGTAGG CGGGTTTGAGAAGGAAATTGAGAAGATAAGTTTCGACGTCTTCAAAC AGACGAGATCCACCACCTCCAGAACC
oKS 3471	GTAGACACATAACCAATAATAAATCTCC
oKS 3472	AGATCCACCACCTCCAGAACCTCCTCCACCCTTGTATAACTCATCCAT TCCTAAGG
oKS 3473	ACTGAATCCACTCGTTGATATGGCG
oKS 3474	TCCACTCGTTGATATGGCGTATCCC
oKS 3507	TTAACGCAGGAATCAACGGTTATCAGTAAAGAGCAAGTTAAAATGTTT ACTCAAATTATTATCGAAAAATATTTCAATCCAGCATCTGGAGGGTCG TCTGGTGGCTCGGCTGGAGGGTCG
oKS 3508	TTTCAATCCAGCATCTCCACATGAAGTTATGCTACCACCACAGCTCGT TCAACCTATTTTAGATTGCAAGGAACATCAAAGACAAGACGGAGGGT CGTCTGGTGGCTCGGCTGGAGGGTC
oKS 3531	CGGATCCCCGGGTTAATTAACATG

oKS 3532	GCTTATTTAGAAGTGGCGCGCCTTA
oKS 3533	GTATGCTCTATTGCATTCC
oKS 3534	TTTACGCGGTTTAGGTCAGC
oKS 3535	TCCTTTAACTTGCACAGGG
oKS 3536	AAAGAGAAATTTGTGAAGC
oKS 3537	AGGACCGAAAGATTGAATCG
oKS 3623	ATCCGCTGTATTTTTTTTGATACACATTAAAATCGGATTAATTTAGGAACTCTAGTACTTGTCTTGAGGTGGTTGTCTGAGAATTCGAGCTCGTTTAAAC
oKS 3624	TAAATGTAAAAGTTGTATAAACTCAACGGTGGAAGATTTTTTTTGGTTAAAACTTCTGAAACTCTCGGGGCGGAAGCCATTTTGTATAGTTCATCCATGC
oKS 3633	GGAGGGTCGTCTGGTGGCTCGGCTGGAGGGTCGAACAGTAAAGGAGAAGAAC
oKS 3634	AGATCCACCACCTCCAGAACCTCCTCCACCTTTGTATAGTTCATCCATGC
oKS 3641	TGATAATGTCGGGATCTATAGTTGTTGAGATTATTCATTGGTTCTTTTCGGAGCATGTCGAAACGTTGCACGACTATTCGtaaCGGATCCCCGGGTTAATTAA
oKS 3642	TTATGTTTTTGATAATGTCGGGATCTATAGTTGTTGAGATTATTCATTGGTTCTTTTCGGAGCATGTCGAAACGTTGCACtaaCGGATCCCCGGGTTAATTAA
oKS 3643	TTGGAGTTATGTTTTTGATAATGTCGGGATCTATAGTTGTTGAGATTATTCATTGGTTCTTTTCGGAGCATGTCGAAACGtaaCGGATCCCCGGGTTAATTAA
oKS 3644	TCGGGATAAGCATTGGAGTTATGTTTTTGATAATGTCGGGATCTATAGTTGTTGAGATTATTCATTGGTTCTTTTCGGAGtaaCGGATCCCCGGGTTAATTAA
oKS 3645	CACGTTACGTTGTAATTATCAGTCTCGGGATAAGCATTGGAGTTATGTTTTTGATAATGTCGGGATCTATAGTTGTTGAGtaaCGGATCCCCGGGTTAATTAA
oKS 3727	CGGATCCCCGGGTTAATTAAC
oKS 3728	TCGCTTATTTAGAAGTGGCGC
oKS 3729	GCGCCACTTCTAAATAAGCGA
oKS 3730	GTTAATTAACCCGGGGATCCG
oKS 3787	TTGCTTAGGTTATTAAATGCAAATGG
oKS 3788	AGTTTTTGTAAATGCTAAAAGAATGG
oKS 3789	ATCGTTAAGGCCACCACCATG
oKS 3790	TGATCAGCTAATTGAACAGAGC
oKS 3867	TCATCTACTTATTACCTATAGTTATTTGGACAACTGAAAATATTTTGCGTTTTTTCTAATATTGTTTATTATTGTTAAAACCGGATCCCCGGGTTAATTAA
oKS 3868	ATACTTATATAAGCAATCTGTTCATATTCAAATAATGTGTAGTTAGATAGACAATTGCAATTGATCGTTTCACCTAACTAGAATTCGAGCTCGTTTAAAC

oKS 3869	ATTGCAACCGCAATTTATCTTT
oKS 3870	AGCTAATTTGGTCGTTTTTGGA
oKS 3889	ATTGGAGAATTATCAATCGTGTAGTTGCATGCCTCGGCGTAGCTATC ACATTCCTATTTATTGGTCTCGGCGTTTCTGGT - CGGATCCCCGGGTTAATTAA
oKS 3900	TCATCTACTTATTACCTATAGTTATTTGGACAACTGAAAATATTTTGCG TTTTTCTAATATTGTTTATTATTGTTAAAACGAATTCGAGCTCGTTTAA AC
oKS 3901	TGTCTACCGTCTTCTTCACCCAAACGGTAAGCGCTTTCATCTCTGCGT TGAGCATGTCCACCGAGATTTTCAAAAGTCATTTTGTATAGTTCATCC ATGC
oKS 3902	ATTGCAACCGCAATTTATCTTT
oKS 3903	GGACGATCGGTTTTTACAGAAG
oKS 3931	TAATGCGCTTTAGAAGCATATCATCTACTTATTACCTATAGTTATTTGG ACAACTGAAAATATTTTGCGTTTTTCTAATATTGTTTATTATTGTTAAAA CCGGATCCCCGGGTTAATTAA
oKS 3932	GACGTTTCTTCCTTGAAGACTCTCCTTTCTGTCTACCGTCTTCTTCAC CCAAACGGTAAGCGCTTTCATCTCTGCGTTGAGCATGTCCACCGAGA TTTTCAAAAGTCATGAATTCGAGCTCGTTTAAAC
oKS 3934	GACGTTTCTTCCTTGAAGACTCTCCTTTCTGTCTACCGTCTTCTTCAC CCAAACGGTAAGCGCTTTCATCTCTGCGTTGAGCATGTCCACCGAGA TTTTCAAAAGTCATATTTGTATAGTTCATCCATGC
oKS 3935	CTGCGTTGAGCATGTCCACCGAGA
oKS 3936	CACCCAAACGGTAAGCGCTTTCAT
oKS 3945	TAATGCGCTTTAGAAGCATATCATCTACTTATTACCTATAGTTATTTGG ACAACTGAAAATATTTTGCGTTTTTCTAATATTGTTTATTATTGTTAAAA CAACAGTAAAGGAGAAGAAC
oKS 3946	ACTCTCCTTTCTGTCTACCGTCTTCTTCACCCAAACGGTAAGCGCTTT CATCTCTGCGTTGAGCATGTCCACCGAGATTTTCAAAAGTCATTTTGT ATAGTTCATCCATGC
oKS 3947	TAATGCGCTTTAGAAGCATATCATCTACTTATTACCTATAGTTATTTGG ACAACTGAAAATATTTTGCGTTTTTCTAATATTGTTTATTATTGTTAAAA CATGGTTTCAAAAGGCGAGGAAGAC
oKS 3948	ACTCTCCTTTCTGTCTACCGTCTTCTTCACCCAAACGGTAAGCGCTTT CATCTCTGCGTTGAGCATGTCCACCGAGATTTTCAAAAGTCATTTTGT AAAGTTCGTCCATACC
oKS 3954	AGCGCTTACCGTTTGGGTGA
oKS 3955	ACCAAAATGAAACGTTCGATGG
oKS 3956	TGCGTGTAAAACCAAACCAGCA
oKS 3960	GGTCTCGTTGGCCTCGCTAA
oKS 3961	GCGATACCCTTCAAAAAGAAACGA
oKS 3962	CACGTCCATCCCCGAAACTC
oKS 3963	CAAGAGCTAAAGGGCTTTCTTGTTCA
oKS 3964	TTCTGTCTACCGTCTTCTTCACCCAAACGGTAAGCGCTTTCATCTCTG CGTTGAGCATGTCCACCGAGATTTTCAAAAGTCATGATTTAACAAAGC GACTATA

oKS 3988	GGGAAGGAACCTATGGCGTTG
oKS 3989	AGCTGTGCTAGGAACTCCCTCAGA
oKS 3990	TGTGCGGAATTTTGGCGTTA
oKS 3991	ACCCCGATGCTGCAAACTGT
oKS 3992	GTCCCCGGAGGAAATTCGTT
oKS 3993	GGGGGCGTTGTCCACTTTC
oKS 4046	ACTCTCCTTTCTGTCTACCGTCTTCTTCACCCAAACGGTAAGCGCTTT CATCTCTGCGTTGAGCATGTCCACCGAGATTTTCAAAAGTCATGATC CACCACCTCCAGAACCTC

2.22 Strain list

Identifier	Genotype	Strain Construction	Source
KS 12	cdc25-22 leu1-32 h-		Sawin lab
KS 13	cdc25-22 leu1-32 h+		Sawin lab
KS 136	h- tea1Δ::ura4+ ade6-M210 ura4-D18		Sawin lab
KS 137	h+ tea1Δ::ura4+ ade6-M210 ura4-D18		Sawin lab
KS 515	ade6-M216 ura4-D18 leu1-32 h+		Sawin lab
KS 516	ade6-M210 ura4-D18 leu1-32 h-		Sawin lab
KS 7305	h- adh13-CRIB-3xmCitrine:LEU2 ade6-M210 ura4-D18 leu1-32		Sawin lab
KS 7306	h- adh31-CRIB-3xmCitrine:LEU2 ade6-M210 ura4-D18 leu1-32		Sawin lab
KS 7812	h- rax1Δ::KanMX6 CRIB-3xmCitrine:leu2 ade6-M210 Ura4-D18 leu1-32		Sawin lab
KS 7867	h- rax2-3xmCitrine:hphMX6 leu1-32 Ura4-D18 ade6-M216		Sawin lab
KS 7908	h+ rax1Δ::KanMX6adh13-CRIB-3xmCitrine:LEU2 leu1-32 ura4-D18 ade6-M210		Sawin lab
KS 7950	h- rax2Δ::KanMX6 adh13-CRIB-3xmCitrine:LEU2 leu1-32 ura4-D18 ade6-M210		Sawin lab
KS 7951	h+ rax2Δ::KanMX6 tea1Δ::ura4+ adh13-CRIB-3xmCitrine:LEU2 leu1-32 ura4-D18 ade6-M210		Sawin lab
KS 8068	h- rax2-mEcitrine:KanMX6 ade6-M216 ura4-D18 leu1-32		Sawin lab
KS 8069	h+ rax1-3xmcitrine:hphMX6 ade6-M216 ura4-D18 leu1-32		Sawin lab
KS 8072	h+ rpl42.sP56Q leu1.32 ura4.D18		Hagan Lab
KS 8082	h+ rax2Δ::KanMX6 rax1Δ::KanMX6 adh13-CRIB-3xmCitrine:LEU2 leu1-32 ura4-D18 ade6-M210		Sawin lab
KS 8106	h- tea1Δ::Ura4+ CRIB-3xmCitrine:LEU2 ade6-M210 ura4-D18 leu1-32		Sawin lab
KS 8179	h- Pbgs4+::RFP-bgs4+:leu1+ bgs4Δ::ura4+ leu1-32 ura4-D18 his3-D1		J.C Ribas
KS 8180	h+ Pbgs4+::RFP-bgs4+:leu1+ bgs4Δ::ura4+ leu1-32 ura4-D18 his3-D1		J.C Ribas
KS 8196	h+ Pbgs4+::Cher-12A-bgs4+:leu1+ bgs4Δ::ura4+ leu1-32 ura4-D18 his3-D1		J. C. Ribas
KS 8197	h+ tea1Δ::ura4+ rax1Δ::KanMX6adh13-CRIB-3xmCitrine:LEU2 leu1-32 ura4-D18 ade6-M210		Sawin lab

KS 8460	h+ rpl42NatMX6:Rax1 rpl42.sP56Q leu1.32 ura4.D18	pKS 1412 amplified with oKS 2830 and 3312 and transformation into KS 8072	This study
KS 8461	h+rax2∆:rpl42NatMX6-3mCitrine rpl42.sP56Q leu1.32 ura4.D18	pKS 1412 amplified with oKS 2830 and 3312 and transformation into KS 8072	This study
KS 8666	h+ Rax2-3xmCitrine-HTB::hphMX6 ade6-M216 ura4-D18 leu1-32	pKS 1586 amplified with oKS 2834 and oKS 3287, transformed into KS 515	This study
KS 8668	h+ Rax2-3xmCitrine-HBH::hphMX6 ade6-M216 ura4-D18 leu1-32	pKS 1605 amplified with oKS 2828 and oKS 2829, transformed into KS 515	This study
KS 8669	h+ 1xmECitrine::Rax1 rpl42.sP56Q leu1.32 ura4.D18	pKS 1412 amplified with oKS 2830 and oKS 3312 transformed into KS 8460	This study
KS 8672	h+ Rax2-3xmCitrine-HTB::hphMX6 CRIB-3xmECitrine:LEU2 ade6-M216 ura4-D18 leu1-32	KS 8666* KS 8106	This study
KS 8673	h- Rax2-3xmCitrine-HTB::hphMX6 tea1∆::Ura4+ CRIB-3xmCitrine:LEU2 ade6-M216 ura4-D18 leu1-32	KS 8666* KS 8106	This study

KS 8722	h+ rax2ID1[61-720]::3xmCitrine:hphMX6 rpl42sP56Q leu1-32 ura4-D18	pKS1606 amplified with oKS 3327 and 3328 transformed into KS 8461	This study
KS 8723	h+ rax2ID2[721-1380]::3xmCitrine:hphMX6 rpl42sP56Q leu1-32 ura4-D18	pKS1607 amplified with oKS 3327 and 3328 transformed into KS 8460	This study
KS 8724	h+ rax2ID3[1381-2040]::3xmCitrine:hphMX6 rpl42sP56Q leu1-32 ura4-D18	pKS1608 amplified with oKS 3327 and 3328 transformed into KS 8460	This study
KS 8725	h+ rax2ID5[2719-3321]::3xmCitrine:hphMX6 rpl42sP56Q leu1-32 ura4-D18	pKS1609 amplified with oKS 3327 and 3328 transformed into KS 8460	This study
KS 8777	h+ Rax2-HTB::KanMX6 ade6-M216 ura4-D18 leu1-32	KS 515	This study
KS 8784	h+ Rax2-HTB::KanMX6 tea1∆::Ura4+ CRIB-3xmCitrine:LEU2 ura4-D18 leu1-32 ade6-M216	KS 8777 * KS 8106	This study
KS 8785	h- rax2-mEcitrine:KanMX6 tea1∆::Ura4+ adh13-CRIB-3xmCitrine:LEU2 leu1-32 ura4-D18 ade6-M210	KS 8068 * KS 8081	This study
KS 8827	h+ Rax2-HBH:hphMX6 ade6-M216 ura4-D18 leu1-32	515	This study
KS 8838	h- Rax2-HBH::hphMX6 tea1∆::Ura4+ CRIB-3xmECitrine:LEU2 ura4-D18 leu1-32 ade6-M216	8827*8106	This study
KS 8916	h+ Rax1∆::kanMX6 ade6-M210 ura4-D18 leu1-32	KS 516	This study
KS 8947	h- Rax2-HBH-1xmECitrine::hphMX6 ade6-M216 ura4-D18 leu1-32	KS 516	This study
KS 8948	h- Rax2 -1xmECitrine-HBH::hphMX6 ade6-M216 ura4-D18 leu1-32	KS 516	This study
KS 8953	h+ Rax2 -1xmECitrine-HBH::hphMX6 tea1∆::Ura4+ adh13-CRIB-3xmCitrine:LEU2 leu1-32 ura4-D18 ade6-M216	KS 8948* KS 8081	This study

KS 8974	h+ Rax2 –HBH-1xmECitrine::hphMX6 tea1∆::Ura4+ adh13-CRIB-3xmECitrine:LEU2 leu1-32 ura4-D18 ade6-M210	KS 8081* KS 8947	This study
KS 8985	h+ scs2∆::ura4+ scs22∆::ura4+ ura4-D18 leu1-32 ade6		Olifrenko lab
KS 8995	h- Pbip1-mCherry-ADEL::ura4+ ura4-294 ade6M210		Olifrenko lab
KS 8996	h- scs2∆::ura4+ scs22∆::ura4+ Pbip1-mCherry-ADEL::ura4+ ura4-294 ade6		Olifrenko lab
KS 9014	h- slx8-29:KanMX6 pREP42(adh)-BirA:ura4 integrated at ars1		Boddy lab
KS 9043	h- pREP42(adh)-BirA:ura4 integrated at ars1	KS 9014* KS 515	This study
KS 9096	h+ Rax2-HTB::Kan pREP42(adh)-BirA:ura4 integrated at ars1 ade6-M216 ura4-D18 leu1-32	KS 9043* KS 8777	This study
KS 9126	h- Rax2-HBH:hphMX6 pREP42(adh)-BirA:ura4 integrated at ars1 ade6-M210 ura4-D18 leu1-32	KS 9043 * KS 8827	This study
KS 9127	h- Rax1-13Myc tea1∆::Ura4+ CRIB-3xmCitrine:LEU2 ade6-M210 ura4-D18 leu1-32	pKS 1413 amplified with oKS 2826 and 2827 and tranformed into KS 8106	This study
KS 9128	h+ Rax1-13Myc ade6-M216 ura4-D18 leu1-32	pKS 1413 amplified with oKS 2826 and 2827 and tranformed into KS 515	This study
KS 9129	h+ kanMX6-nmt41:mECitrine-Rax1 ade6-M216 ura4-D18 leu1-32	pKS 1332 amplified with oKS 3623 and oKS 3624 and transformed into KS 515	This study
KS 9130	h- Rax2∆9::kanMX6 tea1∆::Ura4+ CRIB-3xmCitrine:LEU2 ade6-M210 ura4-D18 leu1-32	pKS 108 amplified with oks 3641 and 2982 and transformed into KS 8106	This study

KS 9131	h- Rax2Δ12::kanMX6 tea1Δ::Ura4+ CRIB-3xmCitrine:LEU2 ade6-M210 ura4-D18 leu1-32	pKS 108 amplified with oks 3642 and 2982 and transformed into KS 8106	This study
KS 9132	h- Rax2Δ15::kanMX6 tea1Δ::Ura4+ CRIB-3xmCitrine:LEU2 ade6-M210 ura4-D18 leu1-32	pKS 108 amplified with oks 3643 and 2982 and transformed into KS 8106	This study
KS 9133	h- Rax2Δ18::kanMX6 tea1Δ::Ura4+ CRIB-3xmCitrine:LEU2 ade6-M210 ura4-D18 leu1-32	pKS 108 amplified with oks 3644 and 2982 and transformed into KS 8106	This study
KS 9134	h- Rax2Δ26::kanMX6 tea1Δ::Ura4+ CRIB-3xmCitrine:LEU2 ade6-M210 ura4-D18 leu1-32	pKS 108 amplified with oks 3645 and 2982 and transformed into KS 810**6**	This study
KS 9135	h- Tea1Δ::hphMX6 Pbgs4+::Cher-12A-bgs4+:leu1+ bgs4Δ::ura4+ leu1-32 ura4-D18 ade6-M210	KS 8828 * KS 8335	This study
KS 9136	h+ kanMX6::nmt81-2xmcherry-Rax1 ade6-M216 ura4-D18 leu1-32	KS 515	This study
kS 9137	h- rax2Δ::KanMX6 leu1-32 ura4-D18 ade6-M210	KS 7951* KS 516	This study
KS 9194	h+ kanMX6-nmt41-YFP-Rax1 rax2Δ::KanMX6 ura4-D18 leu1-32 ade6-M21?	KS 9129* KS 9137	This study
KS 9357	h- Rax2-HTB::KanMX6 ade6-M216 ura4-D18 leu1-32	KS 8777* KS 516	This study
KS 9383	h+ Rax2-Citrine-avitag-his:KanMX6 tea1Δ::Ura4+ CRIB-3xmECitrine:LEU2 ade6-M210 ura4-D18 leu1-32	KS 9378* KS 8106	This study
KS 9461	h- rax2-mEcitrine:KanMX6 tea1::ura4+ Pbgs4+::Cher-12A-bgs4+:leu1+ bgs4Δ::ura4+ ade6-M210 ura4-D18 leu1-32	KS 9473* KS 8335	This study
KS 9462	h+ Rax2-Citrine-avitag-his:KanMX6 pREP42(adh)-BirA:ura4 integrated at ars1b KanMX6 ade6-M216 ura4-D18 leu1-32	KS 9043* KS 9378	This study
KS 9473	h- rax2-mEcitrine:KanMX6 tea1::ura4+ ade6-M210 ura4-D18 leu1-32	KS 137* KS 8068	This study

KS 9552	h+ Rax2Δ9mECitrine::KanMX6 ade6-M216 ura4-D18 leu1-32	pKS 1330 amplified with oks 3641 and 2929 and transformed into KS 515	This study
KS 9553	h+ Rax2Δ12mECitrine::KanMX6 ade6-M216 ura4-D18 leu1-32	pKS 1330 amplified with oks 3642 and 2929 and transformed into KS 515	This study
KS 9554	h+ Rax2Δ15mECitrine::KanMX6 ade6-M216 ura4-D18 leu1-32	pKS 1330 amplified with oks 3643 and 2929 and transformed into KS 515	This study
KS 9555	h+ Rax2Δ18mECitrine::KanMX6 ade6-M216 ura4-D18 leu1-32	pKS 1330 amplified with oks 3644 and 2929 and transformed into KS 515	This study
KS 9556	h+ Rax2Δ26mECitrine::KanMX6 ade6-M216 ura4-D18 leu1-32	pKS 1330 amplified with oks 3645 and 2929 and transformed into KS 515	This study
KS 9587	h+ lrx1Δ::NatMX6 tea1Δ::Ura4+ adh13-CRIB-3xmCitrine:LEU2 leu1-32 ura4-D18 ade6-M210	pKS 113 amplified with oKS 3867 and 3868 and transformed into KS 8081	This study
KS 9588	h+ lrx1Δ::NatMX6 adh13-CRIB-3xmECitrine:LEU2 leu1-32 ura4-D18 ade6-M210	KS 9587 * KS 8068	This study
KS 9589	h+ SPBC405.02cΔ::Nat MX6 rax2-mEcitrine:KanMX6 ade6-M210 ura4-D18 leu1-32	KS 9587* KS 8068	This study

KS 9669	h+kanMX6 nmt41-citrine-lrx1 ade6-M216 ura4-D18 leu1-32	pKS 1332 amplified with oKS 3900 and 3901 and transformed into KS 515	This study
KS 9691	h+ SPBC405.02c∆::NatMX6 kanMX6-nmt41-YFP-Rax1 ade6-M216 ura4-D18 leu1-32	KS 9588* KS 9129	This study
KS 9701	h- rax2-mEcitrine:KanMX6 Pbgs4+::Cher-12A-bgs4+:leu1+ bgs4∆::ura4+ leu1-32 ura4-D18 ade6+	KS 8068* KS 8335	This study
KS 9732	h+ KanMX6:nmt41lrx1 ade6-M216 ura4-D18 leu1-32	pKS 706 amplified with oKS3900 and 3964 and tranformed into KS 515	This study
KS 9733	h- KanMX6: nmt81lrx1 ade6-M216 ura4-D18 leu1-32	pKS 705 amplified with oKS3900 and 3964 and tranformed into KS 516	This study
KS 9758	h+ rax2-mEcitrine:KanMX6 lrx1∆:Nat-MX6 Pbgs4+::Cher-12A-bgs4+:leu1+ bgs4∆::ura4+ leu1-32 ura4-D18 ade6M210	KS 9701 * KS 9587	This study
KS 9773	h- KanMX6:nmt41lrx1 adh13-CRIB-3xmCitrine:LEU2 ade6-M216 ura4-D18 leu1-32	KS 9732* KS 7305	This study
KS 9774	h- KanMX6:nmt81lrx1 adh13-CRIB-3xmECitrine:LEU2 ade6-M210 ura4-D18 leu1-32	KS 9733* KS 7305	This study
KS 9775	h- KanMX6:nmt41lrx1 rax2-mEcitrine:KanMX6 ade6-M210 ura4-D18 leu1-32	KS 9732* KS 8068	This study
KS 9776	h- KanMX6:nmt81lrx1 rax2-mEcitrine:KanMX6 ade6-M216 ura4-D18 leu1-32	KS 9733* KS 8068	This study
KS 9845	h+ rax2-mEcitrine:KanMX6 Pbgs4+::Cher-12A-bgs4+:leu1+ bgs4∆::ura4+ leu1-32 ura4-D18 ade6+	KS 9701* KS 8335	This study
KS 9847	h+ kan::nmt81-citrine-lrx1ade6-M216 ura4-D18 leu1-32	KS 515	This study
KS 9875	h+ rax2-mEcitrine:KanMX6 rax1∆::KanMX6 ade6-M216 ura4-D18 leu1-32	KS8068* KS 7908	This study
KS 9896	h- rax2-mEcitrine:KanMX6 scs2∆::ura4+ scs22∆::ura4+ leu1-32 ura4-D18 ade6M210	KS 9701* KS 8985	This study
KS 9903	h+ rax1∆::KanMX6 scs2∆::ura4+ scs22∆::ura4+ ura4-D18 leu1-32 ade6M216	KS 8985* KS 7812	This study

KS 9904	h- rax2Δ::KanMX6 rax1Δ::KanMX6 lrx1Δ:Nat adh13-CRIB-3xmCitrine:LEU2 leu1-32 ura4-D18 ade6-M210	KS 9588 * KS 7952	This study
KS 9913	h- rax2Δ::KanMX6 leu1-32 ura4-D18 ade6-M210	KS 7950* KS 515	This study
KS 9914	h+ rax2Δ::KanMX6 leu1-32 ura4-D18 ade6-M210	KS 7950* KS 515	This study
KS 9915	h- 1xmECitrine::Rax1 leu1.32 ura4.D18 ade6-M210	KS 8669* KS 516	This study
KS 9916	h+-1xmECitrine::Rax1 leu1.32 ura4.D18 ade6-M210	KS 8669* KS 516	This study
KS 9917	h- rax2-mEcitrine:KanMX6 rax1Δ::KanMX6 Pbip1-mCherry-ADEL::ura4+ ura4-294 ade6-M210 ura4-D18 leu1-32	KS 9875* KS 8995	This study
KS 9918	h- rax2-mEcitrine:KanMX6 Pbip1-mCherry-ADEL::ura4+ ura4-294 ade6 ade6-M210 ura4-D18 leu1-32	KS 9875* KS 9043	This study
KS 9919	H+ kanMX6::nmt41lrx1 cdc25-22 leu1-32 ade6-M216 ura4-D18 leu1-32	KS 9732* KS 12	This study
KS 9920	h- KanMX6:: nmt81lrx1 cdc25-22 leu1-32 ade6-M216 ura4-D18 leu1-32	KS 9733* KS 13	This study
KS 9921	h- Rax2Δ::KanMX6 rax1Δ::KanMX6 lrx1Δ:NatMX6 tea1Δ::ura4+ adh13-CRIB-3xmECitrine:LEU2 leu1-32 ura4-D18 ade6-M210	KS 9904* KS 7951	This study
KS 9934	h+ 1xmECitrine::Rax1 rax2Δ::KanMX6 leu1-32 ura4-D18 ade6-M210	KS 9914* KS 9915	This study
KS 9936	h+ h- rax2-mEcitrine:KanMX6 rax1Δ::KanMX6 scs2Δ::ura4+ scs22Δ::ura4+ leu1-32 ura4-D18 ade6M216	KS 9896* KS 9903	This study
KS 9937	h- rax2-mEcitrine:KanMX6 lrx1Δ:Nat-MX6 Pbip1-mCherry-ADEL::ura4+ leu1-32 ura4-D18 ade6M210	KS 9758* KS 8996	This study
KS 9938	h+ rax2-mEcitrine:KanMX6 lrx1Δ:Nat-MX6 rax1Δ::KanMX6 leu1-32 ura4-D18 ade6M210	KS 9758* KS 9917	This study
KS 9945	h- rax2-mEcitrine:KanMX6 rax1Δ::KanMX6 scs2Δ::ura4+ scs22Δ::ura4+ Pbip1-mCherry-ADEL::ura4+ ura4-294leu1-32 ura4-D18 ade6M216	KS 9936* KS 8996	This study
KS 9946	h- rax2-mEcitrine:KanMX6 rax1Δ::KanMX6 scs2Δ::ura4+ scs22Δ::ura4+ Pbip1-mCherry-ADEL::ura4+ ura4-294leu1-32 ura4-D18 ade6M216	KS 9936* KS 8996	This study
KS 9955	h+ kanMX6 nmt41-citrine-lrx1 rax2Δ::KanMX6 ade6-M216 ura4-D18 leu1-32	KS 9913* KS 9669	This study
KS 9960	h+ Rax2-Citrine-avitag-his:KanMX6 pREP42(adh)-BirA:ura4 tea1Δ::Ura4+ CRIB-3xmCitrine:LEU2 integrated at ars1b KanMX6 ade6-M216 ura4-D18 leu1-32	KS 9462* KS 8106	This study

KS 9975	h+kanMX6 nmt41-citrine-lrx1 rax1Δ::KanMX6 ade6-M216 ura4-D18 leu1-32	KS 9669* KS 7812	This study

Chapter Three: Characterisation of Rax1 and Rax2

3.1 Introduction

As described in Chapter 1, Rax1 and Rax2 are part of a cell-polarity cue based on "memory" of previous cell tip growth. The involvement of the Rax1-Rax2 cue in directing tip growth is most evident in *tea1Δ* cells. *tea1Δ* cells grow in a monopolar *Syn* pattern, in which one daughter cell grows from its old end and the other daughter grows from its new end. The daughter cell that inherits the cell tip that grew in the monopolar mother cell always grows that (old) end. This suggests that this cell tip is able to "remember" growth from the previous cell cycle, even through an intervening period of non-growth (i.e. during septation). Rax1 and Rax2 are the proteins involved in this memory of previous growth. *tea1Δ rax1Δ* and *tea1Δ rax2Δ* cells are no longer able to remember previous tip growth and as a result grow exclusively from their new ends, in a monopolar *Axial* pattern. This growth is thought to be initiated by a remnant of cytokinesis (S.Ashraf, thesis). It is not currently known how Rax1 and Rax2 localise to the cell tips and how they are retained at the cell tips as part of the memory-based cue.

$Rax1^{Sc}$ and $Rax2^{Sc}$ were first identified in budding yeast, and the Rax1 and Rax2 are their fission yeast homologs. $Rax1^{Sc}$ and $Rax2^{Sc}$ localise to the bud sites and are stably retained for multiple generations (Chen, Hiroko et al. 2000). Bud-site selection proteins $Bud8^{Sc}$ and $Bud9^{Sc}$ co-purify with $Rax1^{Sc}$ (and it is assumed also $Rax2^{Sc}$) (Kang, Angerman et al. 2004). $Bud8^{Sc}$ plays a role in $Rax1^{Sc}$ and $Rax2^{Sc}$ localisation to the bud sites, However, $Bud8^{Sc}$ and $Bud9^{Sc}$ do not have apparent homologs in fission yeast. It is possible that there is a functional homolog of $Bud8^{Sc}$ and $Bud9^{Sc}$ that plays a role in Rax1 and Rax2 localisation to the cell tips. In order to identify novel interactors of Rax1 and Rax2 I used the broad approach of cross-linking and mass spectrometry. First, I needed to generate the tools required for these experiments.

In this chapter, to begin to address the outstanding questions regarding Rax1 and Rax2. I characterised anti-Rax1 and anti-Rax2 antisera. I explain how

the antisera were generated and how I optimised detection of Rax1 and Rax2 I characterise anti-Rax1 and anti-Rax2 antisera to be used to investigate Rax1 and Rax2 protein levels in different genetic backgrounds. The anti-Rax2 antisera was fundamental for the experiments discussed in Chapter 4, where I identify interactors of Rax2.

I describe tagged versions of Rax1 and Rax2 for use in live-cell imaging and protein purification. Rax1^{Sc} and Rax2^{Sc} localise to the bud sites and are stably retained for multiple generations (Chen, Hiroko et al. 2000). Consistent with the budding yeast data, previous work in the Sawin lab determined that Rax2 localises to the cell tips. Additionally, it was shown that Rax2 stably localises to the cell tips, consistent with its role in the growth-memory polarity cue (S.Ashraf, Thesis). These experiments used a Rax2-3mCitrine strain. Because Rax2-3mCitrine is localised to cell tips, it was assumed that this protein was functional. However, early in my experiments, I discovered that Rax2-3mCitrine is largely impaired in function. Therefore, I needed to create different tagged versions of Rax2 and confirm that they were functional before continuing with further experiments.

Rax1^{Sc} and Rax2^{Sc} are co-dependent for their localisation to the bud sites (Kang, Angerman et al. 2004). Rax1 is required for Rax2 localisation to the cell tips (S.Ashraf, thesis). I hypothesise that Rax1 localises to cell tips in fission yeast and may require Rax2 for tip localisation. In this chapter I show that Rax1, which has not been previously imaged in fission yeast, localises to cell tips and that Rax2 is indeed required for this localisation.

There is no published data in budding or fission yeast as to which domains of Rax2 are important for function. Therefore, I made a series of truncations of both the cytoplasmic and extracellular regions of Rax2 to investigate whether there was a specific region essential for Rax2 function. It is possible that the small cytoplasmic region could interact with cytoplasmic proteins that may be important for Rax2 function. I speculate that the extracellular region could participate in interactions with other

transmembrane proteins or with the cell wall. These interactions may be required for the function or stable localisation of Rax2 at the cell tips.

3.2 Generation of anti-Rax1 and anti-Rax2 antibodies

Because there are no commercial antibodies available for Rax1 or Rax2, we generated antibodies in-house. Specific antiserum against a protein of interest has several benefits compared to antibodies that detect an exogenously added tag. Specific antibodies towards a protein of interest allow detection of any changes in expression levels of tagged vs. untagged versions of the protein. They also allow direct comparison, and enable better consistency in western blotting, instead of using different antibodies for different-tagged versions of the protein. Additionally, tagging a protein may impair its function. However, for applications such as live-cell imaging and protein purification, tagging, and some impairment of function, may be unavoidable.

Recombinant Rax1 and Rax2 protein fragments were cloned, expressed, and purified from *E.coli* by other lab members, Harish Thakur and Kristina Stakyte. Because Rax2 is a large protein (130 kDa) it was split into N- and C-terminal fragments to improve expression in bacteria. Transmembrane domains (TMDs) were removed from each construct, because expression was not detectable or was toxic when transmembrane domains were present. Each coding sequence was followed by a C-terminal 6xHis Tag for purification. The final plasmids used for expression in bacteria are listed in Table 3.1.

Table 3.1

Protein	Full length (amino acids)	Fragment Name	Fragment length (amino acids)	Fragment size (kDa)	Plasmid number
Rax1	343	Rax1ΔTMD	1-235	32	pKS1540
Rax2	1155	Rax2NΔsignal peptide	1-11 34-620	72	pKS1541
Rax2	1155	Rax2CΔTMD	623-1104 1128-1155	62	pKS1542

Recombinant proteins were purified from bacterial inclusion bodies, solublised in 180 mM Guanidine, using NiNTA beads in an IMAC column. Each protein was gel-purified, ground to a fine powder using a pestle and mortar on dry ice, lyophilised, and injected into sheep for immunisation.

My role in this work began by testing antisera on Western blots. In my initial experiments I found that the Rax2CΔTMD antiserum was able to successfully detect Rax2 (discussed below). Detection of Rax1 required further experimentation and will be discussed later in this chapter.

3.3 Anti-Rax2 antisera detects Rax2 in cell lysates and membrane-enriched fractions

In my initial experiments testing Rax2CΔTMD anti-sera, I prepared protein from whole-cell extracts (WCE). On Western blots, I detected a band in wild-type (*rax2+*) cells that was not present in *rax2Δ* cells (Figure 3.1). While this suggested that I was specifically detecting Rax2, the signal from wild-type cells was weak, and there were also non-specific bands on the blot. Because Rax2 is a transmembrane protein, I performed a membrane-enrichment step to enrich for Rax2 prior to Western blotting. This protocol was adapted from (Kang, Angerman et al. 2004), who used it to detect $Rax2^{Sc}$. The membrane-enrichment step involved a low-speed spin of the cell lysate to pellet cell debris and then a medium-speed spin to pellet the membrane-enriched fraction (MEF). Membrane-enrichment improved the quality of the anti-Rax2 western blots; it decreased the intensity of non-specific bands present in the whole-cell lysate and increased the intensity of the Rax2 band, due to the increased proportion of Rax2 present in the lane (Figure 3.1).

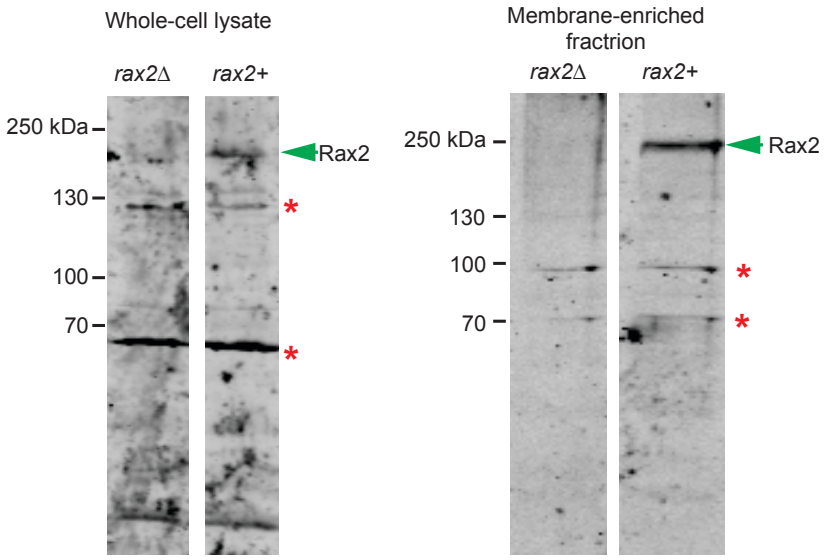

Figure 3.1: Rax2 is enriched in the membrane-enriched fraction compared to whole-cell lysates. Anti-Rax2 western blot. Asterisks adjacent to non-specific bands.

In my initial experiments, the Rax2 band was detected a higher molecular weight (250 kDa) than the calculated weight based on Rax2's constituent amino acids (130 kDa). It is possible that this is because Rax2 is glycosylated. $Rax2^{Sc}$ is highly glycosylated (Kang, Angerman et al. 2004). $Rax2^{Sc}$ from MEFs was detected at a much higher molecular weight when left untreated but was detected at its predicted molecular weight when treated with the deglycosylation enzyme Peptide-N-Glycosidase F (PNGase F). (Kang, Angerman et al. 2004) PNGase F is the most effective enzyme for removal of N-linked oligosaccharides from glycoproteins (Maley, Trimble et al. 1989). PNGase F removes high mannose, hybrid and complex oligosaccharides through cleavage between the innermost GlcNAc and asparagine residues that are connected to the glycoprotein (Maley, Trimble et al. 1989). I treated fission yeast MEFs with PNGase F, and this lead to Rax2 being detected at its predicted molecular weight (Figure 3.2). This confirms that Rax2 is highly glycosylated in fission yeast.

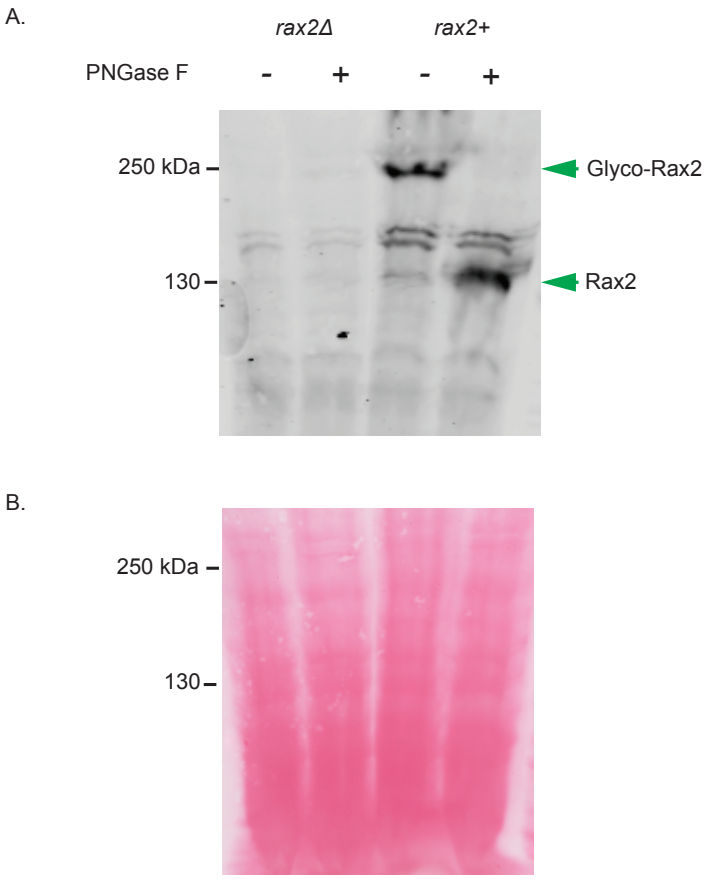

Figure 3.2: Rax2 is highly glycosylated. A. Anti-Rax2 western blot of membrane enriched fractions derived from *rax2+* and *rax2*Δ cells, with and without PNGase F treatment . B. Ponceau S stain of the same region of the blot.

3.4 Anti-Rax1 antisera can detect Rax1 only when Rax1 is overexpressed

Unlike Rax2, Rax1 could not be detected by western blotting of WCE. $Rax1^{Sc}$-Myc could be detected in budding yeast whole cell lysates with anti-Myc antibody (Kang, Angerman et al. 2004). $Rax1^{Sc}$-Myc is fully functional (Kang, Angerman et al. 2004). However, I found that Rax1-Myc was largely impaired in function and therefore I did not perform a western blot of Rax1 in similar conditions to that of $Rax1^{Sc}$-Myc by Kang et al., 2004. To confirm that the anti-Rax1 antiserum was active, I performed western blotting of WCE after spiking in varying amounts of the purified Rax1ΔTMD protein used for immunisation. I easily detected bands of the expected molecular weight for Rax1ΔTMD, confirming that the antibody was active (Figure 3.3). In addition, the purified Rax1ΔTMD was analysed by mass spectrometry; this confirmed that the protein used for immunisation was indeed a Rax1ΔTMD.

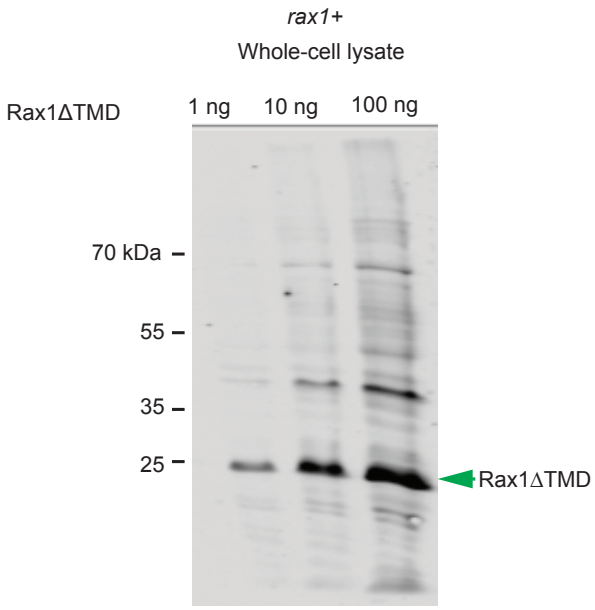

Figure 3.3: Anti-Rax1 antisera can recognise Rax1. Anti-Rax1 western blot of whole cell lysates supplemented with1, 10 and 100 ng of Rax1ΔTMD

As Rax1 contains three transmembrane domains, it was possible that Rax1 was difficult to solubilise from the WCE. Previously, I had used laemmli sample buffer to solubilise Rax1, maybe a different detergent was required. Two buffers with high concentrations of detergent were tested. Buffer 1 was composed of 1 % Triton-X, 0.5 % Tween-20 and 0.5% CHAPS. Buffer 2 was composed of 8 % N-lauryl-sarcosine. These different buffers did not lead to detection of Rax1 with the anti-Rax1 antibody. In order to attempt to increase the specificity of the antibody towards Rax1, the antibody was purified using Rax1ΔTMD protein. This still led to no improvement in Rax1 detection. It was therefore possible that the problem was not related to antibody specificity or Rax1 solubility, but rather to the fact that endogenous levels of Rax1 may be very low.

I therefore overexpressed mECitrine-Rax1 from the thiamine-repressible *nmt41* (no message in thiamine) promoter (Basi, Schmid et al. 1993). In growth media lacking thiamine, the *nmt41* promoter is derepressed, leading to expression of the gene of interest. Upon overexpression, I could now detect *nmt41*:mECitrine-Rax1 by Western blotting of WCE (Figure 3.4). As I am unable to detect endogenous levels of Rax1, I do not know how much I am overexpressing Rax1 compared to endogenous levels.

As described above for Rax2, in order to attempt to improve the detection of overexpressed Rax1, I performed a western blot of the MEF from Rax1-overexpressing cells. Repressed *nmt41*:mECitrine-Rax1 is detected in the MEF but not in the WCE. This suggests that the MEF enriches for Rax1. This also demonstrates low-level expression from the promoter in medium containing thiamine, as expected. The repressed *nmt41* expression levels are approximately 4 % compared to actively expressed *nmt41*(Basi, Schmid et al. 1993) Surprisingly, the amount of detection of Rax1 in the MEF was similar in both presence and absence of thiamine (Figure 3.4). In contrast to the WCE, where *nmt41*:mECitrine-Rax1 repressed was not detected, and *nmt41*:mECitrine-Rax1 actively expressed had a distinct band (Figure 3.4). These data suggest that a large proportion of actively expressed *nmt41*:mECitrine-Rax1 is not in the membrane fraction.

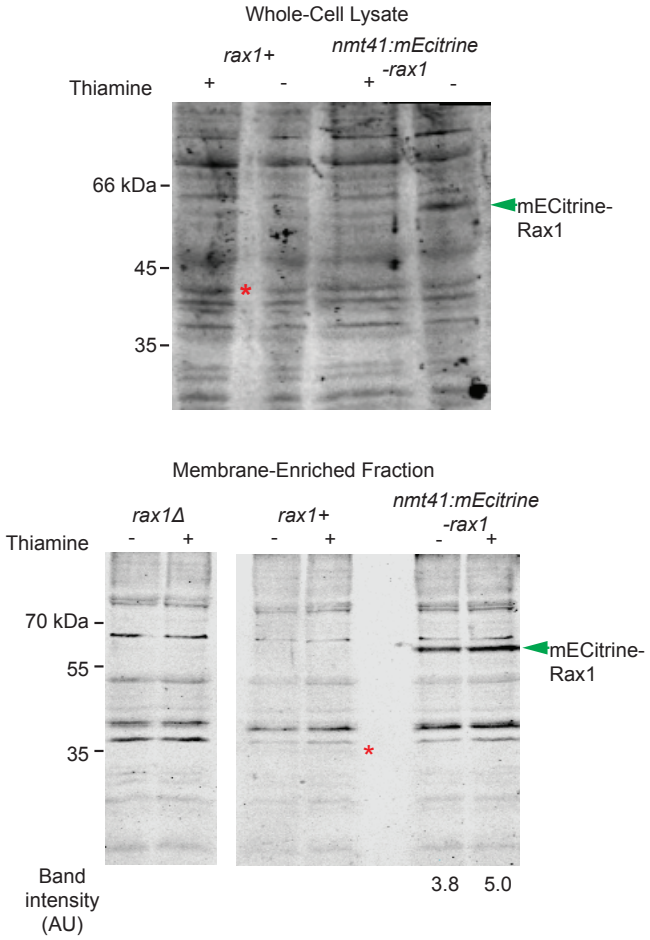

Figure 3.4: Anti-Rax1 can detect overexpressed mECitrine-Rax1 in whole-cell lysate and membrane-enriched fractions. Anti-Rax1 western blot of *rax1*Δ, wild-type and *nmt41:mEcitrine-rax1* cells grown in media with and without thiamine. Red asterisks indicate the expected position of endogenous Rax1. A. Whole-cell lysates show increased mECitrine-Rax1 in media lacking thiamine as expected. B.Membrane-enriched fractions show similar levels of mECitrine-Rax1 in media with and without thiamine.

3.5 Strain construction: Large tags impair Rax2 function; Rax2 function is retained with small tags

I am now able to detect both Rax1 and Rax2 by western blot. In order to further characterise Rax2, I tagged it with a variety of fluorescent and purification tags. For live-cell fluorescence imaging, Rax2 was tagged with mECitrine and 3mCitrine instead of GFP. This is because the 488 nm laser used to excite GFP can also excite molecules such as flavin and lead to cellular autofluorescence (Billinton and Knight 2001). This is particularly important for this project, as a high laser power was required to detect Rax1 and Rax2. The 514nm laser used to excite mECitrine does not lead to autofluorescence. For use in protein purification with harsh denaturing conditions (described in Chapter 4), Rax2 was tagged His-Tev-Biotin (HTB) and His-Biotin-His (HBH) tags. HTB and HBH binding to the purification matrix is unaffected by harsh denaturing conditions because the interaction does not depend on their protein structure (Tagwerker, Flick et al. 2006). I also generated combined fluorescent and purification tags: 3mCitrine-HBH, mECitrine-HBH, HBH-mECitrine and mECitrine-Avitag-His (Avitag is a shortened biotinylation sequence to the one in HBH and HTB). Combined tags would allow me to both image and purify Rax2 from the same strain.

Following tagging of any protein, it is essential to verify that protein function is retained. To be functional, Rax2 must not only localise to cell tips but also recruit growth machinery to cell tips. I imaged the localisation of all fluorescent-tagged versions of Rax2 and assessed their function by analysing cell growth patterns in a *tea1Δ CRIB-3mCitrine* background. *rax2+ tea1Δ CRIB-3mCitrine* cells grow in a *Syn* pattern, but *rax2Δ tea1ΔCRIB-3mCitrine* cells grow in an *Axial* pattern (Figure 1.6). I found that all fluorescently tagged versions of Rax2 were correctly localised to the cell tips (Figure 3.5). However, growth patterns indicated that many of the tags affected Rax2 function (Figure 3.6). Larger tags such as Rax2-3mCitrine-HTB, Rax2-3mCitrine, Rax2-mECitirne-HBH and Rax2-HBH-mECitrine resulted in the majority of daughter pairs growing in an *Axial* fashion in *tea1Δ*, despite the fact that they all correctly localised at the cell tip (Figure

3.6, Figure 3.5). The largest tag 3mCitrine-HTB (95 kDa) had the largest impairment of all of the tags on Rax2 function (Figure 3.6).

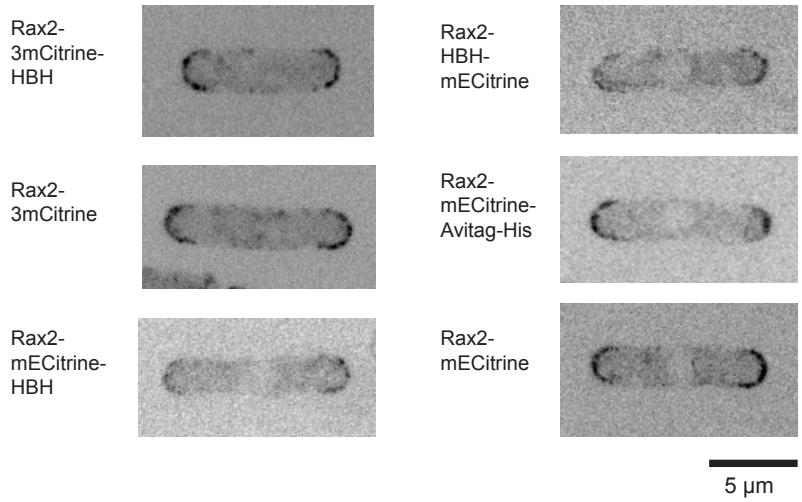

Figure 3.5: All fluorescently tagged versions of Rax2 correctly localise to the cell tips. Localisation of fluroescently tagged Rax2. Images taken using the confocal spinning disk microscope. All image brightness and contrast adjusted independently for optimal image quality. mECitrine-HBH and HBH-mECitrine have a weaker tip signal than mECitrine-Avitag-His and mECitrine alone.

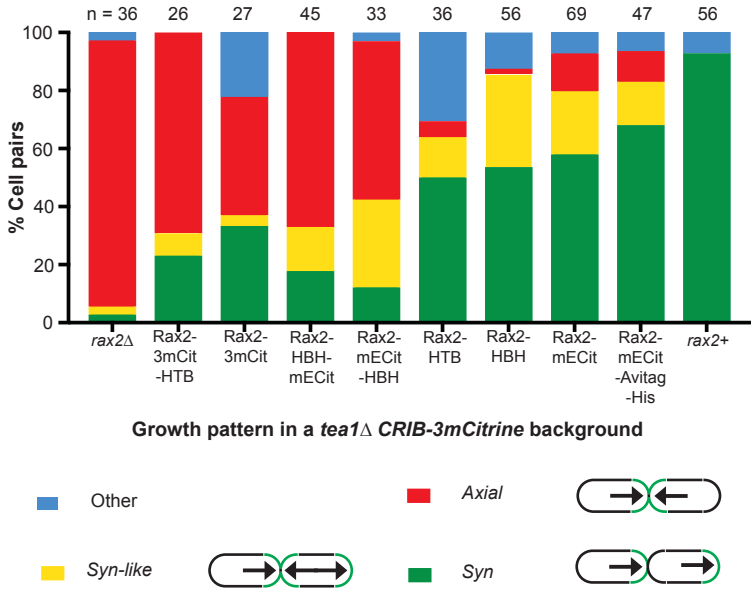

Figure 3.6: Rax2 function is impaired by larger tags. Quantification of growth patterns of daughter-cell pairs. Growth patterns were classed as either *Axial* (new end growth only, in both daughter cells). *Syn* (one daughter grows from its old end; one daughter grows from its new end). *Syn-like* (one daughter grows bipolar; one daughter from its new end). Other (any other growth pattern or any cells which stop growing). 3mCit (3mCitrine), mECit (mECitrine), HTB (His-Tev-Biotin), HBH (His-Biotin-His). n= number of daughter pairs.

During image analysis of Rax2 tagged with smaller tags in a *tea1Δ* background, I noticed an additional prominent growth pattern. In this pattern, the daughter cell that inherits a previously growing end grows at this (old) end but also at its new end, while the other daughter cell grows only from its new end. I called this growth pattern "*Syn-like*", because it suggests that (tagged) Rax2 is partially functional in the growth-memory polarity cue but not sufficiently strong to completely override or outcompete the "default" growth at the new end. Cells with smaller tags on Rax2, such as mECitrine (27 kDa) and HTB (12 kDa), grew mostly in a *Syn* or a *Syn-like* pattern in a *tea1Δ* background, suggesting that Rax2 was partially or mostly functional. Accordingly, very few of these cells showed *Axial* growth (Figure 3.6). Although Rax2-mECitrine and Rax2-HTB had some growth impairment compared to untagged Rax2, I judged the functionality of Rax2-mECitrine and Rax2-HTB to be acceptable for use in future microscopy and biochemical experiments (Figure 3.6, Table 3.2).

While mECitrine-HBH and HBH-mECitrine tags impaired the function of Rax2 and thus were not suitable for future experiments (Figure 3.6, Table 3.2), it would still be desirable to combine an imaging tag with a purification tag. I therefore created a smaller combined mECitrine and biotinylation tag: mECitrine-Avitag-His (CAH). Avitag is the minimum peptide sequence sufficient for biotinylation, although it requires cells to express bacterial biotin ligase BirA for biotinylation (Fairhead and Howarth 2015). The CAH tag is 29 kDa, whereas the mECitrine-HBH and mECitrine-HTB tags are 37 kDa. *rax2-CAH tea1Δ* cells grew in mostly *Syn* and *Syn-like* patterns (Figure 3.6, Table 3.2), suggesting that they retain sufficient Rax2 function to be used in future experiments. Characterisation of the CAH tag for Rax2 purification will be described in Chapter 4.

From this assessment of functionality, I have shown that Rax2-HTB, Rax2-HBH, Rax2-mECitrine and Rax2-CAH are physiologically suitable for use in characterisation of Rax2 using live-cell imaging and/or biochemistry.

Table 3.2

Rax2 Tag	Localised to cell tips?	Functional?	Suitable for use in future experiments?
3mCitrine-HBH	Yes	No	No
3mCitrine	Yes	No	No
HBH-mECitrine	Yes	No	No
mECitrine-HBH	Yes	No	No
HTB	ND*	Partially	Yes
HBH	ND*	Partially	Yes
mECitrine	Yes	Partially	Yes
mECitrine-Avitag-His	Yes	Partially	Yes

* Not determined. Because these tags are not fluorescent, their localisation cannot be determined through live-cell imaging. However, because their function is retained, it is likely they are correctly localised

3.6 Rax2-mECitrine localises to the cell tips and is retained at the cell tips during septation

Introducing the growth marker mCherry-Bgs4 into a *rax2-mEcitrine* strain allowed me to simultaneously image both active growth and Rax2 localisation (Cortes, Carnero et al. 2005). Bgs4 is a component of the (1,3) β-glucan synthase involved in biosynthesis and maintenance of the cell wall during cytokinesis and for polarised growth (Cortes, Carnero et al. 2005). Interestingly, Rax2 and Bgs4 localisation were similar during interphase cell tip extension but different during cell division. During tip extension, both Rax2 and Bgs4 localised to cell tips (Figure 3.7). However, prior to cytokinesis, Bgs4 completely and rapidly relocalised to the cell septum, while the majority of Rax2 remained at cell tips during septation, with only a small proportion localising to the septum (Figure 3.7). This result agrees with previous data from our lab that showed that Rax2-3mCitrine is retained at the cell tips during septation, supporting the model that Rax2 is a stable cue that is inherited by the old-ends of daughter cells following septation (S.Ashraf thesis).

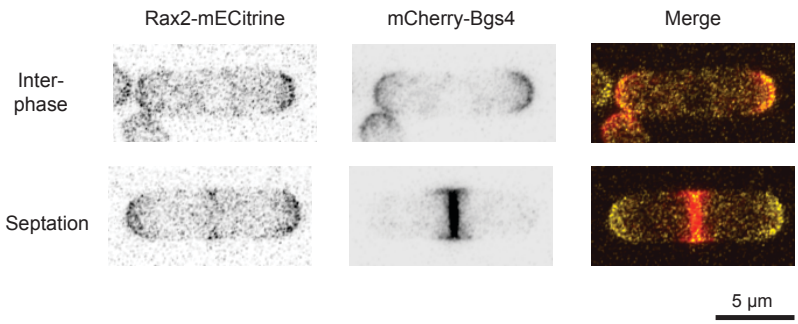

Figure 3.7: During septation, Rax2 is retained at the cell tips. Localisation of Rax2-mECitrine and mCherry-Beta glucan synthase (Bgs)4 . Rax2-mECitrine and mCherry-Bgs4 co-localise at cell tips during interphase but not during septation.

3.7 Rax1 localisation at the cell tips can be seen when imaged using very high exposure

In budding yeast, GFP-Rax1^{Sc} expressed from its endogenous promoter is visible at the bud sites (Kang, Angerman et al. 2004). In order to image Rax1 expressed from its endogenous promoter, I made several strains with various fluorescent tags at the Rax1 N- and C-termini (Table 3.3), However, none of these constructs were visible by microscopy when imaged using the same conditions as for Rax2.

Because Rax1 could only be detected by western blotting when overexpressed from the *nmt41* promoter (Figure 3.4), I hypothesised that to image Rax1 by microscopy, I could either overexpress Rax1 to generate a brighter signal, or optimise Rax1 imaging conditions to detect the much weaker Rax1 signal.

Table 3.3

Construct	Visible by microscopy
mECitrine-Rax1	Only with high exposure
3mCitrine-Rax1	No
Rax1-mECitrine	No
Rax1-mCherry	No
2mCherry-Rax1	No
nmt41-mECitrine-Rax1 “ON”	Vacuoles
nmt41-mECitrine-Rax1 “OFF”	Tip signal

When Rax1 was expressed from the *nmt41* promoter, I was able to image it using the same conditions as used for Rax2. *nmt41*:mECitrine-Rax1 had a tip signal only in the presence of thiamine, where the promoter is repressed (Figure 3.8). In media lacking thiamine, and the promoter is active, *nmt41*:mECitrine-Rax1 has a strong signal and appears to be targeted to vacuoles, possibly for degradation (Figure 3.8). YE5S (a rich, yeast extract based medium which contains thiamine) is the optimal media for imaging tip localisation of *nmt41:*mECitrine-Rax1 (Figure 3.8). The difference in *nmt41*:mECitrine-Rax1 detection in YE5S versus EMM (minimal media) containing thiamine is striking and surprising. It would be expected that the detection of *nmt41*:mECitrine-Rax1 would be similar in both thiamine containing media. I propose that maybe associated with yeast sensing the levels of nutrients in the media. Media that is rich in nutrients may strengthen the polarity cue to promote more growth when the supply of nutrients is high (it has previously been shown that the transition to NETO is delayed in minimal media which suggests that nutrient availability regulates cell growth (Mitchison and Nurse 1985)). This may result in the increased signal of *nmt41:*mECitrine-Rax1 at the cell tips. (It is important to note that Rax2-3mCitrine also has increased signal at the cell tips and cell septum in YE5S compared to EMM (S.Ashraf., thesis)).

I trialed very high exposure conditions, using the Airyscan microscope, to see if I could detect any mECitrine-Rax1 expressed under its endogenous promoter. Indeed, I was able to detect mECitrine-Rax1 signal at the cell tips (Figure 3.9). Despite the fact that imaging endogenous mECitrine-Rax1 is much more challenging than imaging *nmt41:*mECitrine-Rax1, imaging an endogenously expressed transmembrane protein is preferable over overexpression. This is because by overexpressing *rax1* I am affecting the stoichiometry of the Rax1-Rax2 complex. Additionally, overexpression of transmembrane proteins can be costly to cell fitness by overloading the membrane network (Osterberg, Kim et al. 2006, Tomala and Korona 2013). *nmt41:*mECitrine-Rax1 imaged in repressive conditions in YE5S has

approximately four times the protein levels of mECitrine-Rax1, as measured by fluorescence intensity of the cell tips (Figure 3.8).

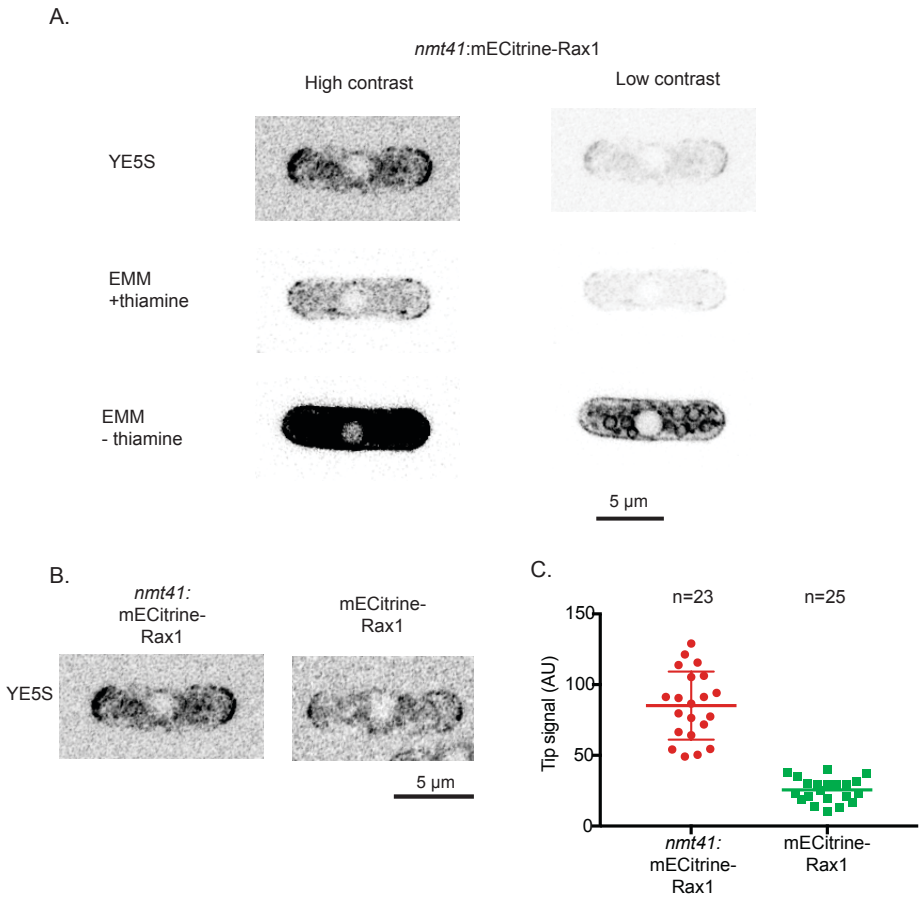

Figure 3.8: In media lacking thiamine, *nmt41:*mECitrine-Rax1 is highly overexpressed and appears to be trapped in vacuoles.In media containing thiamine, *nmt41:*mECitrine-Rax1 localises to the cell tips and protein levels are approximately double endogenous mECitrine-Rax1. All cells imaged with the same conditions on Airyscan micoscope. A. Comparison of *nmt41:*mECitrine-Rax1 in different media. Contrast settings: High: Minimum 0 Maximum 216; Low: Minimum 0, Maximum 1218 B.Comparison of *nmt41:*mECitrine-Rax1 and mECitrine-Rax1 with high contrast settings. C. Quantication of fluorescence signal at the cell tips in *nmt41*:mECitrine-Rax1 and mECitrine-Rax1 cells. Normalisation as described in materials and methods 2.13.3. Median and interquartile ranges are shown.

3.8 Rax2 protein levels are four times higher than Rax1 levels

Live-cell imaging and western blotting experiments suggested that Rax2 protein levels are higher than Rax1 protein levels. To quantify the difference in Rax1 and Rax2 levels I imaged mECitrine-Rax1 and Rax2-mECitrine under the same conditions and measured the total fluorescent signal at cell tips, as described in Chapter 2.13.3 (Figure 3.9). The Rax2-mECitrine tip signal is four times higher than the mECitrine-Rax1 signal (Figure 3.9). Currently, I do not know if the interaction of Rax1 and Rax2 is direct or whether there are other members of the Rax1-Rax complex. Therefore, I cannot propose how important the 1:4 ratio of Rax1 to Rax2 is for complex formation or function of the Rax1-Rax2 growth-memory cue.

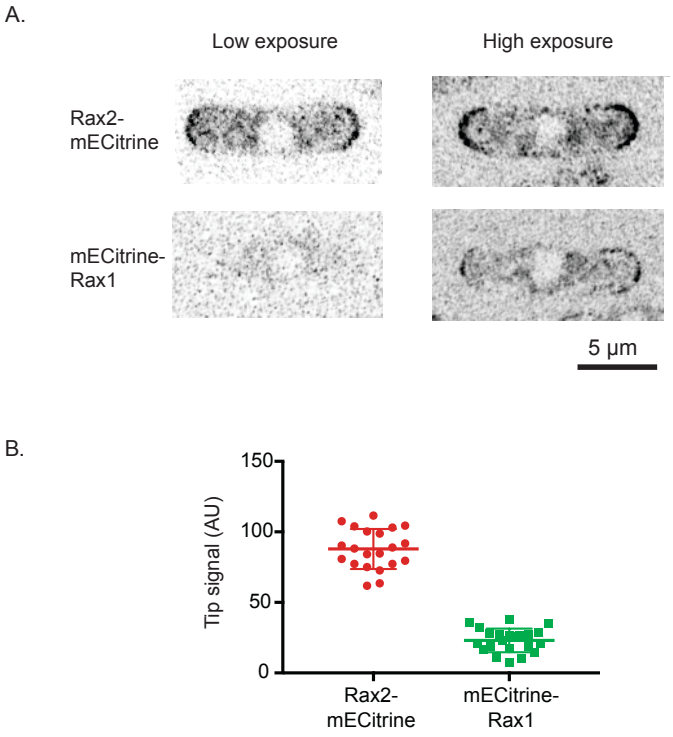

Figure 3.9: Endogenous Rax1 levels are lower than endogenous Rax2 levels. A. Live-cell images of Rax2-Citrine and Citrine-Rax1. Low exposure: 10 % Laser Power, 514 nm, 7 Z sections. High exposure 15 % Laser power, 514 nm, 4 x averaging, 5 Z sections. B. Quantification of tip signal, as described in materials and methods 2.13.3. Median and interquartile ranges are shown.

3.9 Rax1 and Rax2 are co-dependent for localisation to cell tips

In budding yeast, Rax1^{Sc} and Rax2^{Sc} are co-dependent for localisation to bud sites (Chen, Hiroko et al. 2000, Kang, Angerman et al. 2004). I imaged Rax1 in a *rax2Δ* background and Rax2 in a *rax1Δ* background and found that Rax1 and Rax2 are also co-dependent for localisation (Figure 3.10). In *rax1Δ* cells, Rax2 is no longer tip localised. Rax2 appeared to be retained in the ER. The ER is localised close to the plasma membrane and is contiguous with the nuclear envelope (Zhang, Vjestica et al. 2010). To confirm that Rax2 was localised in the ER, Rax2-mECitrine was co-imaged with the luminal marker ADEL-mCherry (Figure 3.10A) (Zhang, Vjestica et al. 2010). Indeed, Rax2-mECitrine and ADEL-mCherry co-localised. Rax2-mECitrine was also imaged in *scs2*Δ *scs22*Δ ER-to-plasma membrane tethering mutant cells. In *scs2*Δ *scs22*Δ cells, the ER membrane is largely dissociated from the cell periphery and, at the cell tips in particular, the ER accumulates in the cytoplasm (Zhang, Vjestica et al. 2012). In *scs2*Δ *scs22*Δ cells, Rax2 correctly localises to the cell tips. In *rax1*Δ *scs2*Δ *scs22*Δ cells, Rax2 is localised in the dissociated ER and in the cytoplasmic accumulations of the ER (Figure 3.10). This further supports that Rax2 is retained in the ER in *rax1*Δ cells rather than, for example, being ectopically targeted to the cortical plasma membrane. ER retention of Rax2 is clearly detectable only in specific imaging conditions using the spinning disk at 50 % 514 nm laser power and imaged in a single Z section. mECitrine-Rax1 was not visible using these imaging conditions due to its weaker fluorescence intensity, and was also not detected at higher laser powers on the spinning disk. However, *nmt41:*mECitrine-Rax1 was detectable in these imaging conditions. *nmt41:*mECitrine-Rax1 appeared to be retained in the ER in *rax2*Δ cells (Figure 3.10B). This suggests that Rax1 and Rax2 are co-dependent for trafficking out of the ER. Interestingly, Rax2 protein levels, as assessed by western blotting, were increased approximately two-fold in *rax1*Δ cells compared to wild type (Figure 3.10C). I propose there may be some kind of sensing mechanism in the cells to ensure there are sufficient levels of Rax2 at the cell tips. When Rax2 is mislocalised the cell may increase the

expression of Rax2 and consequently supply more Rax2 to be delivered to the cell tips.

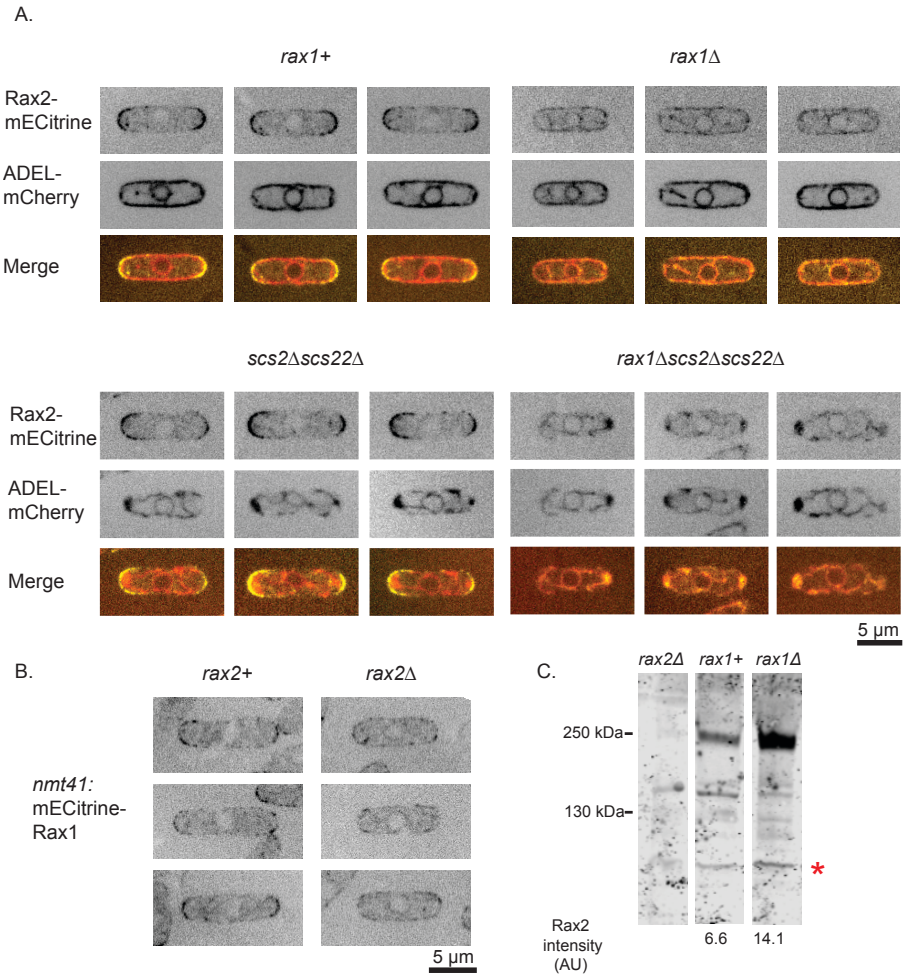

Figure 3.10: Rax1 and Rax2 are co-dependent for trafficking out of the ER and localisation to the cell tips. A. Live-cell imaging of Rax2-mECitrine and the ER maker ADEL-mCherry in YE5S media taken on confocal spinning disk. B. Live-cell imaging of *nmt41*-mECitrine-Rax1 in YE5sS media taken on the confocal spinning disk . C. Anti-Rax2 Western blot. Rax2 intensity normalised to the non-specific band adjacent to the asterisk.

3.10 Large internal deletions within the Rax2 extracellular region cause severe defects in protein expression and localisation

The large (1106 amino acids), glycosylated extracellular region of Rax2 could be important for protein-protein interactions and/or interactions between the plasma membrane and cell wall, which could be important for Rax2 retention at the cell tips. The extracellular region has no predicted structural features, apart form an N-terminal signal peptide (amino acids 1-20). I made four internal deletions of 100 amino acids each in Rax2-3mCitrine and imaged them to investigate whether Rax2 localisation was affected (these internal deletions were made before 3mCitrine was found to affect Rax2 function). No signal was detected at the cell tips for any of the internal deletions (Table 3.3). I investigated the expression levels of the internal deletions by western blotting. Internal deletions ID1 and ID3 were detected at levels similar to full length Rax2. All other internal deletions had either low or undetectable protein levels (Table 3.3). The internal deletions appear to have a strong effect on protein stability and localisation, most likely due to disruption of protein glycosylation and folding.

Table 3.3

Rax2 fragment	Signal at the cell tips	Signal by Western blotting
Full-Length: Rax2 -3mCitrine	Yes	Yes
ID1: Rax2Δ21-120 -3mCitrine	No	Yes
ID2: Rax2Δ121-220 -3mCitrine	No	No
ID3: Rax2Δ221-320 -3mCitrine	No	Yes
ID4: Rax2Δ421-520 -3mCitrine	No	Weak

3.11 Deletion of the Rax2 cytoplasmic tail results in its mislocalisation and loss-of-function

In budding yeast, the Rax2^{Sc} cytoplasmic tail is 37 amino acids long. When whole cytoplasmic region of Rax2^{Sc} is removed (Rax2^{Sc}Δ1184-1220), Rax1^{Sc} can no longer localise to the bud sites (Meitinger, Khmelinskii et al. 2014). Because Rax2^{Sc} and Rax1^{Sc} are co-dependent for their localisation to the bud sites, it is most likely Rax2^{Sc}Δ1184-1220 also mislocalised (Kang, Angerman et al. 2004). In fission yeast, Rax2 has a small C-terminal cytoplasmic tail of 26 amino acids. I hypothesised that the Rax2 cytoplasmic tail is required for the interaction with Rax1, and consequently, for localisation to the cell tips. Additionally, the cytoplasmic region may be involved in the interaction of Rax2 with the cytoplasmic growth machinery proteins for re-initiation of growth at a previously growing tip. I therefore was interested whether a particular region of cytoplasmic tail was important for Rax2 localisation and function. To investigate the role of the cytoplasmic tail in Rax2 function, I made five Rax2 C-terminal truncations, removing 9, 12, 15, 18 or 26 amino acids, in a *tea1Δ CRIB-3mCitrine* background (Figure 3.11). Analysis of daughter-cell growth patterns showed that truncations from CΔ9 to CΔ18 amino acids had a mild effect on Rax2 function, with the majority of cells growing in either a *Syn* or *Syn-like* pattern (Figure 3.11). This indicates that Rax2 is still able to lead to the re-initiation of growth at a previously growing tip with a cytoplasmic tail of just 8 amino acids.

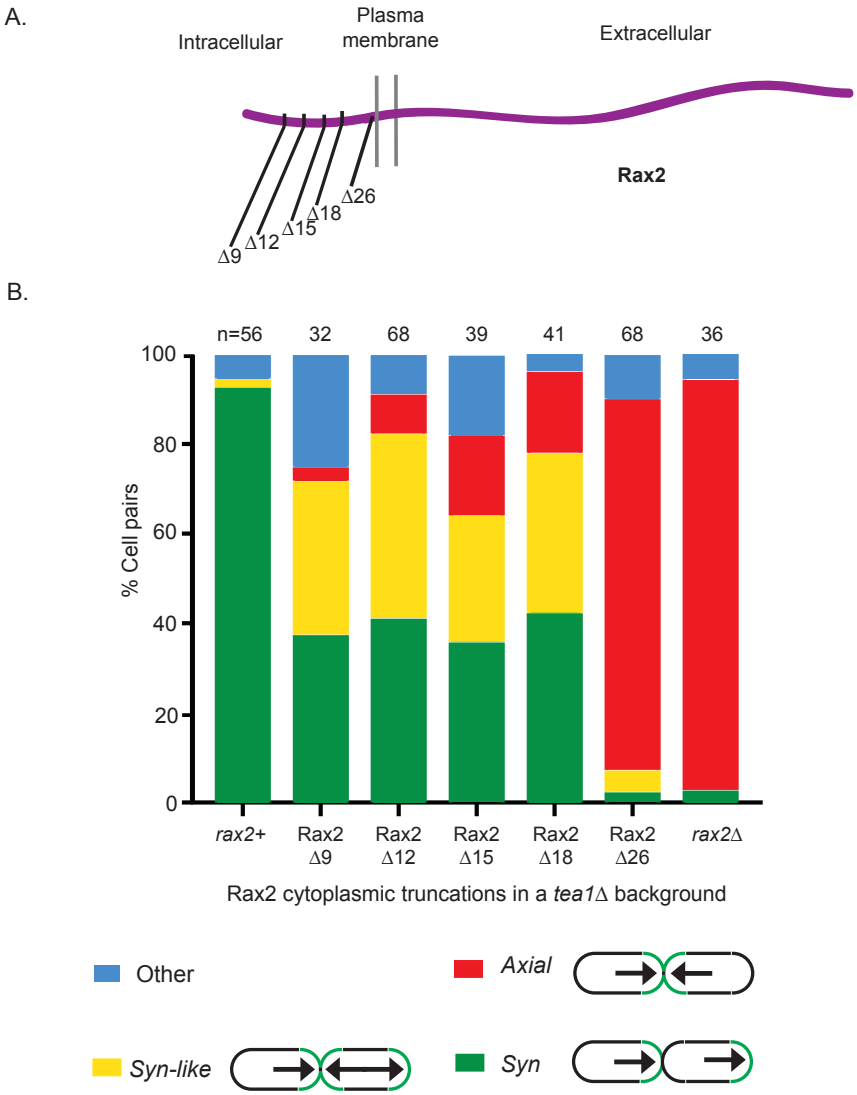

Figure 3.11: Removing the entire Rax2 cytoplasmic region leads to a loss of function of Rax2. A. Cartoon illustrating each of the truncations.The cytoplasmic region of Rax2 is 26 amino acids long. Five truncations were made by removing 9, 12, 15, 18 and 26 amino acids from the C-terminus. B. Quantification of growth patterns of daughter-cell pairs. *Axial* (new end growth only, in both daughter cells). *Syn* (one daughter grows from its old end; one daughter grows from its new end). *Syn-like* (one daughter grows bipolar; one daughter from its new end). Other (any other growth pattern or any cells which stop growing). HTB (His-Tev-Biotin). HBH (His-Biotin-His). n= number of daughter pairs.

By contrast, truncation of the entire cytoplasmic region led to nearly complete loss-of-function of Rax2 (Figure 3.11). In *rax2-CΔ26 tea1Δ* cells, growth was mostly *Axial*. This is similar to *rax2Δtea1Δ* cells. I therefore wanted to know if Rax2-CΔ26 was correctly localised to cell tips (it was most likely the other truncations were correctly localised due to their retention of function). Because tagging can impair Rax2 function (Figure 3.6), my original Rax2 truncations were untagged, to ensure that any impaired Rax2 function was due to truncation and not to tagging. To investigate whether Rax2-CΔ26 was localised to cell tips, I tagged all of the truncations with a C-terminal mECitrine tag. Rax2-CΔ26-mECitrine was completely mis-localised from the cell tips. Similarly to Rax2 in a *rax1Δ,* Rax2-CΔ26-mECitrine appeared to be trapped in the ER. This suggests that mislocalisation is responsible for Rax2-CΔ26 loss-of-function (Figure 3.11B). It is quite likely this is due to Rax2Δ26 being unable to interact with Rax1 to be trafficked out of the ER. Rax2-CΔ9-mECitrine and Rax2-CΔ12-mECitrine localised to cell tips similarly to full-length Rax2-mECitrine. This confirms that the mECitrine tag does not contribute to mislocalisation of the Rax2Δ26 (Figure 3.12A). Rax2-CΔ15-mECitrine and Rax2-CΔ18-mECitrine showed some apparent ER localisation, but also significant cell-tip enrichment. As the ER is not strongly enriched at cell tips (Zhang, Vjestica et al. 2010) this suggests that Rax2-CΔ15 and Rax2-CΔ18 enriched at the cell tips is localised to the plasma membrane (not due to ER enrichment at the cell tips) and thus is capable of trafficking out of the ER, albeit not as efficiently as full-length Rax2.

Western blotting showed that, similar to Rax2 in *rax1Δ* cells, Rax2-CΔ26 levels are increased about two-fold relative to wild-type cells (Figure 3.10C, Figure 3.12B). In addition, Rax2-CΔ18 levels are increased ~1.5 times compared to wild-type (Figure 3.12B). This suggests again that Rax2 ER retention is in some way responsible for the increased protein levels of Rax2. This is possibly due to a sensing mechanism for Rax2 localisation at the cell tips as described in Section 3.9.

A.

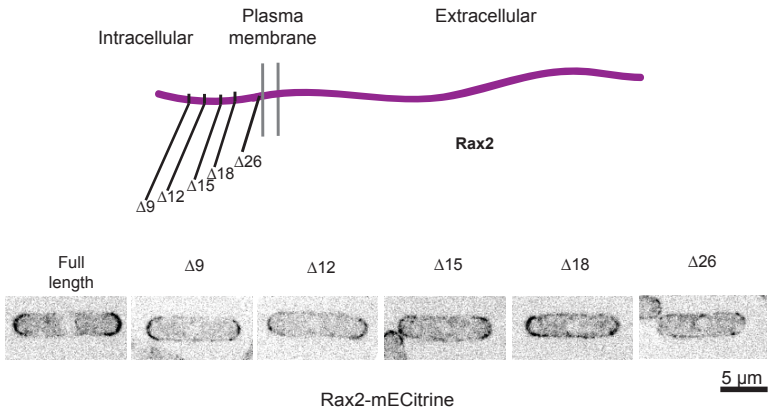

B.

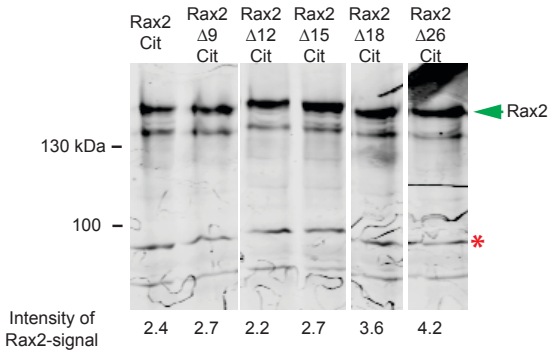

Figure 3.12: Removing the entire Rax2 cytoplasmic region prevents localisation to the cell tips. A. Cartoon illustrating cytoplasmic truncations. Live-cell images of truncations tagged with mECitrine. Rax2 is localised to the cell tips when truncated by up to 18 amino acids. Rax2 is not tip localised with 26 amino acid truncation.Images taken on the confocal spinning disk B. Anti-Rax2 western blot of PNGase F treated membrane-enriched fraction. Rax2 specific band marked by the arrow. Rax2 signal is normalised to a non-specific band adjacent to the asterisks.

3.12 Discussion

In this chapter I have developed tools for studying Rax1 and Rax2 in molecular detail. These will be used in the next chapters to identify and characterise interacting partners of Rax1 and Rax2. I will discuss the similarities and differences between the data I have generated when studying Rax1 and Rax2 in fission yeast to what has been reported in studies of $Rax1^{Sc}$ and $Rax2^{Sc}$ in budding yeast.

3.12.1 $Rax1^{Sc}$ can be detected by western blot expressed under its endogenous promoter but Rax1 needs to be overexpressed for detection in anti-Rax1 western blot

$Rax1^{Sc}$ can be detected by western blotting when expressed under its endogenous promoter, whereas I was unable to detect Rax1 expressed at endogenous levels (Kang, Angerman et al. 2004) (Figure 3.4). (Kang, Angerman et al. 2004) detected a C-terminally Myc-tagged $Rax1^{Sc}$ with an anti-Myc antibody, and they described $Rax1^{Sc}$-Myc as being fully functional (Kang, Angerman et al. 2004). However, I found that Rax1-Myc was largely impaired in function and therefore I did not perform a western blot of Rax1 in similar conditions to that of $Rax1^{Sc}$-Myc. This difference may be due to anti-Myc antibody having higher affinity towards Myc than the anti-Rax1 antisera has towards Rax1, or that the endogenous levels of $Rax1^{Sc}$ are higher than Rax1.

3.12.2 mECitrine-Rax1 has four-fold lower protein levels than Rax2-mECitrine.

Endogenously expressed mECitrine-Rax1 can be detected by fluorescence microscopy only with very high exposures on the Airyscan microscope, 15 % laser power with averaging over four scans per Z-section, and not under conditions similar to those used for imaging Rax2, 10 % laser power with only one scan per Z-section. Quantification through fluorescence microscopy suggests that Rax1 protein levels are approximately four-fold lower than Rax2 protein levels at the cell tips (Figure 3.9).

On the spinning disk microscope, mECitrine-Rax1 can only be detected at the cells tips when expressed under repressible conditions for the *nmt41* promoter. In these conditions the ratio of Rax1 to Rax2 is 1:1, rather than 1:4 when Rax1 is expressed under its endogenous promoter. (Figure 3.8, Figure 3.9). Overexpression of Rax1 may either improve or reduce the efficiency of Rax1 and Rax2 complex formation and function. Without further biochemical experiments to identify the following:

1. Whether the Rax1-Rax2 interaction is direct
2. Whether any other proteins are involved in the complex
3. The stoichiometry of the complex

I am unable to suggest how the relative Rax1 and Rax2 levels might be important to their tip localisation and role as a growth-memory cue.

3.12.3 Large tags at the C-terminus of Rax2 may prevent important protein interactions for Rax2 function

I am unable to use Rax2-3mCitrine for imaging because this tag impairs Rax2 function, but I am able to use Rax2-mECitrine. A single mEcitrine tag generates a weaker fluorescent signal, and this is a problem because endogenous Rax2 levels appear to be low. Because I have to use high laser powers to observe the Rax2-mECitrine signal, making time-lapse movies is difficult, due to photobleaching. Currently I am unable to image any Rax2 accumulation at the new end of a cell as it grows, whereas this was possible with Rax2-3mCitrine (S.Ashraf, thesis).

Large tags such as 3mCitrine may create steric hindrance, preventing Rax2 from interacting with downstream partners involved in cell polarity regulation. However, the tags do not affect Rax2 localisation to the cell tips (Figure 3.5). This suggests that the interactions between Rax2 and the proteins involved in its own localisation, such as the interaction with Rax1, are not affected by tagging. Potentially, the C-terminal region could be interacting with downstream effectors for polarized growth. Conversely, truncating the cytoplasmic tail to just 8 amino acids has only a very mild effect on Rax2 function as a growth-memory cue (Figure 3.10). This suggests that the large tags at the Rax2 C-terminus are not disrupting an

interaction that occurs at the Rax2 cytoplasmic domain but somehow interfere with an interaction may occur elsewhere, for example at the transmembrane domain, or potentially interfere with an interaction between different proteins that are localised in the vicinity of the Rax2 C-terminus.

A combined fluorescence- and purification-tag would allow me to do imaging and biochemistry experiments with the same strain. Previous work in the lab investigating Mto1 used a fluorescence tag (GFP) at the N-terminus and a purification tag (HTB) at C-terminus of Mto1 (Bao, Spanos et al. 2018). However, I was unable to do an analogous experiment, because of the signal peptide at the Rax2 N-terminus. Combined C-terminal mECitrine-HBH or HBH-mECitrine tags lead to an impairment of Rax2 function (Figure 3.6). However, the CAH and the HTB alone tag do not, because they are smaller. Protein purification involving Rax2-HTB and Rax2-CAH are described in Chapter 4.

3.12.4 Rax1 and Rax2 may be co-dependent for intracellular trafficking

Rax1 and Rax2 are co-dependent for localisation to cell tips, and my data support the idea that Rax1 and Rax2 are co-dependent for trafficking out of the ER. I can detect Rax2 and *nmt41*:mECitrine-Rax1 retained in the ER only under specific imaging conditions (very high laser powers and imaging a single Z section). In budding yeast, $Rax1^{Sc}$ and $Rax2^{Sc}$ are co-dependent for bud site localisation. Mislocalised $Rax2^{Sc}$ in $rax1^{Sc}\Delta$ cells was not obviously trapped in the ER but instead appears to be localised in small patches or vesicles (Chen, Hiroko et al. 2000, Fujita, Lord et al. 2004, Kang, Angerman et al. 2004). It is possible that ER localisation could have been observed with improved imaging conditions or potentially the trafficking of Rax2 out of the ER is not dependent on Rax1 in budding yeast.

Rax2 protein levels are approximately doubled in *rax1*Δ cells. There is no published data as to whether there is a change in $Rax2^{Sc}$ levels in a $rax1^{Sc}\Delta$. As mentioned previously, there could be a sensing mechanism to detect if there are sufficient levels of Rax1 and Rax2 at the cell tips. If there is insufficient Rax1 or Rax2 at the cell tips, the expression of *rax1 or rax2* may be increased to provide sufficient Rax1 and Rax2. This sensing mechanism

may ensure that, following cell division, the polarity cue will be sufficiently stronger at the old end than the new end. And consequently lead to initial monopolar growth from the old end.

3.12.5 Large extracellular deletions of affect expression/stability of Rax2, cytoplasmic truncations affect localisation of Rax2

I made five 100 amino-acid internal deletions in the Rax2 extracellular region. None of these localised to the cell tips (Table 3.4). Additionally, only ID1 and ID3 were detected at wild-type protein levels (Table 3.4). The glycosylation levels of ID1 and ID3 were unaffected, suggesting that their mislocalisation was not due to insufficient glycosylation. The internal deletions ID2 and ID4 may have lead to mis-folding of the proteins and consequently their targeting for degradation.

In budding yeast, the $Rax2^{Sc}$ cytoplasmic region is 37 amino acids long. When the $Rax2^{Sc}$ cytoplasmic region is removed, $Rax1^{Sc}$ can no longer localise to the bud sites (Meitinger, Khmelinskii et al. 2014). This suggests that the cytoplasmic region may be involved in the Rax1-Rax2 interaction and consequently trafficking of the Rax1-Rax2 complex out of the ER. Rax2 in a *rax1*Δ and Rax2-CΔ26 are not transported out of the ER. Rax2-CΔ15 and Δ18 appear to have some impairment in trafficking out of the ER. Potentially Rax2-CΔ26, Δ18 and Δ15 may have impaired interaction with Rax1, which may be responsible for their impaired trafficking out of the ER. Oligomerisation of TM proteins can be either partially of fully mediated by the transmembrane domain (TMD) and may involve amino acids adjacent to the TMD (Fink, Sal-Man et al. 2012). One possibility is that Rax1 and Rax2 interact via their TMDs, and the amino acids adjacent to the TMD are required for this interaction to be stable. For recognition by COPII vesicles and transport out of the Golgi, protein complexes must be correctly formed (Barlowe 2003, Sato and Nakano 2007). This ensures that only correctly folded and fully synthesised cargos are targeted for export from the ER (Barlowe 2003) (Sato and Nakano 2007). Therefore, it appears that correct Rax1-Rax2 complex formation, which may be mediated by their TMDs, may

be required for recognition by COPII vesicles for transport from the ER to the Golgi.

So far it is not known how Rax1 and Rax2 form a complex in either budding yeast or fission yeast. It is also not known whether any other proteins participate in the interaction in fission yeast. In budding yeast, $Bud8^{Sc}$ plays a role in $Rax1^{Sc}$ and $Rax2^{Sc}$ localisation to the bud sites (Kang, Angerman et al. 2004). It is possible that there is a protein in fission yeast that is also required for correct localisation of Rax1 and Rax2. Despite no sequence homologs of $Bud8^{Sc}$ or identified in fission yeast, there may be a functional homolog of $Bud8^{Sc}$ that plays a role in Rax1 and Rax2 localisation to the cell tips.

3.13 Future directions

I would next like to use the strains I have generated and the antisera I have characterised to investigate the interactors of Rax2. In the following chapter I will look into the Rax2-HTB and Rax2-CAH and optimise their purification and cross-linking conditions and identify interactors of Rax2.

$Rax1^{Sc}$ and $Rax2^{Sc}$ have been shown to interact, although it is not known whether this interaction is direct or indirect (Kang, Angerman et al. 2004). Future work that would be of interest to carry out is investigating whether Rax1 and Rax2 directly interact. Additionally, I would be interested to see whether Rax2-CΔ26, Δ18 and Δ15 impair the Rax1 to Rax2 interaction *in vitro*.

Chapter four: Identification of Rax2 interactors using cross-linking and mass spectrometry

4.1 Introduction

There are currently no known interactors of Rax1 or Rax2. The known interactors of Rax1^{Sc} and Rax2^{Sc} are Bud8^{Sc}, Bud9^{Sc} and Nis1^{Sc}, and they do not have obvious homologs in fission yeast. To identify interactors of Rax2, I first carried out cross-linking, followed by purification in harsh denaturing conditions, and analysed any interacting partners by mass spectrometry and label-free quantification.

For purification, Rax2 was tagged with either an HTB or CAH tag. The HTB tag contains six histidines, a TEV cleavage site and an *in vivo* biotinylation signal sequence. The biotinylation signal sequence is 75 amino acids long and derived from *E.coli* (Tagwerker, Flick et al. 2006). The biotinylation sequence is highly conserved between organisms and is efficiently biotinylated via endogenous biotin ligases found in yeast and mammalian cells (Tagwerker, Flick et al. 2006). The CAH tag contains mECitrine, AviTag biotinylation sequence and six histidines. The AviTag is a minimal biotinylation sequence of 15 amino acids (Cull and Schatz 2000). For complete biotinylation of the AviTag sequence, the bacterial biotin ligase, *BirA* must be co-expressed in the yeast cells (van Werven and Timmers 2006, Fairhead and Howarth 2015). The AviTag is the minimal sequence for recognition and biotinylation specifically by BirA, and is not biotinylated by the yeast endogenous biotin protein ligase Bpl1 (Li and Sousa 2012)

Samples were cross-linked prior to purification of tagged Rax2 to retain protein-protein interactions throughout the purification process. Chemical cross-linkers react with residues of proteins that are in close proximity and form stable covalent links between these proteins. Cross-linking allows weak or transiently interacting partners to be purified along with Rax2. These interactions may be lost during a native pull down. Cross-linking also prevents the formation of non-physiological protein complexes during the purification process (however, it should be noted that it is possible that some non-specific cross-linking may occur). Additionally, cross-linking

enables protein complexes to be purified in harsh denaturing conditions. Harsh denaturing conditions decrease the amount of non-specific binding to the beads (Spriestersbach, Kubicek et al. 2015). Denaturing conditions allow purification tags to be more exposed and more accessible to bind to the purification matrix (Spriestersbach, Kubicek et al. 2015). However, any tags that require their secondary structure to be maintained to bind to the purification matrix will not work under denaturing conditions.

The HTB and the CAH tags are ideal for purification in denaturing conditions. The binding of 6xHis and the biotin to Ni-NTA and streptavidin (respectively) does not require the tag to have a secondary structure (Spriestersbach, Kubicek et al. 2015). Additionally, the biotin-streptavidin interaction is one of the strongest available in biochemistry, the K_d is approximately 10^{-14} to 10^{-16} M(Laitinen, Hytonen et al. 2006). Therefore, less tagged protein will be lost in washes during purification and thus results in a higher yield of the tagged protein following elution from the beads.

After purification of Rax2 and any cross-linked interacting partners, the samples can be analysed by mass spectrometry. Any differences in protein levels between the cross-linked tagged Rax2-HTB sample and cross-linked untagged negative control were quantified with Label-Free Quantification (LFQ). LFQ provides semi-quantitative information inferred from total peptide counts or spectral counts. Proteins found enriched in the Rax2-HTB sample are potential Rax2 interacting partners.

In this chapter I describe optimisation of the purification of Rax2-HTB. However, I was unable to purify an acceptable yield of Rax2-CAH. Following cross-linking, purification and mass spectrometry analysis I identified 20 candidate interacting proteins for Rax2. Rax1 was found to be an interactor, consistent with budding yeast data that showed co-purification of $Rax1^{Sc}$ with $Rax2^{Sc}$ (Kang, Angerman et al. 2004). Four of the interactors, glucan synthase components Bgs1 and Bgs3 and Rho GAPs Rga1 and Rga3, are known polarity proteins. In this chapter I will discuss the potential relevance of the all identified interactors for Rax2 function.

4.2 Rax2-HTB can be purified using streptavidin beads in denaturing conditions

A previous lab member, Xun Bao, identified interactors of GFP-Mto1-HTB through cross-linking, purification and mass spectrometry. Xun purified GFP-Mto1-HTB using a two-step purification, first with Ni-Fractogel beads and then streptavidin beads. I based my initial experiments on the work carried out by Xun for GFP-Mto1-HTB, and I then optimised the conditions for purification Rax2-HTB.

To test whether the HTB tag added to Rax2 was biotinylated in vivo, and thus capable of binding to streptavidin, I performed a streptavidin gel shift assay. 2 µg of streptavidin was added to membrane-enriched fraction (MEF, described in Chapter 3.3) protein samples in Laemmli sample buffer prior to loading onto the gel. Streptavidin is a tetramer with a molecular weight of 55 kDa, and therefore, if Rax2-HTB is bound to streptavidin there will be an increase in the apparent molecular weight of Rax2-HTB from 130 kDa to 185 kDa. Indeed, 75 % of Rax2-HTB is detected at an increased molecular weight when streptavidin is added (Figure 4.1). This suggests that the HTB tag is biotinylated and able to bind to streptavidin. As expected, untagged Rax2 did not show any increase in molecular weight after streptavidin addition.

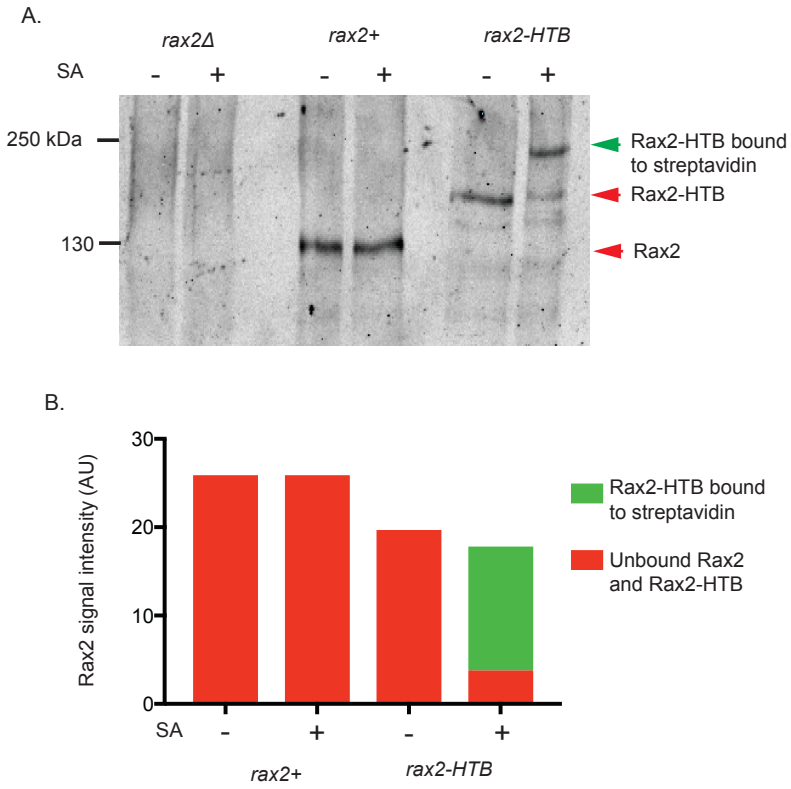

Figure 4.1: Rax2-HTB is biotinylated *in vivo.* A. Anti Rax2 Western blot of PNGase F treated samples. When streptavidin is added to the protein sample the interaction between streptavidin and the biotinylated sequence leads to a band shift to an increased molecular weight of Rax2-HTB. B. Quantification of panel A. SA = streptavidin .

I first attempted to purify Rax2-HTB using the same protocol Xun had designed for the purification of GFP-Mto1-HTB. This involves first a Ni+ fractogel purification followed by a streptavidin purification. I firstly adapted this protocol to first enrich for Rax2 by creating a MEF prior to binding the protein sample to the beads (Figure 3.1). I was unable to detect any Rax2 following the His pull-down (Figure 4.2). Because the His purification was unsuccessful, I attempted a streptavidin pull-down without the prior Ni+ fractogel purification step. Initially, this approach still did not lead to detectable levels of Rax2 from the streptavidin pull-down (Figure 4.2). I had expected to be able to purify Rax2-HTB with the streptavidin beads because Rax2-HTB was able to bind to soluble streptavidin protein in the gel shift assay (Figure 4.1). Because samples in the gel shift assay were treated with PNGase F prior to incubation with streptavidin (to make the molecular weight shift more apparent), I hypothesised that the glycosylation of Rax2-HTB may interfere with its binding to streptavidin.

I therefore repeated the purification and treated the protein samples with PNGase F treatment prior to bead binding. This allowed me to purify Rax2 from the beads (Figure 4.2). A mock treatment, without adding PNGase F enzyme, leads to a similar efficiency of Rax2 purified from the beads as PNGase F treatment (Figure 4.2, Table 4.1). The mock treatment involves a glycoprotein denaturation step by boiling the sample in 40 mM DTT, followed by incubation at 37 ˚C in 1 % Triton-X and 50 mM $NaPO_4$ pH 7.5.

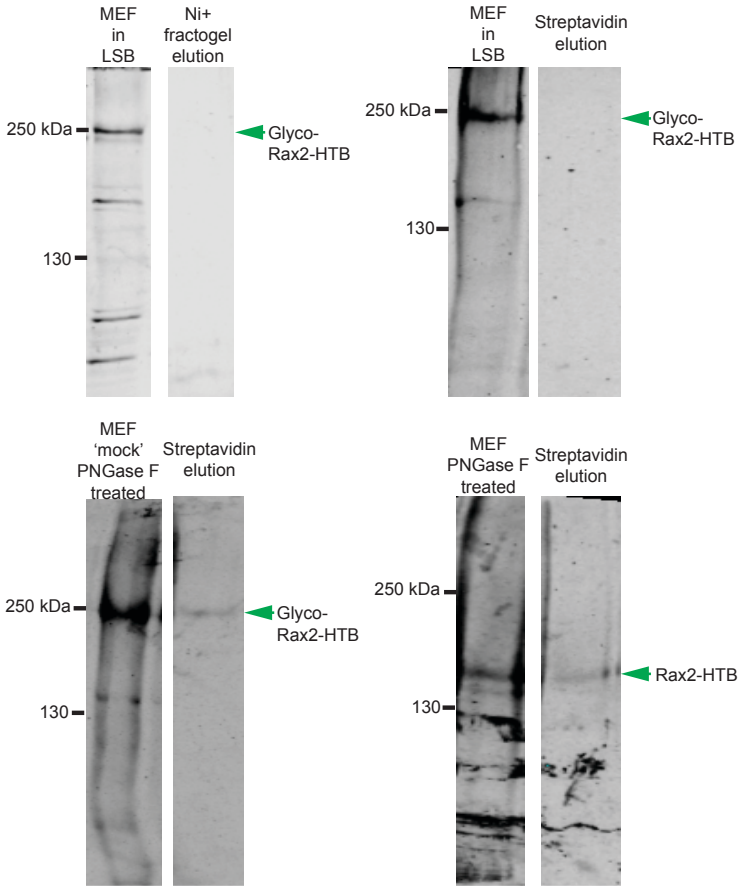

Figure 4.2: Rax2-HTB is purified from 'mock' and PNGase F treated membrane-enriched fractions (MEFs) with streptavidin beads. Anti-Rax2 Western blot. Equal cell equivalents are loaded into each lane.

I investigated whether the initial glycoprotein denaturation step was sufficient to increase binding of Rax2-HTB. There was no detectable Rax2 purified from just the denaturation step (Table 4.1). Using homemade buffers lead to equal efficiency of Rax2 purification to those supplied by NEB as part of the PNGase F kit (Table 4.1). Treatment with PNGase F did not lead to a significant increase in Rax2 yield compared to mock treatment.

Table 4.1.

Condition	Rax2 levels as equal cell equivalents compared to input
LSB boil	Not detected
Boil in 40 mM DTT (NEB buffers)	Not detected
Mock-treatment (NEB buffers)	7.4 %
PNGaseF treatment (NEB buffers)	8.0 %
40 mM DTT boil (Homemade buffers)	Not detected
Mock-treatment (Homemade buffers)	7.8 %
PNGaseF treatment (Homemade buffers)	8.2 %

In subsequent experiments I treated protein samples with a mock-treatment with homemade buffers prior to bead binding. These experiments involved investigating the efficiency of the purification of Rax2-CAH (which was ultimately unsuccessful), purification of cross-linked Rax2, and large-scale purification of cross-linked Rax2 for identification of interacting partners through mass spectrometry.

4.3 Rax2-CAH is biotinylated but has decreased protein levels in a *birA*+ background

As described in section 4.2 for Rax2-HTB, I needed to confirm that Rax2-CAH was biotinylated and able to bind to streptavidin. To do this, I carried out a streptavidin spike-in gel shift assay. As mentioned previously, efficient biotinylation of the Avitag sequence in Rax2-CAH requires expression of *birA* . A large proportion of Rax2-CAH bound to streptavidin in a *birA*+ strain but not in a *birA*- strain (Figure 4.3A). Surprisingly, the levels of Rax2-CAH in *birA*+ cells was only about half of that in the *birA*- cells, in spite of equal loading of lanes (as judged by non-specific bands on the blot) (Figure 4.3A). A reduced fluorescence intensity of Rax2-CAH at the cell tips in *birA*+ cells compared to *birA*- cells was observed through live-cell imaging. The average fluorescence signal observed at the tips in *birA*- cells was 23 AU versus 15 AU for *birA*+ cells (Figure 4.3C). This again suggests that there are reduced protein levels of Rax2-CAH in *birA*+ cells compared to *birA*-. Additionally, compared to Rax2-CAH *birA*-, Rax2-CAH *birA*+ leads to a mild impairment of Rax2 function as a growth-memory cue. The functionality of Rax2-CAH *birA*- and Rax2-CAH *birA*+ was investigated in a *tea1*∆ background, as described in Chapter 3.5. *tea1*∆ cells grow in a *Syn* pattern when Rax2 is fully functional (Figure 1.6 and 4.3D). 68 % of daughter pairs grew in a *Syn* pattern in Rax2-CAH *birA*- cells and 14 % grew in a Syn-like pattern (suggesting a weakened but functional memory-cue, see Chapter 3.5) (Figure 4.3D). This suggests that Rax2-CAH *birA*- is largely functional. The number of daughter pairs growing in a Syn pattern is reduced in Rax2-CAH *birA*+ cells compared to Rax2-CAH *birA*- cells. In Rax2-CAH *birA*+ cells, 30 % of daughter cell pairs grew in a *Syn* pattern and 31 % grew in a *Syn*-like pattern (Figure 4.3D). This suggests that the growth-memory cue is still functional in Rax2-CAH *birA*+, but weakened in comparison to Rax2-CAH *birA*- cells. This is likely due to the reduced Rax2-CAH levels in *birA*+ cells.

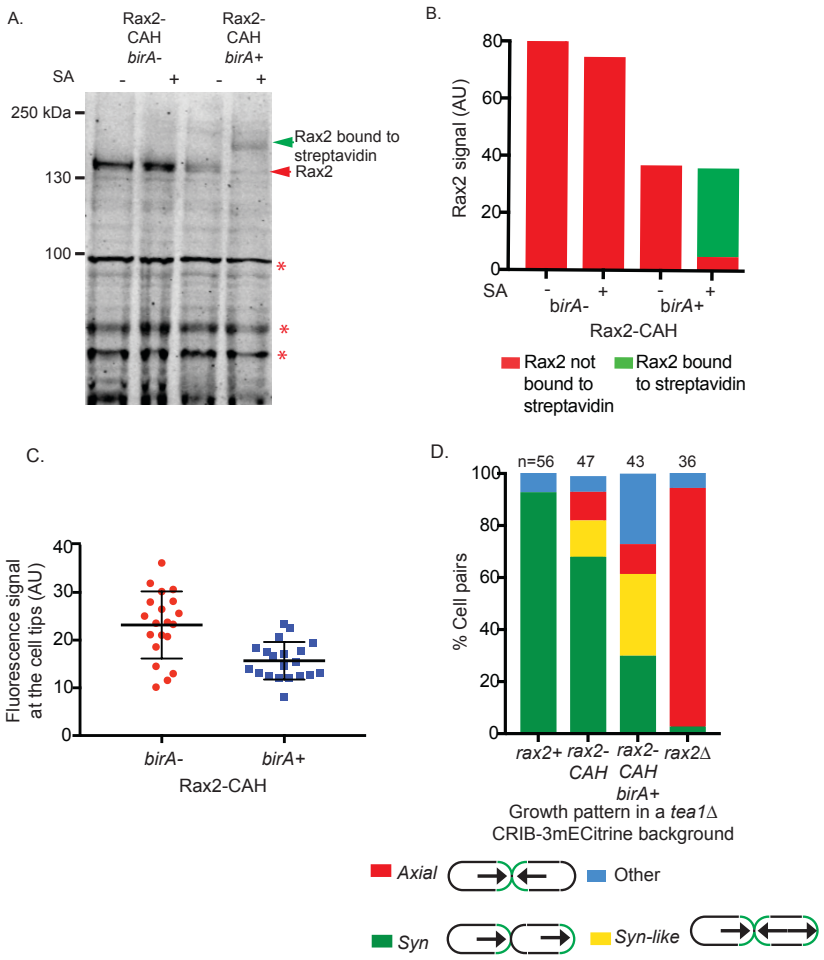

Figure 4.3: Rax2-CAH is expressed at lower levels in *birA+* cells. A. Anti-Rax2 western blot of streptavidin gel shift assay of Rax2-CAH in *birA+* and birA- strains. Asterisks indicate non-specific bands that show equal loading B. Quantification of Rax2-CAH protein levels of the western blot in pannel A. C. Total fluorscence signal of Rax2-CAH at the cell tips in *birA+* and *birA-* cells. Quantified as described in materials and methods.Median and interquartile ranges are shown. D. Quantification of growth patterns of daughter cell pairs.Growth patterns were classed as either *Axial* (new end growth only, in both daughter cells). *Syn* (one daughter grows from its old end; one daughter grows from its new end). *Syn-like* (one daughter grows bipolar; one daughter from its new end). Other (any other growth pattern or any cells which stop growing).

I purified Rax2-CAH *birA*+ using streptavidin beads using the optimised protocol described in section 4.2. Per gram of cells, the Rax2-CAH *birA*+ yield is only one third of that of Rax2-HTB. This is most likely due to the decreased protein levels of Rax2-CAH compared to Rax2-HTB in the input (Figure 4.4).

I decided to optimise the conditions for Rax2-HTB purification and carry out live-cell imaging in a separate Rax2-mECitrine strain rather than troubleshoot why the protein levels of Rax2-CAH vary between *birA*+ and *birA*- strains. It would have been possible to simply increase the cell mass used for purification to counteract the decreased protein yield per gram of cells. However, the Rax2-CAH protein levels in *birA*+ background were abnormally low compared to wild type and this lead to an impairment of Rax2 functional as a growth-memory cue. Therefore, this strain is not suitable for use in purification and imaging experiments. It is possible that Rax2-CAH in a *birA*+ background is degraded at a higher rate than wild type Rax2. This may lead to an increase in the number of proteins involved in protein degradation interacting with Rax2. Proteins involved in degradation may be detected as Rax2 interactors in cross-linking and mass spectrometry experiments of Rax2-CAH *birA*+, which may not normally interact with wild-type Rax2.

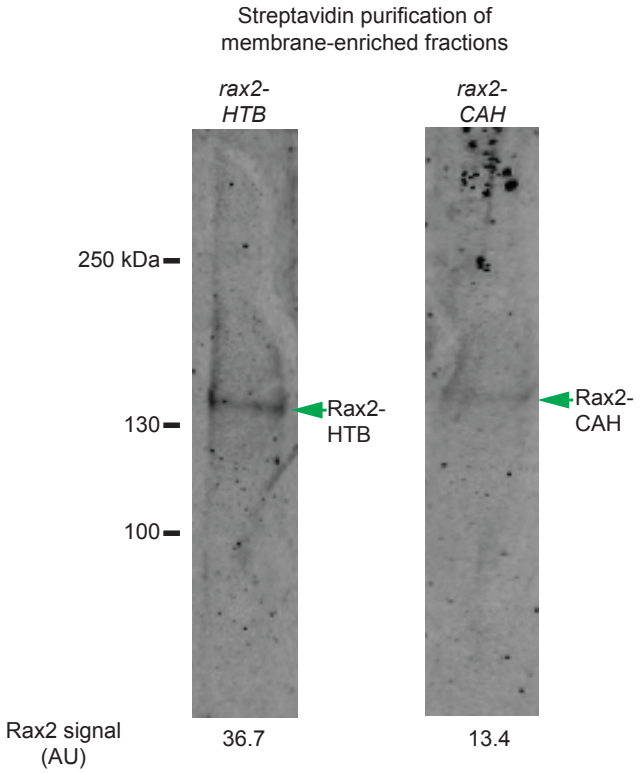

Figure 4.4: The yield of purified Rax2-CAH per gram of cells is approixmately one third of the yield of Rax2-HTB. Anti-Rax2 Western blot, protein samples treated with PNGase F. Equal cell equivalents loaded per lane..

4.4 Rax2-HTB purification conditions were optimised for bead volume, cross-linker conditions and incubation times

In my initial experiments described in sections 4.2 and 4.3 I used Nanolink beads. Nanolink beads are 0.8 µm in diameter with multilayers of covalently cross-linked streptavidin. Their large surface area means that they have a high binding capacity for biotin. However, during boiling, which is required for protein elution from the beads, a large amount of streptavidin dissociates from the beads. The cross-linked streptavidin eluted from the beads forms a ladder of bands on the gel (Figure 4.5A).

The ladder of cross-linked streptavidin could have interfered with my subsequent experiments, which involved gel purification of cross-linked and purified Rax2-HTB. If streptavidin was eluted in large amounts relative to my proteins of interest, the streptavidin may have contaminated the sample sent for mass spectrometry. Additionally, any streptavidin that eluted at a similar molecular weight to Rax2-HTB would make identification of the Rax2-HTB band difficult. Therefore, I trialled a range of different streptavidin beads to see if less streptavidin eluted from the beads during boiling, and if they would be more suitable for my experiments.

I investigated how much streptavidin elutes from four different streptavidin Dynabeads. Streptavidin Dynabeads beads have a single layer of streptavidin attached directly to their surface, and as a result, the streptavidin may be less likely to dissociate from beads during elution.

1. M-270: 2.8 µm diameter, blocked with BSA
2. M-280: 2.8 µm diameter
3. C1: 1 µm diameter
4. T1: 1 µm diameter, blocked with BSA

M-270 and T1 beads are blocked with BSA and are mainly used for RNA/DNA based studies where the proteome will not be assessed and therefore any dissociated BSA will not affect the results. Streptavidin does not dissociate from the Dynabeads during boiling (Figure 4.5A). A faint band

corresponding to BSA was eluted from the M-270 and T1 beads (Figure 4.5A).

Next, I compared the binding efficiency of 4 µl of each bead slurry (as provided by the manufacturer) to purify Rax2-HTB from 1 g of frozen cell powder. The NanoLink beads had by far the highest binding efficiency Rax2-HTB (Figure 4.5B). The 1 µm C1 beads had better binding efficiency than the 2.8 µm M-280 beads (Figure 4.5B). This is most likely due to the increased surface area of the C1 beads. BSA blocking of the beads does not lead to a significant difference in the amount of Rax2-HTB purified from either the 1 µm or the 2.8 µm beads (Figure 4.5B).

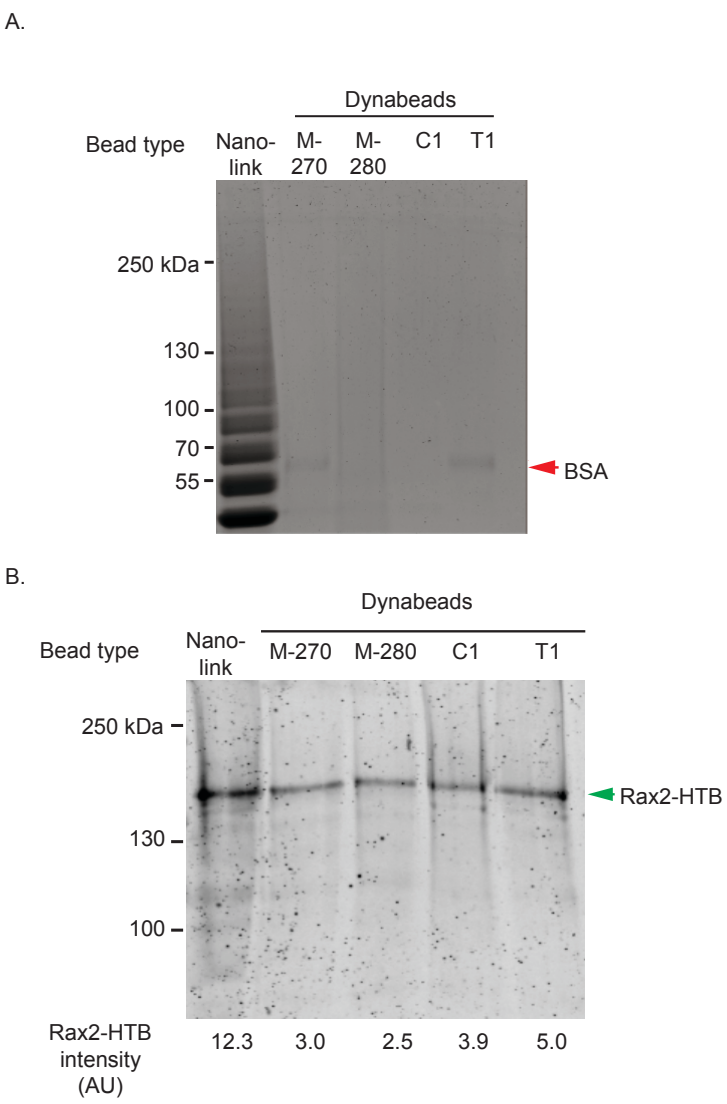

Figure 4.5: Streptavidin does not elute from Dynabeads during boiling but Dynabeads have a lower binding efficiency per µl of bead slurry than Nanolink beads . A. Coomassie stain of beads boiled as a mock elution. B. Anti-Rax2 Western blot of PNGase F treated elutions. An equal volume of bead slurry, as provided by the manufactuers, was used for each bead type.Rax2-HTB band intensity normalised to a region below the Rax2-HTB band, of the appropriate lane, that doesn't contain a protein band.

Ideally, I would like to use beads that do not elute either streptavidin or BSA during boiling. The most suitable candidates are the C1 beads, which are not blocked with BSA, and have streptavidin stably bound. However, per µl of bead slurry, the C1 beads had only one third of the binding efficiency of the Nanolink beads. To increase the yield of Rax2-HTB purified per gram of cells, I increased the bead volume to find the optimum bead volume for Rax2-HTB binding.

Originally I used 4 µl of beads slurry per gram of frozen cell powder. This was optimal for Rax2-HTB binding to Solulink beads. However, due to the decreased binding of Rax2-HTB per µl of C1 beads compared to Solulink, an increased bead volume for the C1 beads may be more optimal. However, adding too many beads may lead to non-specific binding to the beads. I compared the yield of Rax2-HTB by incubating mock PNGase F treated MEFs from 10 g of frozen cell powder and incubated them with 40 µl, 80 µl and 120 µl beads overnight. I increased the scale of the experiment so that it would be more relevant to future large-scale pull-down experiments involving subsequent mass spectrometry analysis. Increasing the bead slurry volume from 40 µl to 80 µl increased the Rax2-HTB yield approximately two-fold, while 120 µl of bead slurry did not further increase the yield (Figure 4.6).

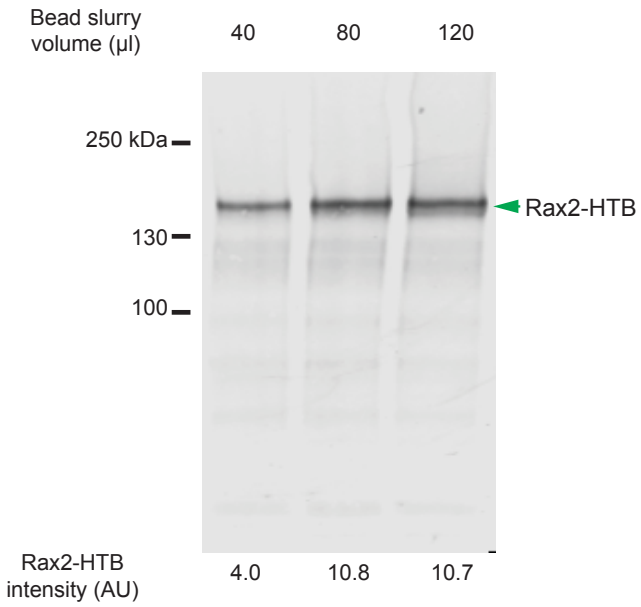

Figure 4.6: 80 µl C1 bead slurry is optimal for Rax2-HTB purification. Anti-Rax2 Western blot of PNGase F treated protein elutions.

The cross-linker disuccinimidyl suberate (DSS) was used to identify interactors of Rax2 through cross-linking and mass spectrometry. DSS forms irreversible cross-links with primary amines and is most reactive with lysine side-chains but also has some reactivity towards serine, threonine and tyrosine side-chains (Kalkhof and Sinz 2008). DSS is suitable for both *in vivo* and *in vitro* cross-linking because it is able to cross cell membranes (Kalkhof and Sinz 2008). However, this means that DSS is not particularly soluble in aqueous solutions and may precipitate if its concentration is greater than a few micromolar.

In my experiments, I have carried out *in vitro* cross-linking in frozen cell grindate. Following cross-linking I created a MEF to enrich for Rax2 and treated samples with PNGase F. For all of my previous experiments I have used a Tris-based buffer. However, a Tris-based buffer is not compatible with DSS cross-linking because Tris contains a primary amino group that DSS will react with. Therefore, I needed to use an alternative buffer that would both be compatible with DSS cross-linking and, following cross-linking, would be compatible for making a MEF to enrich for Rax2 for the first stage of Rax2 purification. The alternative buffer is an $NaPO_4$-based buffer, which is a variant on the buffer Xun used to purify GFP-Mto1-HTB (but without detergent, in order to preserve the integrity of my membrane fraction) (Bao, Spanos et al. 2018). To optimise the cross-linking reaction I first investigated varying the pH of the $NaPO_4$ buffer. Under physiological conditions (pH 7.0-7.5) DSS has a half-life of hours. When the pH of the cross-linking solution is increased the hydrolysis and amine reactivity of DSS increases, resulting in faster cross-linking reaction (Kalkhof and Sinz 2008). After 1 hour of cross-linking at room temperature, I found no difference in the level of cross-linking at pH 7.5, 8.0, or 9.0 (Figure 4.7A). I therefore decided to use pH 7.5, because it is closest to physiological pH. I also investigated a range of temperatures and times for the cross-linking reaction. Decreasing the temperature slows down the rate of the cross-linking reaction and prevents the formation of large cross-linked protein aggregates. Additionally, proteins may be more stable at decreased temperatures as the rate of proteolysis that

may occur in the sample is slowed down. Cross-linking was carried out on ice, at 4 ˚C and at room temperature for both one and two hours. Cross-linking at room temperature for 2 hours was most effective (Figure 4.7B). The chosen reaction conditions were cross-linking in $NaPO_4$ buffer pH 7.5 at room temperature for two hours.

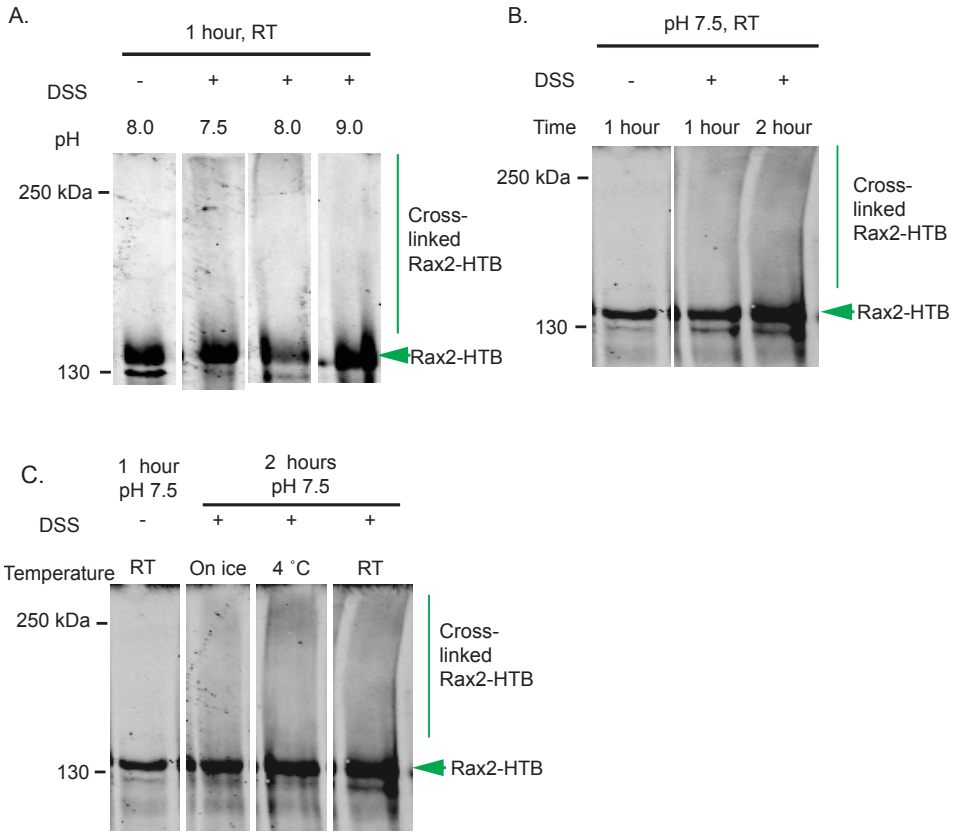

Figure 4.7: Optimal cross-linking conditions are in NaPO4 pH7.5 at RT for 2 hours. Anti-Rax2 Western blot. Membrane enrichment and PNGase F treatment following cross-linking. RT = room temperature.

4.5 Mass spectrometry identification of Rax2 interactors after cross-linking and purification

To isolate proteins from the gel for the mass spectrometry experiment my protocol involved cutting a region of interest from the gel. I cut just above the non-cross-linked Rax2-HTB band and include all of the cross-linked protein above the Rax2-HTB band. This region of the gel then underwent trypsin digestion and mass spectrometry analysis. I chose in-gel digestion over on-bead digestion as this minimises contamination from non-cross-linked Rax2 and other low- molecular weight non-specifically bound proteins. In order to accurately cut out the region of interest I need to be able to clearly detect the Rax2-HTB band using a Coomassie stain. I originally attempted to purify Rax2 from 7 g of frozen cell powder, because this is the amount of frozen cell powder Xun used for purification of GFP-Mto1-HTB. She found that further increasing the cell mass did not increase the peptide intensities detected in mass-spectrometry as identified by label-free quantification (X.Bao thesis). However, after purifying Rax2 from 7 g of frozen cell powder, I could not detect any Rax2 by Coomassie stain. I therefore tested increasing amount of input frozen cell powder (15 , 30 and 60 g). With 60 g of frozen cell powder I observed a distinct Rax2 band by Coomassie staining (Figure 4.8).

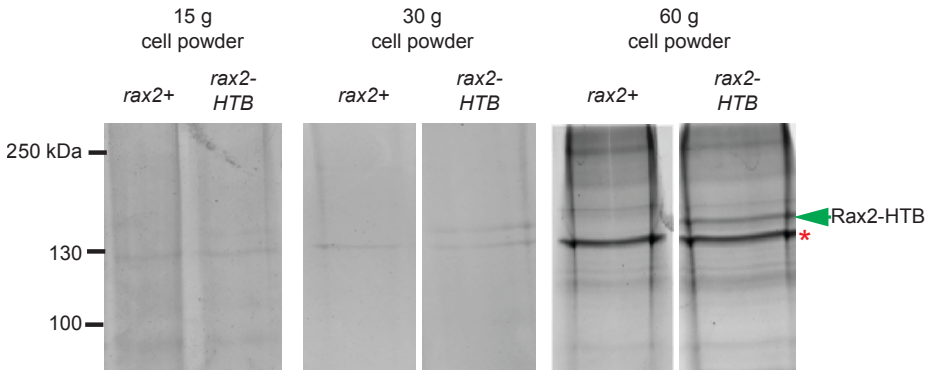

Figure 4.8: A clear band of Rax2-HTB is visible when purified from 60 g of frozen cell powder. Coomassie stain of protein elutions from *rax2+* and Rax2-HTB cell powder incubated with C1 dynabeads. Asterisk next to non-specific band

I performed three rounds of mass spectrometry with independent biological repeat samples of cross-linked wild type (untagged Rax2) and cross-linked Rax2-HTB cells. I used label-free quantification (LFQ) to compare peptide intensities detected in the Rax2-HTB sample to the untagged negative control. Any proteins detected at similar intensities in both Rax2-HTB and negative control are likely to have bound non-specifically to the beads or are also naturally biotinylated proteins. To filter my dataset for proteins that are likely to be true interactors of Rax2, I selected for proteins whose peptide intensity was increased 2-fold or greater in the Rax2-HTB sample relative to the negative control in all three biological replicates (Table 4.2). The identified interactors and their possible relevance to the Rax1-Rax2 memory-based polarity cue are discussed in section 4.6.

Table 4.2: Label-Free Quantification of Rax2-HTB interacting proteins. Three individual runs of mass spectrometry for untagged and Rax2-HTB samples were performed. Each run is a biological repeat. List of proteins that are increased in intensity by greater than two-fold in the *rax2-HTB* sample relative to the *rax2+* control for all three mass spectrometry repeats . Protein column shows the proteins that were identified by mass spectrometry. Peptide counts column represents the number of peptides within one protein that was identified by mass spectrometry. Combined Peptide Intensity is the intestiy of all of the identified peptides of one proteins analysed by MAXQUANT.

Gene ID	Common name	Combined peptide intensity 1		Combined peptide intensity 2		Combined peptide intensity 3	
		rax2+	*rax2-HTB*	*rax2+*	*rax2-HTB*	*rax2+*	*rax2-HTB*
SPAC6F6.06c	*rax2*	0.00E+00	2.13E+09	0.00E+00	1.22E+09	4.31E+07	1.49E+09
SPAC23G3.05c	*SPAC23G3.05c*	0.00E+00	1.30E+08	0.00E+00	1.69E+08	0.00E+00	9.73E+07
SPBC405.02c	*SPBC405.02c*	0.00E+00	1.03E+08	0.00E+00	1.07E+08	0.00E+00	1.00E+08
SPBC29A10.01	*ccr1*	3.66E+07	7.92E+07	1.57E+07	6.29E+07	3.80E+06	3.18E+07
SPBC3F6.05	*rga1*	1.47E+07	4.54E+07	0.00E+00	2.26E+07	0.00E+00	2.25E+07
SPCC663.03	*pmd1*	1.13E+07	4.52E+07	0.00E+00	2.04E+07	0.00E+00	1.37E+07
SPBC19G7.05c	*bgs1*	1.15E+07	4.09E+07	0.00E+00	2.28E+07	0.00E+00	1.39E+07
SPAC19B12.03	*bgs3*	1.78E+07	4.09E+07	3.97E+06	3.61E+07	0.00E+00	8.88E+06
SPAC17D4.03c	*cis4*	0.00E+00	3.31E+07	0.00E+00	4.37E+07	0.00E+00	2.09E+07
SPBC1347.05c	*SPBC1347.05c*	9.66E+06	2.47E+07	0.00E+00	1.38E+07	0.00E+00	2.24E+07
SPBC36B7.03	*sec63*	7.60E+06	1.83E+07	0.00E+00	1.71E+07	0.00E+00	4.03E+07
SPBC16E9.14c	*zrg17*	0.00E+00	1.13E+07	0.00E+00	3.32E+07	0.00E+00	1.18E+07
SPBC13A2.04c	*ptr2*	3.27E+06	1.07E+07	0.00E+00	7.72E+06	0.00E+00	4.34E+06
SPAC1687.16c	*erg31*	0.00E+00	1.01E+07	0.00E+00	4.89E+06	0.00E+00	2.13E+06
SPBC4F6.06	*kin1*	4.57E+06	1.01E+07	0.00E+00	5.41E+06	0.00E+00	8.61E+05
SPBC20F10.07	*SPBC20F10.07*	0.00E+00	6.66E+06	0.00E+00	1.17E+07	0.00E+00	8.75E+06
SPAC22E12.17c	*glo3*	0.00E+00	6.16E+06	0.00E+00	1.74E+06	0.00E+00	7.17E+05
SPAC2C4.17c	*msy2*	0.00E+00	5.70E+06	0.00E+00	9.53E+05	0.00E+00	2.54E+06
SPCC1450.15	*SPCC1450.15*	2.72E+06	5.65E+06	0.00E+00	5.59E+06	0.00E+00	2.62E+06
SPAC29A4.11	*rga3*	0.00E+00	5.14E+06	0.00E+00	1.74E+06	0.00E+00	5.49E+06
SPBC1652.02	*SPBC1652.02*	0.00E+00	3.18E+06	0.00E+00	4.37E+06	0.00E+00	9.07E+05

4.6 Discussion

In this chapter I have described optimisation of Rax2-HTB purification both with and without cross-linking, and I have identified Rax2 interacting partners by cross-linking and mass spectrometry. Below is a discussion for how some of these interactors may play a direct or indirect role in Rax1 and Rax2 function as a growth-memory polarity cue.

4.6.1 Rax1 interacts with Rax2

I expected Rax1 to be an interactor of Rax2 because Rax1 and Rax2 are co-dependent for localisation to the cell tips, and it has previously been shown that $Rax1^{Sc}$ is co-purified with $Rax2^{Sc}$ (Kang, Angerman et al. 2004).

I would be interested to know if the interaction between Rax1 and Rax2 is direct, and if so which regions of Rax1 and Rax2 participate in this interaction. Ideally, I would like to carry out a protein interaction study with purified Rax1 and Rax2. Unfortunately, I am currently unable to generate purified full-length fragments of Rax1 and Rax2. Rax1 and Rax2 fragments can only be expressed at detectable levels in bacteria when their transmembrane domains are removed. However, these shortened fragments may be able to give some insights into which regions of Rax1 and Rax2 participate in the interaction.

4.6.2 Cell-polarity proteins Rga1, Rga3, and Kin1 interact with Rax2

Rga1 and Rga3 are GTPase activating proteins (GAPs) for the Rho-family GTPase Rho1 (Nakano, Arai et al. 1997). Rho1 is an essential gene involved in polarisation of the actin cytoskeleton, cell wall biogenesis and maintenance of the cell wall, but neither Rga1 nor Rga3 are essential (Nakano, Arai et al. 1997). *rga1*∆ cells have delocalised F-actin patches and thickened cell walls and septum (Nakano, Mutoh et al. 2001). *rga3*∆ cells have no significant defects in cell growth, however overexpression of rga3 inhibits cell growth (Nakano, Mutoh et al. 2001) Rga1 and Rga3 localise to the cell tips during tip extension and to the septum during cytokinesis (Nakano, Mutoh et al. 2001) (Ding, Tomita et al. 2000).

Rga1 has been shown to be strongly associated with the insoluble (membrane fraction) and that this association is not simply through its

association with Rho1 (Nakano, Arai et al. 1997). It was proposed that Rga1 might interact with transmembrane proteins at the cell tips (Nakano, Arai et al. 1997). Rax2 may be one of the transmembrane proteins involved in Rga1 localisation at the cell tips. This is likely to be a transient interaction, as Rga1 doesn't remain stably localised at the cell tips during cytokinesis like Rax2 (Nakano, Mutoh et al. 2001). Rax2 could also be involved in Rga3 localisation at the cell tips. However, it has not been shown whether Rga3 is strongly associated with the insoluble fraction like Rga1.

Kin1 is a tyrosine specific protein kinase of the Par-1/MARK protein kinase family (Tassan and Le Goff 2004). Kin1 localises to the cell tips and cell septum and phosphorylates Tea4 and Mod5 (at non-overlapping site with Pom1) (Tassan and Le Goff 2004). Additionally, *kin1*∆ cells have a thicker cell wall than wild type and ß-glucan containing deposits are visible on the lateral cortex (Cadou, Couturier et al. 2010). It is possible that Rax2 is involved in Kin1's role in cell wall organisation at the growing cell tips, as Rax2 had also cross-linked to the cell wall synthesis proteins Bgs1 and Bgs3.

4.6.3 Cell wall synthesis proteins Bgs1 and Bgs3 are Rax2 interactors

(1,3)β-D-glucan is a major component of the cell wall (Cortes, Ishiguro et al. 2002). (1,3)β-D-glucan is synthesised by the enzyme(1,3) ß-D-glucan synthase and two catalytic subunits of the (1,3) ß-D-glucan synthase, Bgs1 and Bgs3, were identified as Rax2-HTB interactors. Bgs3 is essential for cell wall biosynthesis during cell elongation (Martin, Garcia et al. 2003). Bgs1 is involved in cell wall growth and repair and is essential for correct septum formation (Cortes, Ishiguro et al. 2002, Cortes, Konomi et al. 2007). Both Bgs1 and Bgs3 localise to the growing tips during tip extension and to the cell septum during cytokinesis (Cortes, Ishiguro et al. 2002) (Martin, Garcia et al. 2003). Rax2 may be involved in recruiting Bgs3 to the cell tips for cell wall synthesis; Rax2 could be involved in Bgs1 localisation to the cell tips that may be a mechanism to prevent ectopic activity of Bgs1 during interphase.

4.6.4 Rax2 interacts with Erg31, SPCC1450.15 and Ccr1, transmembrane proteins involved in lipid metabolism

Cell growth requires expansion of both the cell wall and plasma membrane. Lipid metabolism is required for plasma membrane growth and remodelling. Erg31 and Ccr1 are involved in ergosterol biosynthesis and SPCC1450.15 is predicted to be involved in lipid metabolism (Iwaki, Iefuji et al. 2008). Ergosterol is the end product of sterol biosynthetic pathways and is the major sterol in yeast (Iwaki, Iefuji et al. 2008). Ergosterol is important for plasma membrane structure and function and for the localisation of plasma membrane proteins (Iwaki, Iefuji et al. 2008). Sterol-rich domains (SRMs) play an important role in polarised growth in yeast (Makushok, Alves et al. 2016). SRMs polarise to the cell tips in a Tea1/Tea4 dependent manner and act as platforms on which growth and polarity machinery assemble (Makushok, Alves et al. 2016). In *tea1*∆ cells, SRMs only localise to the growing cell tip, it is possible that Rax1 and Rax2 could be involved in polarising SRMs to the old end of *tea1*∆ cells.

4.6.5 Proteins involved in the secretory pathway, Cis4, Zrg17, Sec63 and Glo3, interact with Rax2

Rax2 is trafficked to the cell tips through the secretory pathway (S.Ashraf, pers. Comm.). Rax2 may be interacting with Cis4, Zrg17, Sec63 and Gki3 on its journey to the cell tips. Sec63 is predicted to be involved in translocation of proteins across the ER membrane. Glo3 is involved in ER-to-Golgi mediated transport and retrograde transport of proteins from the Golgi to the ER. And Cis4 and Zrg17 are involved in Golgi-to-plasma-membrane transport (Fang, Sugiura et al. 2008).

Limited data is available for Sec63 and Glo3. Sec63 is component of a tetrameric complex consisting of Sec62, Sec63, Sec71 and Sec72. The complex is localised in the ER membrane and is involved in post-translationally targeting proteins to the ER (Vjestica, Tang et al. 2008). Glo3 is predicted to be a GTPase activating protein for ADP ribosylation factor Arf1 and is essential for cell viability. Glo3 is localised in the ER-to-Golgi

intermediate component and is involved in ER-to-Golgi and Golgi-to-ER transport (Hayles, Wood et al. 2013).

Cis4 and Zrg17 are ion channels that form a heteromeric complex to function in Zinc homeostasis in the Golgi (Fang, Sugiura et al. 2008). Deletion of either Cis4 or Zrg17 leads to defects in secretion and cell wall integrity. (Fang, Sugiura et al. 2008) Localisation of the Syb1, a vesicle-associated membrane protein, to the cell tips was greatly decreased in *cis4*Δ in cells and was seen retained in the Golgi (Fang, Sugiura et al. 2008). This demonstrates the requirement for Cis4 and Zrg17 for Golgi-to-plasma-membrane transport of secreted proteins. Cis4 and Zrg17 are not likely to be directly involved in Rax2 localisation or function. However, Rax2 trafficking from the Golgi to the plasma membrane could be impaired in *cis4*Δ and *zrg17*Δ cells.

4.6.6 Transmembrane transport proteins Pmd1, Msy2 and SPBC1652.02 and the protein folding protein SPBC1347.05c are interactors of Rax2

Pmd1, Msy2 and SPBC1652.02 are transmembrane proteins involved in the transport of various cargoes across membranes. Pmd1 is a transporter for the drug Leptomycin across the plasma membrane, Leptomycin B inhibits nuclear export through inactivation of the exportin CRM1, which leads to the nuclear accumulation of proteins that shuttle between the cytoplasm and the nucleus (Kudo, Matsumori et al. 1999) (Iwaki, Giga-Hama et al. 2006). Msy2 is a mechanosensitive calcium ion channel and is localised in the ER membrane. Its role is to control cytoplasmic calcium ion levels as part of the hypoosmotic response (Nakayama, Hirata et al. 2014). SPBC1652.02 is predicted to be an amino acid transmembrane transporter and is localised in the lumen of the ER.

Based on the functions or predicted functions of these proteins as transport channels, it is not immediately apparent how these proteins are functionally relevant interactors or Rax2 as part of the growth-memory cue. They may cross-link with Rax2 due to their close proximity in the membrane or may function in combination with Rax2 in a role independent from Rax2's role as a growth-memory cue.

SPBC1347.05c contains a DNAJ domain, which is a hallmark of chaperone proteins. Because of this domain SPBC1347.05c is predicted to be involved in protein folding, and most likely may have a role in ensuring that Rax2 is folded correctly (Qiu, Shao et al. 2006).

4.6.7 SPBC405.02c is a promising candidate as a Rax2 interactor

SPBC405.02c is an uncharacterised transmembrane protein. However, together with Rax1 and Rax2 itself, it was one of the top three proteins most increased in abundance in the Rax2-HTB sample relative to the untagged negative control. In the next chapter I describe experiments that show that SPBC405.02c is involved in the Rax1-Rax2 growth-memory cue. For reasons described in the next chapter, I have named *SPBC405.02c lrx1.*

Chapter Five: Lrx1 is required for Rax1 and Rax2 localisation at the cell tips

5.1 Introduction

In Chapter four, I carried out cross-linking and mass spectrometry, with the aim to identify novel interactors of Rax2 that play a functional role in the growth-memory cue. A protein of interest identified in these experiments was a previously uncharacterised transmembrane protein, SPBC405.02c, which I shall refer to as Lrx1. Lrx1 was a notable hit as an interactor because it was detected consistently in the top three most abundant proteins along with Rax1 and Rax2 (Table 4.2).

At the beginning of this work, there was limited data available regarding *lrx1*. Lrx1 is predicted to be a transmembrane protein by TOPCONS, transmembrane topology prediction software (Bernsel, Viklund et al. 2009), and is a fission yeast specific protein (Zerbino, Achuthan et al. 2018). *lrx1*Δ cells are viable with no morphological defects (Kim, Hayles et al. 2010) (Hayles, Wood et al. 2013). Additionally, Cyclebase 3.0 data suggests that *lrx1* expression may be cell-cycle regulated (Santos, Wernersson et al. 2015).

I first investigated whether Lrx1 plays a role in the growth-memory cue. The growth-memory cue is required for the initial old-end monopolar growth in a wild type background and for old-end growth in *tea1*Δ cells (Figure 1.6). I created *lrx1*Δ *CRIB-3mCitrine* and *lrx1*Δ *tea1*Δ *CRIB-3mCitrine* strains and assessed the growth patterns. I fluorescently tagged Lrx1 to identify its localisation and also investigated whether Lrx1 plays a role in the localisation of Rax1 and Rax2. Finally, I carried out RT-Q-PCR of synchronised cell cultures to confirm whether *lrx1* expression is cell cycle regulated and created non-cell cycle regulated versions of Lrx1 to investigate whether the cell cycle regulation of Lrx1 is important for its role in the growth-memory cue.

In this chapter, I show that Lrx1 is a novel component of the growth-memory cue and plays a role in trafficking Rax1 and Rax2 from the ER to the cell tips. I also confirm that Lrx1 is cell cycle regulated and that disruption of Lrx1 cell-cycle regulation leads to slight growth pattern defects.

5.2 Lrx1 is predicted to be a transmembrane protein

Lrx1 is predicted to have two transmembrane domains, with a N-terminal extracellular region of 385 amino acids, a 21 amino acid cytoplasmic loop and a C-terminal region of just 2 amino acids (Figure 5.1). This topology was generated by TOPCONS (Bernsel, Viklund et al. 2009). TOPCONS generates a consensus of five independent predictions that combine protein hydrophobicity profiles, residue preference on whether the protein is inside or outside the membrane (based on charge because of the 'positive inside rule'), as well as using multiple sequence alignments (Viklund and Elofsson 2008, Bernsel, Viklund et al. 2009) (Reynolds, Kall et al. 2008).

Lrx1 does not have any clear homologs in any other species. In-depth multiple sequence alignments were carried out to identify any evolutionary conserved functional domains of Lrx1. Our collaborator Luis Sanchez-Pulido (Chris Ponting lab, University of Edinburgh) carried out an in-depth alignment of Lrx1 protein sequence against animal and fungal sequences. Lrx1 transmembrane domains were found to have homology with the human protein presenilin enhancer 2 (PEN-2). PEN-2 is a regulatory component of the Alzheimer's disease (AD) -associated γ −secretase complex (Hu, Xu et al. 2017) (Hasegawa, Sanjo et al. 2004). AD-associated γ −secretase is involved in the proteolysis of transmembrane proteins including Amyloid ß precursor protein, which constitutes the amyloid plaques of AD (Hu, Xu et al. 2017) (Dries and Yu 2008). The first transmembrane region of PEN-2 is a reentrant loop, in which the protein enters partly through the membrane and then folds back to exit at the same side it enters, rather than passing across the membrane (Yan and Luo 2010) (Zhang, Yu et al. 2015). The second transmembrane region passes directly across the membrane (Zhang, Yu et al. 2015). Because Lrx1 shares homology with PEN-2 across the described transmembrane regions, it is possible that the initial predicted transmembrane region of Lrx1 might be an insertion loop (Figure 5.1). This would mean that the majority of the Lrx1 sequence is cytoplasmic rather than extracellular, as predicted by the topology software (Figure 5.1).

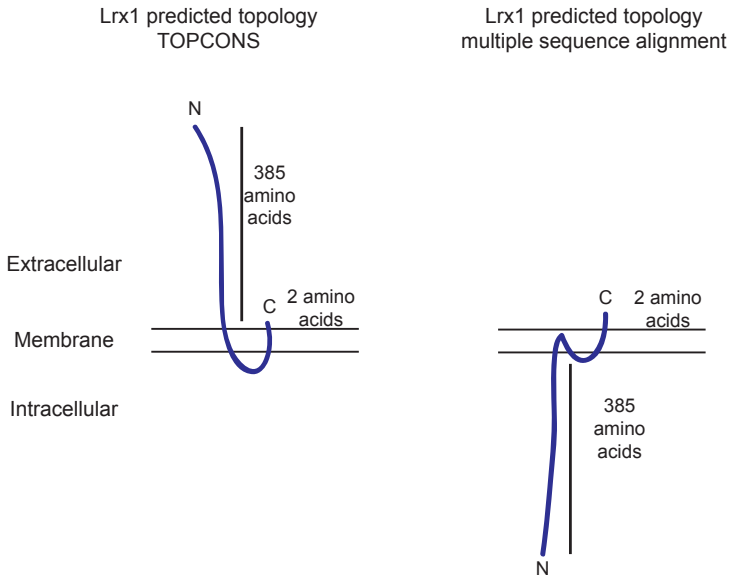

Figure 5.1: Lrx1 is predicted to be a transmembrane protein. Cartoon of the different topologies of Lrx1 generated from TOPCONS and by multiple sequence alignments.

5.3 *lrx1*Δ cells grow in a similar pattern to *rax2*Δ and *rax1*Δ cells

Data from fission yeast genome-wide deletion studies show that *lrx1*Δ cells are viable with no morphological defects (Hayles, Wood et al. 2013) (Kim, Hayles et al. 2010). Consistent with these studies, *lrx1*Δ cells I generated were viable with no morphological defects.

Because I identified Lrx1 as a Rax2-interactor, I wanted to investigate whether *lrx1*Δ cells have growth pattern defects similar to *rax1*Δ and *rax2*Δ. I introduced *lrx1*Δ into a *CRIB-3mCitrine* background and performed time-lapse imaging of daughter-cell growth. 96% of daughter-cell pairs grew in a premature bipolar fashion (Figure 5.2). This is also the most prominent growth pattern of both *rax1*Δ and *rax2*Δ cells (Figure 1.6). A triple deletion of *rax1*Δ *rax2*Δ and *lrx1*Δ resulted in 92% premature bipolar growth. There were no additional growth pattern defects by deleting all three genes, and this suggests that they are working in the same pathway.

The role of Rax1 and Rax2 in the growth-memory cue is most clear from the phenotypes of *rax1*Δ and/or *rax2*Δ in a *tea1*Δ background. In *tea1*Δ cells, the daughter cell that inherits a previously growing cell tip from the monopolar mother is able to reinitiate growth from this old end (due to the Rax1-Rax2 growth-memory cue) (Figure 1.6). By contrast, the *tea1*Δ daughter cell that inherits the cell tip that was not previously growing in the mother cell grows from its new end (Figure 1.6). In *tea1*Δ *rax1*Δ or *tea1*Δ *rax2*Δ cells, both daughter cells grow exclusively from their new ends (Figure 1.6). In *lrx1*Δ *tea1*Δ cells, 80% of daughter-cell pairs grew exclusively from their new ends, in an *Axial* fashion (Figure 5.2). This suggests that in *lrx1*Δ *tea1*Δ cells, the growth-memory cue is lost, as in *rax1*Δ *tea1*Δ and *rax2*Δ *tea1*Δ cells. Daughter-cell pairs in the quadruple mutant *rax1*Δ *rax2*Δ *lrx1*Δ *tea1*Δ also grew in an *Axial* pattern. Again, there were no synergistic effects of deleting a combination of *rax1, rax2* and *lrx1* compared to deleting them individually (for example there was no increase in cells losing polarity or cells forming branches). This again supports the idea that these three genes are involved in the same pathway.

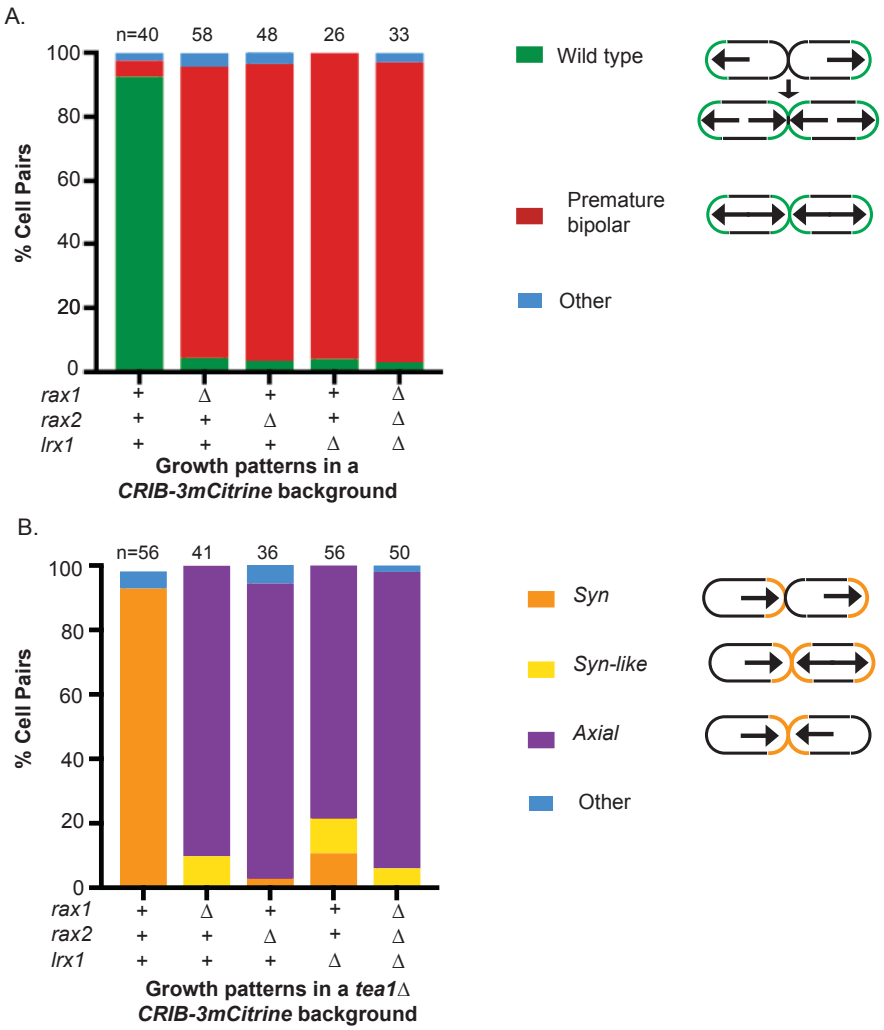

Figure 5.2: *lrx1*Δ cells grow in a similar pattern to *rax1*Δ and *rax2*Δ cells. Quantification of growth patterns of daughter-cell pairs. A. In a *CRIB-3mCitrine* background growth patterns were classed as Bipolar , Premature Bipolar or Other (any other growth pattern or any cells which stop growing) B. In a *tea1*Δ *CRIB-3mCitrine* background growth patterns were classed as *Axial* *Syn*, *Syn-like* or Other (any other growth pattern or any cells which stop growing) .

5.4 Lrx1 is involved in Rax1 and Rax2 localisation to the cell tips

The growth patterns of *lrx1*Δ and *lrx1*Δ *tea1*Δ cells suggested that Lrx1 is involved in the Rax1-Rax2 growth-memory polarity cue. Because Rax1 and Rax2 are co-dependent for their localisation to cell tips, I investigated whether the tip localisation of Rax1 and Rax2 also requires Lrx1. I found that the localisation of both Rax1 and Rax2 to cell tips involved Lrx1 (Figure 5.3). In *lrx1*Δ cells, *nmt41:*mECitrine-Rax1 and Rax2-mECitrine appeared to co-localise with the ER luminal marker ADEL-mCherry, which suggests they are retained in the ER (Figure 5.3A). However, there was still some enrichment of Rax2-mECitrine at the cell tips in *lrx1*Δ cells. Rax2 enrichment at the cell tips in *lrx1*Δ cells was half of that in *lrx1+* cells (Figure 5.3B). This Rax2 tip enrichment in *lrx1*Δ was significantly higher than in *rax1*Δ (Figure 5.3B). Any Rax2 tip signal observed in *rax1*Δ cells was assumed to be due to Rax2 trapped in ER localised at the cell tips (Figure 5.3B). This suggests that additional Rax2 observed at the tips in *lrx1*Δ cells compared to *rax1*Δ cells had trafficked to the plasma membrane. Lrx1 appears to increase the efficiency of Rax2 (and Rax1) trafficking out of the ER, and may be required for appropriate levels of Rax2 to accumulate at the cell tips. Lrx1, **L**ocalisation of **R**a**X** was named for its role in Rax1 and Rax2 localisation to the cell tips.

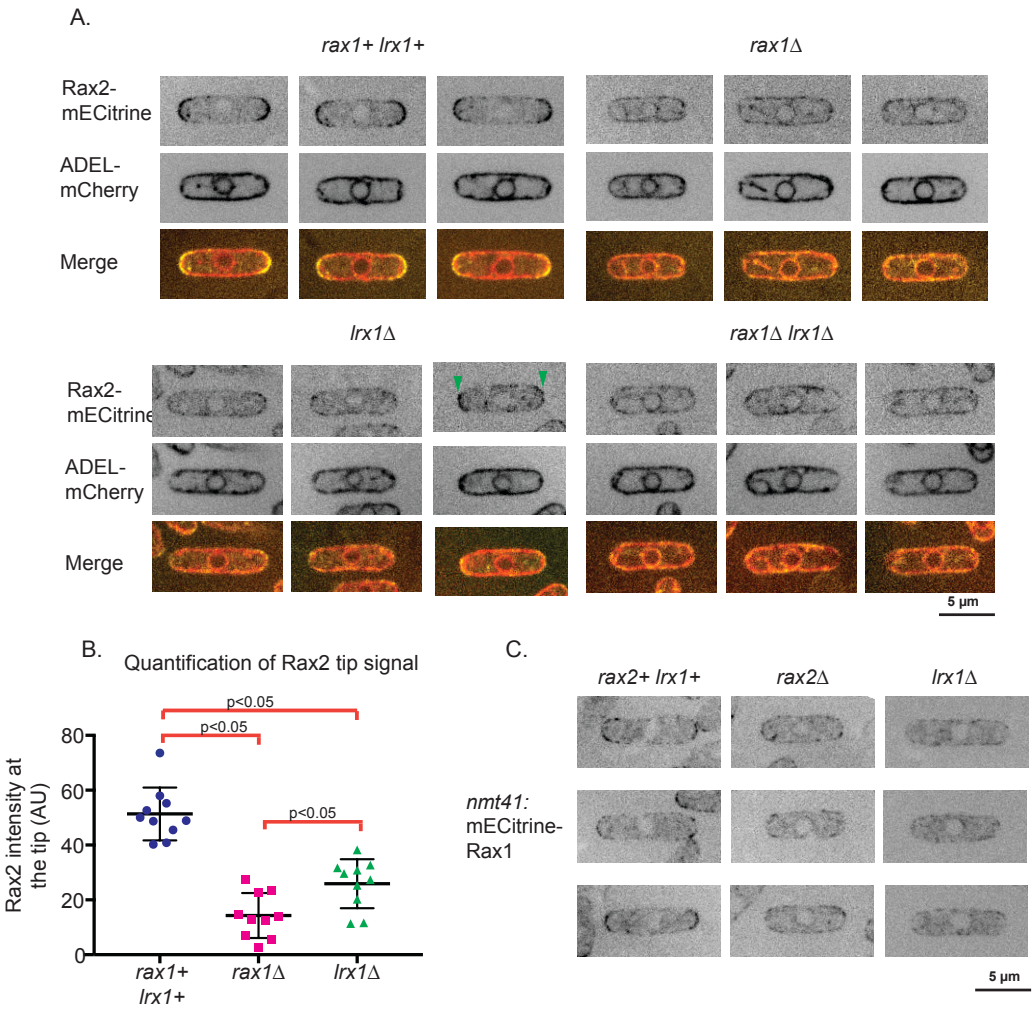

Figure 5.3: Lrx1 is necessary for Rax1 and Rax2 trafficking out of the ER to the cell tips. A. Live-cell imaging of Rax2-mECitrine, ER marker ADEL-mCherry. Images taken on the confocal spinning disk microscope, cells grown in YE5S media. Green arrows indicate mild accumulation of Rax2 at the cell tips of *lrx1*Δ cells. B. Quantification of Rax2 signal at the cell tips in different genetic backgrounds. Normalisation as described in materials and methods 2.13.3. Median and interquartile ranges are shown. All pairwise comparisons were significant (Mann–Whitney test; P<0.05) C. Live-cell imaging of nmt41:mECitrine-Rax1. Images taken on the confocal spinning disk microscope, cells grown in YE5S media.

Furthermore, Rax2 was still observed at the septum in *lrx1*Δ cells (Figure 5.4). In wild-type cells, the intensity of Rax2 signal at the cell septum is weak in comparison to signal at the cell tips (Figure 5.4). I imaged the growth marker mCherry-Bgs4 at the same time as Rax2-mECitrine, which allowed clear identification of septating cells and interphase cells (Cortes, Carnero et al. 2005) (Figure 5.4A). This Rax2 enrichment at the septum was not due ER (containing Rax2) being enriched at the cell tips, as the Rax2 septum enrichment was not co-localised with the ER marker ADEL-mCherry (Figure 5.4C). This implies that Rax2 can be trafficked to the cell septum by a Lrx1 independent mechanism.

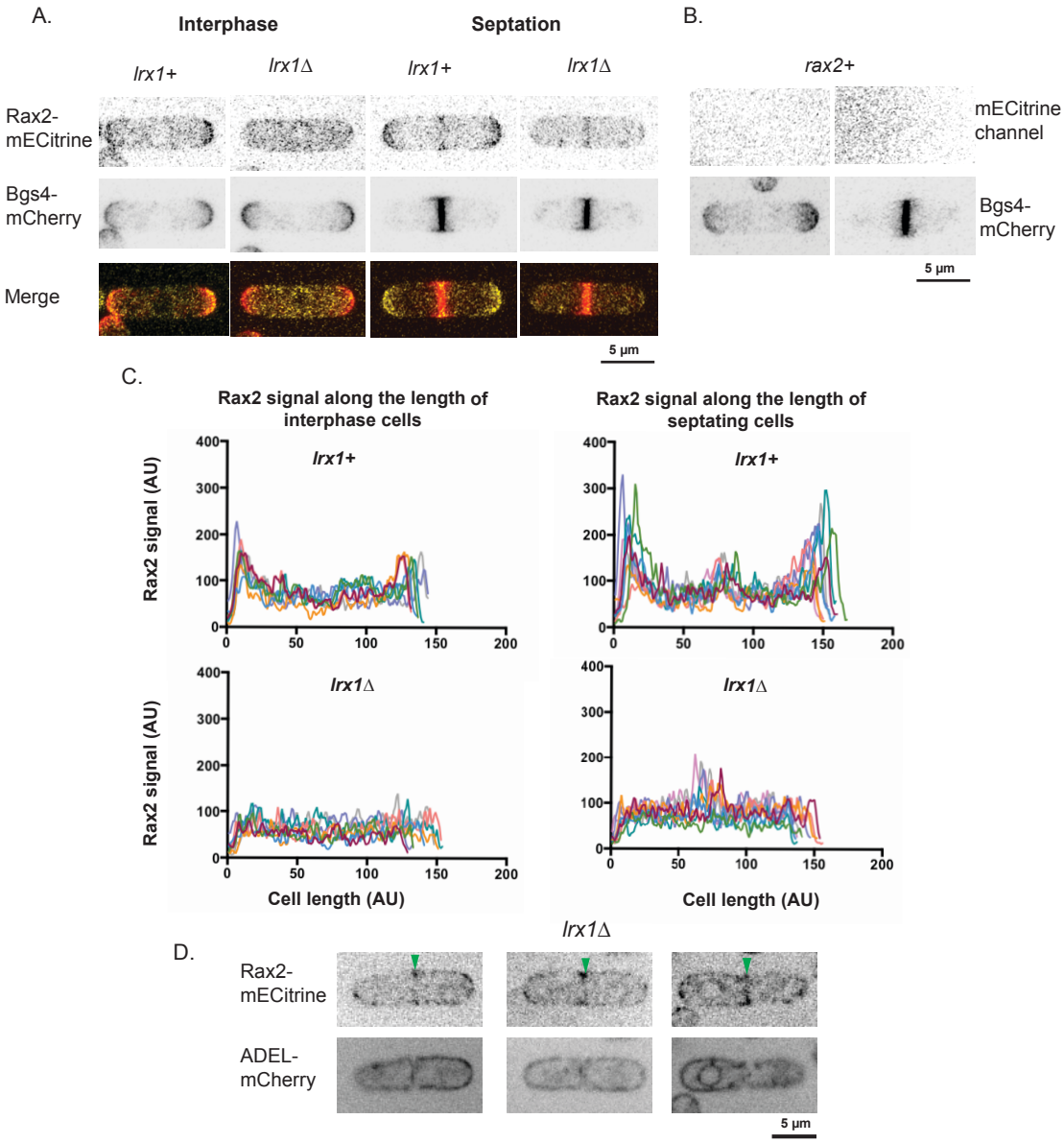

Figure 5.4: Rax2 localises to the septum independently of *lrx1*. A. Live-cell images of Rax2-mECitrine and Beta-glucan synthase mCherry-Bgs4 taken on Airyscan microscope. B.mCherry-Bgs4 imaged without Rax2-mECitrine to demonstrate no bleedthrough C. Rax2 signal intensity profiles. A line 20 pixels wide was drawn along the whole length of the cell. The total signal at each point along the line was plotted for Rax2-mECitrine signal in both *lrx1+* and *lrx1Δ* cells during septating and interphase. D. Rax2 localisation to the septum is independent of ER enrichment. Live-cell images of Rax2-mECitrine and ADEL-mCherry taken on confocal spinning disk microscope. Green arrows indicate Rax2 septum signal.

5.5 Lrx1 is dependent upon Rax1 and Rax2 to localise to the cell tips

I next investigated whether Lrx1 had similar localisation to Rax1 and Rax2. When imaged in repressive conditions for the *nmt41* promoter (media containing thiamine), *nmt41:*mECitrine-Lrx1 was enriched at the cell tips, similar to Rax1 and Rax2 (Figure 5.5). In media lacking thiamine, *nmt41:*mECitrine-Lrx1 is highly expressed and detected throughout the cell in what appears to be many small vacuoles (Figure 5.5). Work is currently in progress to image mECitrine-Lrx1 expressed under its endogenous promoter.

Because Rax1 and Rax2 localisation to cell tips is co-dependent and also dependent upon Lrx1, I was interested as to whether Rax1 and Rax2 are required for Lrx1 localisation to cell tips. I imaged *nmt41:*mECitrine-Lrx1 in *rax1*∆ and *rax2*∆ backgrounds and found that Lrx1 localisation to the cell tips depends on both Rax1 and Rax2 (Figure 5.5). Differently to Rax1 and Rax2, Lrx1 does not appear to be retained in the ER in *rax1*∆ and *rax2*∆ cells (Figure 5.3, Figure 5.5). This suggests that Lrx1 localisation to cell tips is dependent on Rax1 and Rax2 but Lrx1 trafficking out of the ER is not dependent upon Rax1 or Rax2.

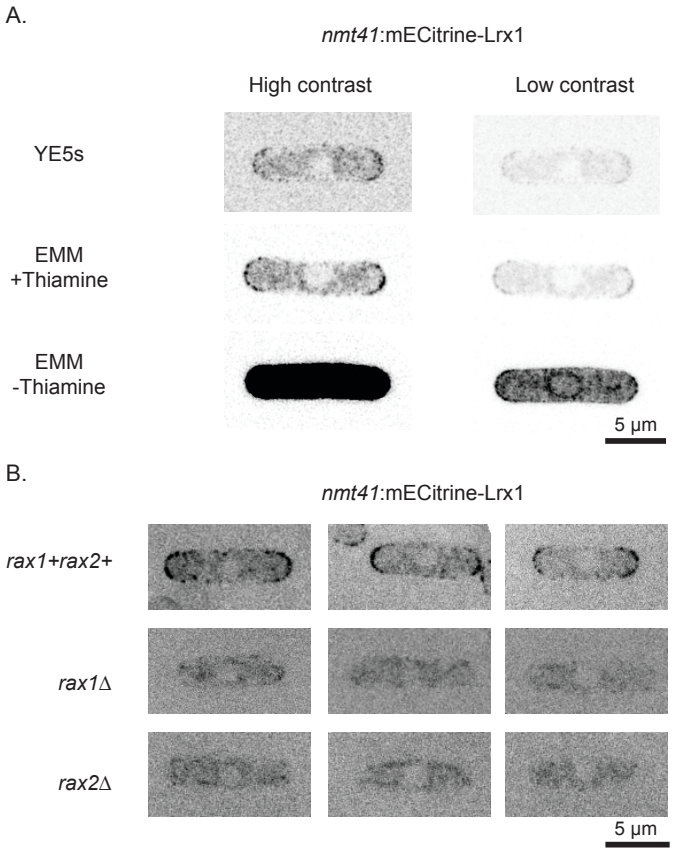

Figure 5.5: *nmt41:*mECitrine-Lrx1 is visible at the cell tips when imaged in media containg thiamine, Lrx1 localisation to the cell tips is dependent upon Rax1 and Rax2. A. Images taken on the Airyscan microscope. High contrast settings Minimum = 0 Maximum = 370. Low contrast settings Minimum = 0 Maximum = 1100. B. Images taken on the confocal spinning disk microscope.

5.6 Lrx1 expression levels peak during interphase

If trafficking of Rax1, Rax2 and Lrx1 out of the ER were increased during interphase compared to during cell division, this could potentially explain how the growth-memory cue accumulates at cell tips and not at the septum. Cyclebase 3.0 data suggests that there is an increase in expression of *lrx1* during interphase (Santos, Wernersson et al. 2015), raising the possibility that Lrx1 regulates trafficking of the growth-memory cue out of the ER. I therefore decided to examine Lrx1 expression levels through the cell cycle in my own experiments.

Because Lrx1 appears to be part of the growth-memory cue, it would be expected to be a stable protein. This means that any regulatory changes in the free pool of Lrx1 throughout the cell cycle may be difficult to distinguish from the stable pool of Lrx1 at the cell tips by western blotting. Instead, I investigated whether *lrx1* mRNA levels are regulated during the cell cycle, using reverse transcriptase-quantitative-polymerase chain reaction (RT-Q-PCR). I measured *lrx1* mRNA levels in synchronised *cdc25-22* mutant cells. Cdc25 activates cyclin dependent kinases through dephosphorylation of the Cdk active site for the cell to enter mitosis (Miller and Johnson 1994). *cdc25-22* mutants arrest at G2/M of the cell cycle at the restrictive temperature (36 ˚C) and re-enter the cell cycle when returned to the permissive temperature (25 ˚C) (Fantes 1979). I synchronised *cdc25-22* mutant cells through temperature-shift and release and analysed levels of *lrx1* mRNA at 20-minute intervals. Firstly, I assessed cell-cycle synchrony by counting the septation index and by analysing two known highly cell-cycle regulated genes, *chr1* and *gas1,* through RT-Q-PCR. Cyclebase 3.0 data suggests that *gas1* mRNA levels peak at late G2 and *chr1* levels peak in early G1 (Santos, Wernersson et al. 2015). My experiments were consistent with Cyclebase 3.0, *chr1* and *gas1* mRNA levels peaked prior to septation and *gas1* RNA levels peak earlier than *chr1,* and this suggests that my cells are synchronised (Figure 5.6). *lrx1* mRNA levels peaked at mid-G2, and at this stage *lrx1* mRNA levels were ten-fold increased compared to the mRNA levels immediately following release from the cell cycle arrest (Figure 5.6).

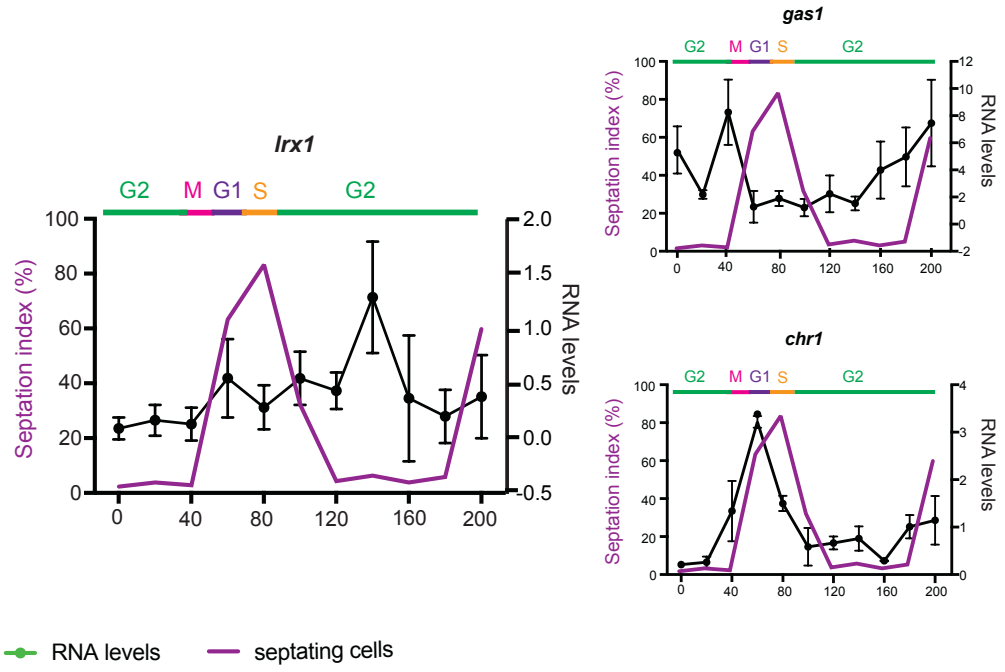

Figure 5.6: Lrx1 RNA levels peak at Mid-G2. RT-Q-PCR of RNA extracted from *cdc25-22* synchronised cell cultures. Time point 0 is immediately following 4 hour incubation at 36 ˚C, samples taken every 20 minutes from cultures incubated at 25 ˚C. Normalisation of *lrx1, gas1* and *chr1* RNA levels described in materials and methods. Black line: mean and standard deviation of RNA levels from 4 replicates (2 repeats of 2 biological replicates). Purple line: septation index.

The l*rx1* mRNA expression profile suggests a model in which Lrx1 plays a regulatory role in targeting the growth-memory cue 1) to cell tips during G2 and 2) not to the septum during cell division (Figure 5.7). Immediately following septation, *lrx1* levels are low. At this time, Rax1 and Rax2 are localised at the old end due to inheritance from the previous cell cycle (Figure 5.7A). Later in G2, cells transition to bipolar growth. Simultaneous with this, Lrx1 expression increases, and Rax1 and Rax2 are trafficked to the cell tips, resulting in Rax1 and Rax2 localised at both cell tips by the end of the cell cycle (Figure 5.7B). Later, during septation, *lrx1* levels are again decreased, so that there is a decrease in Rax1 and Rax2 trafficking out of the ER, and thus decreased levels of Rax1 and Rax2 delivered to the septum (Figure 5.7C).

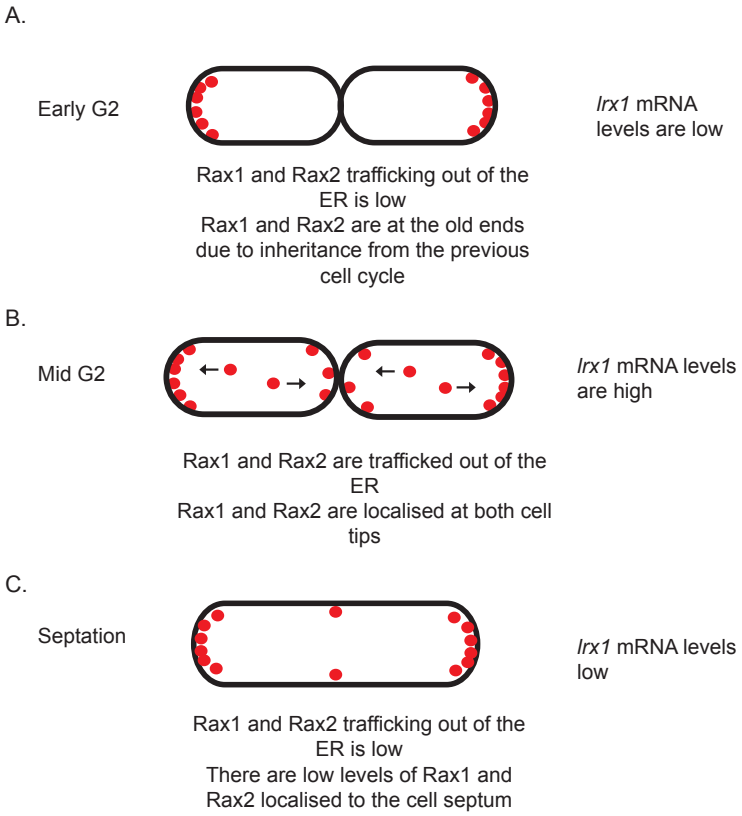

Figure 5.7: Model for how *Irx1* expression levels regulate trafficking of Rax1 and Rax2 to the cell tips. A. At early G2 there is sufficient Rax1 and Rax2 at the old end of the cell, low *Irx1* levels prevent excess Rax1 and Rax2 being delivered to the old end. B. By mid-G2 cells are growing in a bipolar manner, Rax1 and Rax2 are trafficked to the new ends due to increased *Irx1* levels. C. At septation, *Irx1* levels are low and there are low levels of Rax1 and Rax2 delivered to the cell tips.

5.7 Misregulation of Lrx1 expression leads to minor growth pattern defects

If cell-cycle regulation of Lrx1 is responsible for timely Rax2 localisation to cell tips and not the septum, I would expect Rax2 localisation at the septum to be increased following disruption of cell-cycle regulation of *lrx1* expression. I expressed *lrx1* under control of the *nmt41* and *nmt81* promoters to investigate whether non-cell-cycle regulated expression or overexpression of *lrx1* leads to any changes in Rax2 localisation and whether this leads to changes in cell growth patterns. *nmt81:lrx1* and *nmt41:lrx1* RNA levels were compared to the endogenous *lrx1* RNA levels in unsynchronised cell cultures to investigate to the extent of *lrx1* overexpression when controlled by these promoters. In media containing thiamine, average *nmt81*:*lrx1* mRNA levels were similar to endogenous *lrx1* levels. In media lacking thiamine, average *nmt81:lrx1* mRNA levels were approximately double those of endogenous *lrx1* (Figure 5.8A). Average *nmt41:lrx1* mRNA levels were 1.5 fold increased compared to endogenous *lrx1* in media supplemented with thiamine and four-fold increased in media lacking thiamine (Figure 5.8A).

To investigate whether disrupting cell cycle regulation of *lrx1* affects Rax2 localisation I imaged Rax2-mECitrine in *nmt41:lrx1* and *nmt81:lrx1* cells. The cells were imaged in rich media (which contains thiamine) both to be consistent with previous imaging experiments and so that high *lrx1* levels did not affect Rax2 localisation. Rax2 localisation at both the cell tips and the septum was not changed by disruption of *lrx1* cell cycle regulation. The intensity of Rax2-mECitrine was not significantly different at neither the cell tips nor septum between *lrx1+* and *nmt41:lrx1* or *nmt81:lrx1* cells (Figure 5.8B).

Misregulation of *lrx1* expression may lead to changes in the growth pattern independently of the effect of *lrx1* expression has on Rax2 localisation to the septum. I analysed the growth patterns of *nmt81:lrx1* and *nmt41:lrx1* cells. Again, the cells were grown in rich media, to be consistent with previous growth pattern experiments and to prevent any additional growth defects due to *lrx1* overexpression. For both *nmt81:lrx1* and *nmt41:lrx1* cells the number of cells growing in a premature bipolar fashion was increased (Figure 5.8C).

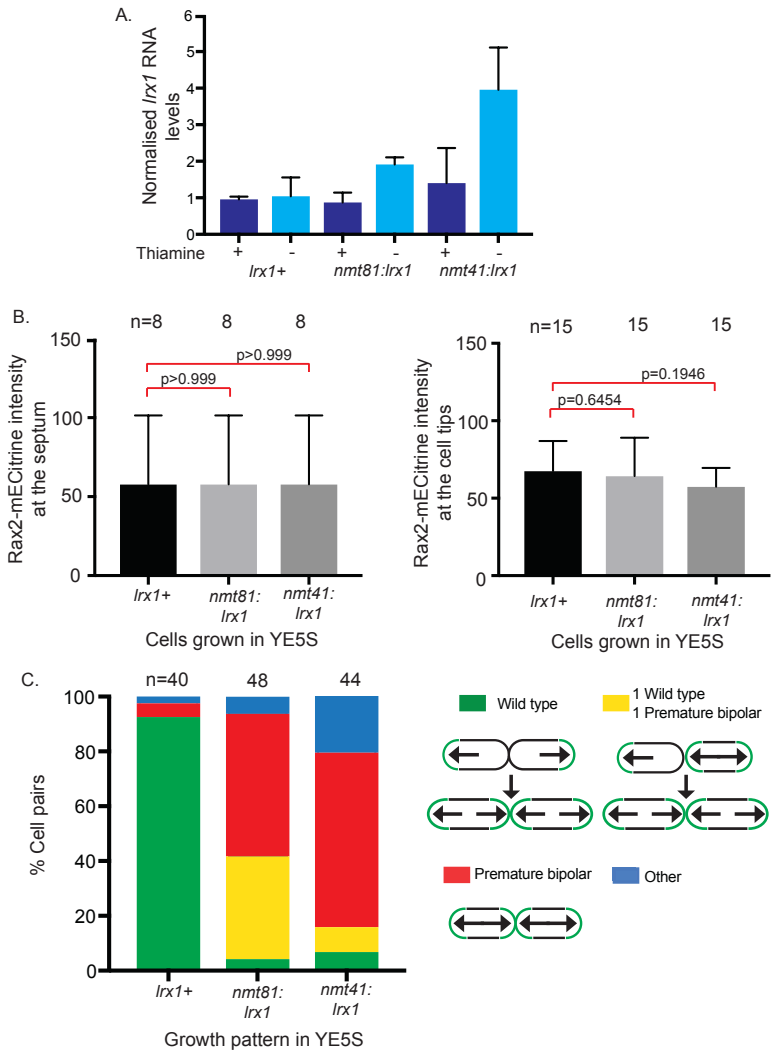

Figure 5.8: *lrx1* overexpression leads to minor growth pattern defects A. *lrx1* RNA levels of unsynchronised cultures grown in minimal media with and without thiamine supplementation, normalised as described in materials and methods. Mean and standard deviation of four repeats (two technical repeats of two biological replicates).All pairwise comparisons were not significant (Mann–Whitney test; P>0.05) B. Rax2-mECitrine intensity at the septum and tips of *lrx1+*, *nmt41:lrx1* and *nmt81:lrx1* cells. Mean and standard deviation. C. Quantification of growth patterns of daughter cell pairs.

There are two possible reasons for why the cells grow in a premature bipolar pattern (Figure 5.9A). Either the growth-memory cue is impaired in function, as premature bipolar growth is seen in *rax1*Δ*, rax2*Δ and *lrx1*Δ cells, or the growth memory cue has ectopic function at the new end (in addition to the old-end) (Figure 5.9A). The current experiments I have carried out are not sufficient to support either of these hypotheses. Further experiments to understand how misregulation of expression of *lrx1* affects the function of the growth-memory cue should be done in a *tea1*Δ background. If non-cell cycle regulated expression of *lrx1* leads to impaired function of the growth-memory cue, cells should grow in an *Axial* pattern in a *tea1*Δ background (similar to *tea1*Δ *lrx1*Δ) (Figure 5.9B). If non-cell cycle regulated expression of *lrx1* in *tea1*Δ cells leads to ectopic function of the growth-memory cue at the new ends in addition to at the old ends, cells should grow in a premature bipolar fashion (Figure 5.9B). Additionally, further experiments could involve expressing *lrx1* under a promoter that peaks in expression during cytokinesis, to see if this leads to increased Rax1 and Rax2 localisation to the septum.

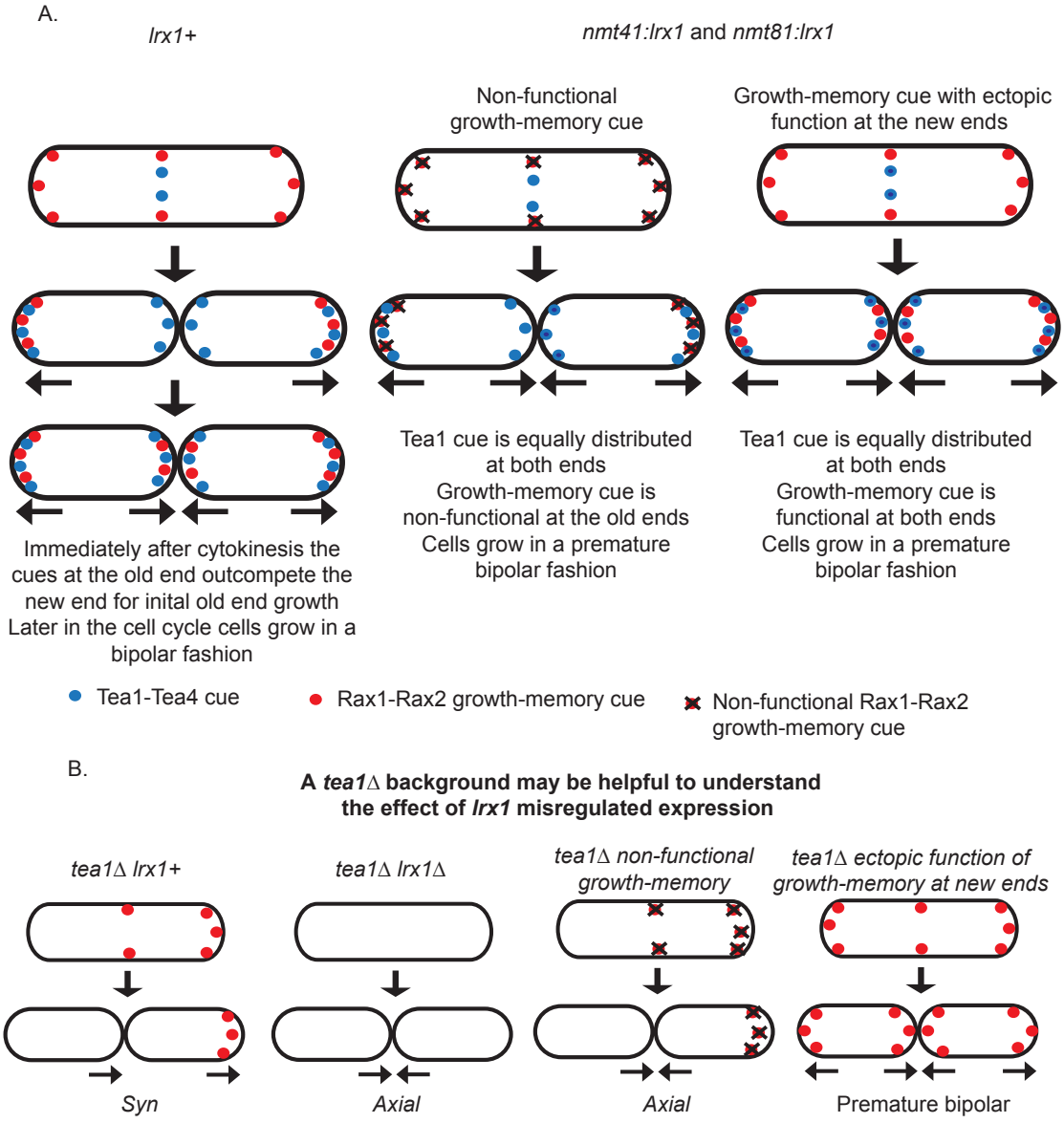

Figure 5.9: *lrx1* misregulation of expression may lead to bipolar growth due to impaired function or ectopic function of the growth-memory cue. A. Cartoon model for premature bipolar growth in *nmt41:lrx1* and *nmt81:lrx1* cells. B. Cartoon model for possible growth patterns in *nmt41:lrx1 tea1*Δ and *nmt81:lrx1 tea1*Δ cells.

5.8 Discussion

In this work, I have characterised a novel component of the growth-memory cue, Lrx1. Lrx1 is essential for the memory of cell-tip growth from one cell cycle to the next, and Lrx1 plays an important role in Rax1 and Rax2 trafficking out of the ER for localisation to the cell tips (Figure 5.2, Figure 5.3). In this discussion I compare the data I have generated regarding Lrx1 to $Bud8^{Sc}$ and $Bud9^{Sc}$ (known interactors of $Rax1^{Sc}$, $Bud8^{Sc}$ and $Bud9^{Sc}$ play an important role in bipolar budding along with $Rax1^{Sc}$ and $Rax2^{Sc}$). I propose that Lrx1 may be a functional homolog of $Bud8^{Sc}$ and $Bud9^{Sc}$.

5.8.1 Lrx1 is a transmembrane protein of undetermined topology

I was not able to confirm the topology of Lrx1 from my experiments. However, I predict that the N-terminus may be extracellular and that Lrx1 has a similar topology to $Bud8^{Sc}$ and $Bud9^{Sc}$ (Figure 5.10A). The N-terminus of $Bud8^{Sc}$ and $Bud9^{Sc}$ is glycosylated, which suggests that the N-termini of $Bud8^{Sc}$ and $Bud9^{Sc}$ are extracellular (Figure 5.10B) (Harkins, Page et al. 2001). I analysed whether Lrx1 has any predicted N-glycosylation sites using the NetNGlyc 1.0 Server (Gupta et al. 2004). The server predicted that Lrx1 has 6 potential N-glycosylation sites. All the predicted N-glycosylation sites are within the N-terminal region, which is predicated to be extracellular by TOPCONS (Figure 5.9).

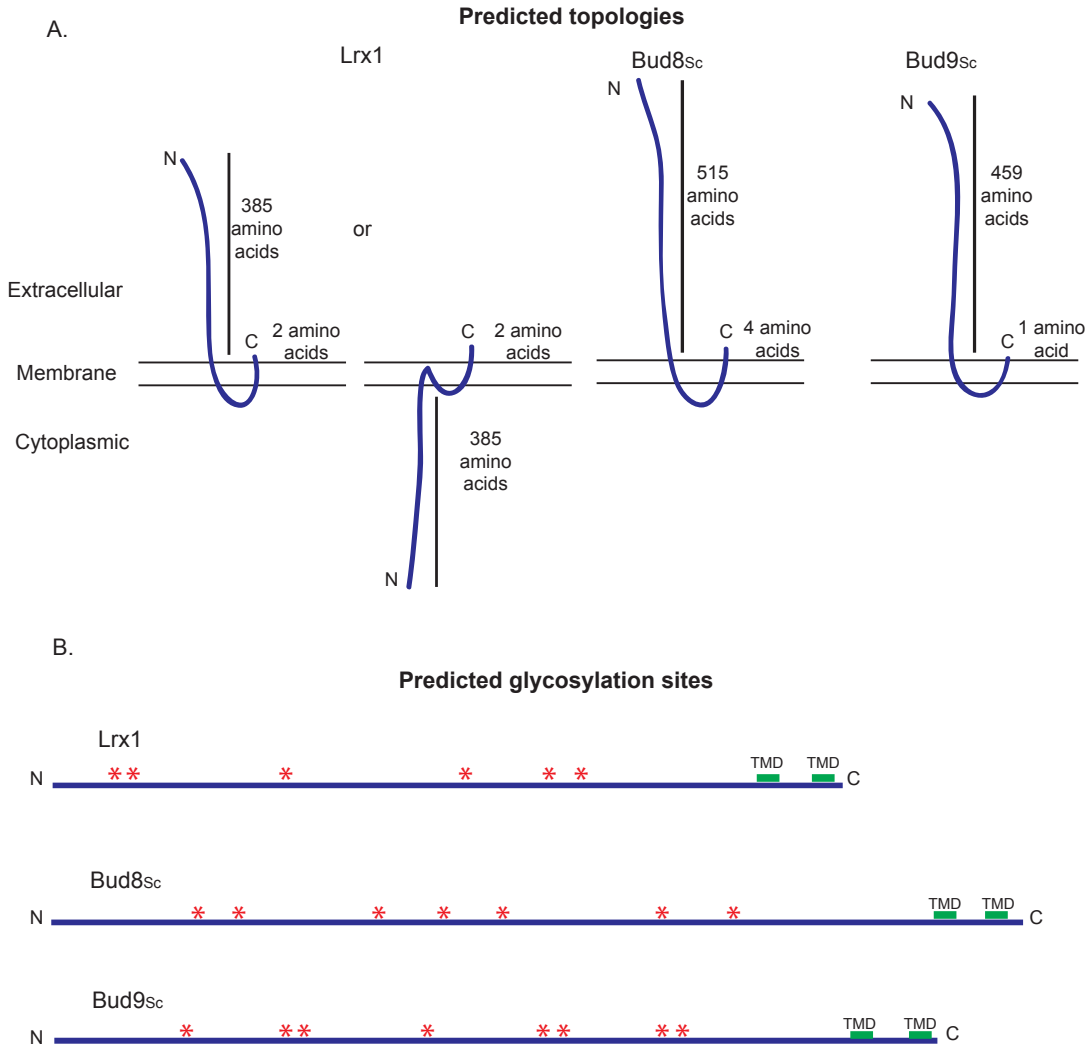

Figure 5.10: Lrx1 may have a similar topology to Bud8Sc and Bud9Sc A. Cartoon of predicted topologies of Lrx1, Bud8Sc and Bud9Sc, adapted from TOPCONS output . B. Cartoon of predicted N-glycosylation sites. Red asterisk =position of predicted N-glycosylation site. TMD = transmembrane domain. Adapted from NetNGlyc 1.0 server (Gupta et al., 2004)

PNGase F treatment and western blotting would confirm whether Lrx1 is N-glycosylated or not and may provide insights into the topology of Lrx1. If Lrx1 has a similar topology to Bud8^{Sc} and Bud9^{Sc}, this would be consistent with the hypothesis that Lrx1 could be a functional homolog of Bud8^{Sc} and Bud9^{Sc}.

5.8.2 Rax1, Rax2 and Lrx1 are co-dependent for localisation to the cell tips

Rax1 and Rax2 required Lrx1 for efficient targeting to the cell tips, in particular for trafficking out of the ER (Figure 5.3). Rax2 enrichment at the cell tips in *lrx1*Δ cells was approximately half that of *lrx1*+ cells (Figure 5.3) and Rax2 localisation to the septum was not affected by *lrx1*Δ (Figure 5.4). Rax2 did not localise to the cell tips or septum in *rax1*Δ cells. This suggests that Rax2 is capable of trafficking out of the ER independently of *lrx1,* albeit inefficiently. This impaired, but not completely abolished localisation of Rax2 to the cell tips in *lrx1*Δ cells was reminiscent of the reduced, but not completely abolished, localisation of Rax2^{Sc} to bud sites in *bud8*^{Sc}Δ/*bud8*^{Sc}Δ cells (Rax1^{Sc} and Rax2^{Sc} localisation to the bud sites is not impaired in *bud9*^{Sc}Δ/*bud9*^{Sc}Δ cells)(Kang, Angerman et al. 2004)(Figure 1.9).

Unlike Rax1 and Rax2, which were retained in the ER when a component of the growth-memory cue was deleted, Lrx1 was mislocalised to vesicles throughout the cytoplasm. This suggests that Lrx1 is able to traffic out of the ER independently of Rax1 and Rax2, but cannot correctly localise to the cell tips. In budding yeast, Bud9^{Sc} is dependent on Rax1^{Sc} and Rax2^{Sc} for localisation to the bud sites, whereas Bud8^{Sc} localisation to bud sites is only partially dependent on Rax1^{Sc} and Rax2^{Sc} (Figure 1.9).

Lrx1 appears to share some similarities with Bud8^{Sc} and Bud9^{Sc}. Like Bud8^{Sc} plays a role in Rax1^{Sc} and Rax2^{Sc} localisation to the bud sites, Lrx1 plays a role in Rax1 and Rax2 localisation to the cell tips. Like Bud9^{Sc} is dependent on Rax1^{Sc} and Rax2^{Sc} for localisation to the bud sites, Lrx1 is dependent on Rax1 and Rax2 its localisation to the cell tips.

5.8.3 Cell-cycle regulation of Lrx1 may have a minor role in regulation of the growth-memory cue independently of its role in Rax1 and Rax2 localisation

lrx1 RNA levels peak at mid-G2, when there is active tip growth. This peak in *lrx1* RNA levels correlates with accumulation of the Rax1-Rax2 growth-memory cue at the cell tips (Figure 5.6). Disrupting the cell cycle expression of *lrx1,* whilst maintaining a similar average expression level, increases the number of cells growing in a premature bipolar manner. Surprisingly, the premature bipolar growth pattern was not due to an increase in Rax2 localised to the cell septum (which would be inherited by the new ends) (Figure 5.8). This suggests that the effect of *lrx1* misregulated expression on the growth pattern is independent of Lrx1's function in the localisation of Rax1 and Rax2.

Cell-cycle regulation of *bud8*^{Sc} and *bud9*^{Sc} is important for their role in bud site selection. *bud8*^{Sc} mRNA peaks at G2/M and *bud9*^{Sc} mRNA peaks at late G1. *bud8*^{Sc} and *bud9*^{Sc} mRNA levels peak just prior to Bud8^{Sc} and Bud9^{Sc} protein delivery to the bud sites (Harkins, Page et al. 2001) (Schenkman, Caruso et al. 2002). The cell-cycle regulation of *bud8*^{Sc} and *bud9*^{Sc} expression plays an important role for their role in bud site selection. Overexpression of *bud8*^{Sc} using the *GAL* promoter leads to random positioning of the growth sites (Harkins, Page et al. 2001). Increased expression (using high-copy plasmids), but with maintenance of cell-cycle regulation of *bud8*^{Sc} and *bud9*^{Sc} under their endogenous promoter leads to a bias of bud-site selection at the distal and proximal pole respectively (Harkins, Page et al. 2001).

The extracellular region of Bud8^{Sc} and Bud9^{Sc} function to recruit the polarity module Rsr1^{Sc}/Bud5^{Sc}/Bud2^{Sc} to the bud sites for bipolar budding. The N-terminus of Bud9^{Sc} (amino acids 91 to 283) and amino acids 72-216 and 268-417 of Bud8^{Sc} are essential for the interaction with Bud5^{Sc} (Cdc25-like protein)(Krappmann, Taheri et al. 2007). It is possible that extracellular region of Lrx1 could form the link between the growth-memory cue in fission yeast and the Cdc42 polarity module. However, Cdc25 was not enriched in Rax2-HTB mass spectrometry (Table 4.2). Lrx1 may promote growth at the cell tips by an

interaction with a different protein to Cdc25, or Cdc25 may be found enriched in cross-linking and mass spectrometry of Lrx1.

5.8.4 Future work

In this chapter I have proposed that Lrx1 could be a functional homolog of $Bud8^{Sc}$ and $Bud9^{Sc}$, but a lot of further work would be required to confirm this. This work should involve making truncations and internal deletions of Lrx1. Amino acids 91 to 283 of $Bud9^{Sc}$ and amino acids 74-216 and 268-417 of $Bud8^{Sc}$ are essential for their interaction with $Bud5^{Sc}$, and thus the polarity module in budding yeast. The interaction domains of $Bud8^{Sc}$ and $Bud9^{Sc}$ with $Bud5^{Sc}$ are independent of their interaction with $Rax1^{Sc}$. Truncations and internal deletions of Lrx1 may lead to the disruption of localisation of the growth-memory cue. This would identify the portions of Lrx1 essential for its interaction with Rax1 and Rax2. The truncations may also lead to a correctly localised, but non-functional memory cue. This could identify the portions of Lrx1 required to recruit the Cdc42 polarity module. This may be through a different mechanism to budding yeast, as Cdc25 was not found enriched in the Rax2-HTB mass spectrometry. Mass spectrometry analysis of the interacting partners of Lrx1 and relevant truncated forms may identify how the memory cue is able to promote growth at cell tips.

Chapter Six: Discussion

6.1 The Rax1-Rax2 memory-based cue promotes initial old end growth in fission yeast

In this work, I have identified a novel component of the Rax1-Rax2 growth-memory polarity cue, Lrx1. Lrx1 plays a role as a regulator of Rax1 and Rax2 trafficking from the ER to the plasma membrane. Lrx1 may be a homologue of $Bud8^{Sc}$ and $Bud9^{Sc}$ and may be the link between the growth-memory cue and the growth machinery.

There are a few possible reasons for why it may be beneficial for fission yeast to have a growth-memory polarity cue. Having two independent polarity cues may enable cells to be more robust to environmental stresses (such as nutrient starvation) or physiological perturbations (such as genetic mutations). Directing cell growth away from the other daughter cell through initial old-end growth may promote increased outward expansion of colonies. Expansion of the colony would allow the cells to make use of a larger pool of nutrients and may reduce cell crowding and starvation if nutrients are limiting. Alternatively, having one strong polarity cue following cytokinesis, rather than two, may increase the fidelity of growth site selection in newly born daughter cells.

6.2 The Rax1-Rax2 growth-memory cue in budding and fission yeast

In both budding yeast and fission yeast, $Rax1^{Sc}$ and $Rax2^{Sc}$ and Rax1 and Rax2 play a role in the positioning of growth sites and are part of a stable growth memory cue. The function of $Rax1^{Sc}$ and $Rax2^{Sc}$ at bud sites appears to be very different to that of Rax1 and Rax2 at cell tips. $Rax1^{Sc}$ and $Rax2^{Sc}$ retained at the bud sites prevent re-budding at the same site through recruitment of the $Cdc42^{Sc}$ antagonist $Nba1^{Sc}$ (Meitinger, Khmelinskii et al. 2014). Contrastingly, Rax1 and Rax2 promote growth at a cell tip that was growing in the previous cell cycle (through a so-far-unidentified mechanism) (S.Ashraf, thesis). In budding yeast, there is a fitness cost when growth-memory cue is lost. Re-budding from the same site leads to narrowing of the bud neck. Prior to cytokinesis, one of the duplicated nuclei has to move from the mother cell to the daughter cell through the bud neck. Transporting the nucleus through

a narrowed bud neck due to bud site re-use can lead to nuclear segregation defects (Meitinger, Khmelinskii et al. 2014). In fission yeast, nuclear inheritance occurs very differently. The nucleus is divided in two and positioned at the appropriate sites in the mother cell prior to cytokinesis, which divides the cell into two equally-sized daughter cells. Re-use of the same growth site in fission yeast should therefore have no effect on the efficiency of nuclear segregation.

In budding yeast, Rax1^{Sc} and Rax2^{Sc} interact with Bud8^{Sc} and Bud9^{Sc} (either indirectly or directly), and all four proteins are required for bipolar budding in diploid cells (Kang, Angerman et al. 2004). Rax1^{Sc} and Rax2^{Sc} are co-dependent for localisation to the bud sites and are partially dependent on Bud8^{Sc} for localisation (Rax1^{Sc} and Rax2^{Sc} localise to some but not all bud sites in *bud8^{Sc}Δ/bud8^{Sc}Δ* cells) (Kang, Angerman et al. 2004). In fission yeast, Lrx1 also plays an essential role in the Rax1-Rax2 growth-memory cue. Rax1, Rax2 and Lrx1 are all co-dependent for tip localisation, but surprisingly, Rax2 is not dependent upon Lrx1 for septum localisation. This suggests that in both fission yeast and budding yeast, Rax1 and Rax2 are partially able to localise to growth sites independently of Lrx1, Bud8^{Sc} and Bud9^{Sc}. Additional Rax1-Rax2 interactors, which have not yet been investigated, could be involved in this tip localisation that occurs independently of Lrx1.

6.3 Directional memory in different organisms

Directional memory has been shown to play a role in systems other than yeast. Heritable cues direct the polarised growth of *Drosophila* sensory neurons. These cues may play a role in co-ordinating the polarised growth of neurons in accordance with neighbouring cells or as a recycling mechanism to save resources (Pollarolo, Schulz et al. 2011). Long-lived cues direct the polarised migration of chemotactic cells such as *Dictyostelium* and neutrophil-like cells in fluctuating gradients of chemotactic signals (Skoge, Yue et al. 2014).

For the polarised growth of *Drosophila* sensory neurons, the cue for polarised growth of the neuronal sprout is a cytokinesis remnant that is inherited from the division of the neuronal precursor cell (Pollarolo, Schulz et al. 2011). Cytokinetic machinery, including Rho1 and Aurora A, is retained at the apical

pole and re-used for cell elongation in the subsequent cell cycle (Pollarolo, Schulz et al. 2011).

Dictyostelium cells migrate to a source of travelling waves of chemoattractant produced during aggregation. The cells always migrate towards the front of the wave and never repolarise as the gradient of chemoattractant changes when the wave passes over the cells(Skoge, Yue et al. 2014). The memory of migrational direction is maintained for up to 10 minutes and is maintained following depolymerisation of the actin cytoskeleton with Latrunculin B. Additionally, the memory cue is cumulative: the longer the cells are subjected to a chemoattractant in a particular direction, the longer the memory lasts following removal of the chemoattractant (Skoge, Yue et al. 2014). The identity of the memory cue is still to be determined; however, it appears to share similarities with Rax2. Like this cue, Rax2 is stable following depolymerisation of the actin cytoskeleton and accumulates with cell growth (S. Ashraf, thesis).

Neutrophil-like cells are model chemotactic cells that have been shown to retain directional memory following removal of the chemoattractant (Prentice-Mott, Meroz et al. 2016). Following a period of depolarisation, 80% of cells are able to repolarise to the original direction within 10 minutes without readdition of the chemoattractant (Prentice-Mott, Meroz et al. 2016). The memory cue was identified as the cytoskeletal Ezrin, Radaxin, Moesin (ERM) family protein Moesin and was shown to have a long turnover time. However, unlike Rax2 and the memory cue in *Dictyostelium*, moesin is not retained independently of the cytoskeleton. Depolymerisation of microtubules disrupts moesin localisation and consequently leads to loss of memory.

These examples of directional memory exhibit key differences relative to each other and to the Rax1 and Rax2 system. In different cell types, the memory may need to have more or less flexibility to be both robust to and amenable towards changing environments. It is likely that many more examples of cells with memory of cell polarity, particularly migratory cells, will be discovered in the future.

6.4 Future directions

From this work I have identified a new component involved in localising the fission yeast growth-memory cell polarity cue to cell tips. However, there are still important unanswered questions regarding Rax1 and Rax2. It is not known how Rax1 and Rax2 are retained so stably at the cell tips. Could the highly glycosylated extracellular domain of Rax2 be interacting with the cell wall for retention? Could there be endocytic recycling of Rax1 and Rax2 to enable these proteins to remain stably localised, despite constant membrane remodelling at the cell tips during growth? Additionally, how do Rax1 and Rax2 ultimately lead to Cdc42 activation and polarised growth at a previously growing cell tip?

References

Bao, X. X., C. Spanos, T. Kojidani, E. M. Lynch, J. Rappsilber, Y. Hiraoka, T. Haraguchi and K. E. Sawin (2018). "Exportin Crm1 is repurposed as a docking protein to generate microtubule organizing centers at the nuclear pore." Elife **7**.

Barlowe, C. (2003). "Signals for COPII-dependent export from the ER: what's the ticket out?" Trends Cell Biol **13**(6): 295-300.

Basi, G., E. Schmid and K. Maundrell (1993). "TATA box mutations in the Schizosaccharomyces pombe nmt1 promoter affect transcription efficiency but not the transcription start point or thiamine repressibility." Gene **123**(1): 131-136.

Baum, B. and M. Georgiou (2011). "Dynamics of adherens junctions in epithelial establishment, maintenance, and remodeling." J Cell Biol **192**(6): 907-917.

Bendezu, F. O. and S. G. Martin (2011). "Actin cables and the exocyst form two independent morphogenesis pathways in the fission yeast." Mol Biol Cell **22**(1): 44-53.

Bendezu, F. O., V. Vincenzetti, D. Vavylonis, R. Wyss, H. Vogel and S. G. Martin (2015). "Spontaneous Cdc42 polarization independent of GDI-mediated extraction and actin-based trafficking." PLoS Biol **13**(4): e1002097.

Bernsel, A., H. Viklund, A. Hennerdal and A. Elofsson (2009). "TOPCONS: consensus prediction of membrane protein topology." Nucleic Acids Res **37**(Web Server issue): W465-468.

Bicho, C. C., D. A. Kelly, H. A. Snaith, A. B. Goryachev and K. E. Sawin (2010). "A catalytic role for Mod5 in the formation of the Tea1 cell polarity landmark." Curr Biol **20**(19): 1752-1757.

Billinton, N. and A. W. Knight (2001). "Seeing the wood through the trees: a review of techniques for distinguishing green fluorescent protein from endogenous autofluorescence." Anal Biochem **291**(2): 175-197.

Bonazzi, D., J. D. Julien, M. Romao, R. Seddiki, M. Piel, A. Boudaoud and N. Minc (2014). "Symmetry breaking in spore germination relies on an interplay between polar cap stability and spore wall mechanics." Dev Cell **28**(5): 534-546.

Browning, H., J. Hayles, J. Mata, L. Aveline, P. Nurse and J. R. McIntosh (2000). "Tea2p is a kinesin-like protein required to generate polarized growth in fission yeast." J Cell Biol **151**(1): 15-28.

Brunner, D. and P. Nurse (2000). "CLIP170-like tip1p spatially organizes microtubular dynamics in fission yeast." Cell **102**(5): 695-704.

Busch, K. E. and D. Brunner (2004). "The microtubule plus end-tracking proteins mal3p and tip1p cooperate for cell-end targeting of interphase microtubules." Curr Biol **14**(7): 548-559.

Busch, K. E., J. Hayles, P. Nurse and D. Brunner (2004). "Tea2p kinesin is involved in spatial microtubule organization by transporting tip1p on microtubules." Dev Cell **6**(6): 831-843.

Cabib, E., P. C. Mol, J. A. Shaw and W. J. Choi (1993). "Biosynthesis of cell wall and septum during yeast growth." Arch Med Res **24**(3): 301-303.

Cadou, A., A. Couturier, C. Le Goff, T. Soto, I. Miklos, M. Sipiczki, L. Xie, J. R. Paulson, J. Cansado and X. Le Goff (2010). "Kin1 is a plasma membrane-associated kinase that regulates the cell surface in fission yeast." Mol Microbiol **77**(5): 1186-1202.

Cansado, J., T. Soto, M. Gacto and P. Perez (2010). "Rga4, a Rho-GAP from fission yeast: Finding specificity within promiscuity." Commun Integr Biol **3**(5): 436-439.

Casamayor, A. and M. Snyder (2002). "Bud-site selection and cell polarity in budding yeast." Curr Opin Microbiol **5**(2): 179-186.

Chang, E. C., M. Barr, Y. Wang, V. Jung, H. P. Xu and M. H. Wigler (1994). "Cooperative interaction of S. pombe proteins required for mating and morphogenesis." Cell **79**(1): 131-141.

Chant, J. (1999). "Cell polarity in yeast." Annu Rev Cell Dev Biol **15**: 365-391.

Chant, J. and J. R. Pringle (1995). "Patterns of bud-site selection in the yeast Saccharomyces cerevisiae." J Cell Biol **129**(3): 751-765.

Chen, T., T. Hiroko, A. Chaudhuri, F. Inose, M. Lord, S. Tanaka, J. Chant and A. Fujita (2000). "Multigenerational cortical inheritance of the Rax2 protein in orienting polarity and division in yeast." Science **290**(5498): 1975-1978.

Chiou, J. G., M. K. Balasubramanian and D. J. Lew (2017). "Cell Polarity in Yeast." Annu Rev Cell Dev Biol **33**: 77-101.

Choi, E., K. Lee and K. Song (2006). "Function of rax2p in the polarized growth of fission yeast." Mol Cells **22**(2): 146-153.

Coll, P. M., Y. Trillo, A. Ametzazurra and P. Perez (2003). "Gef1p, a new guanine nucleotide exchange factor for Cdc42p, regulates polarity in Schizosaccharomyces pombe." Mol Biol Cell **14**(1): 313-323.

Cortes, J. C., E. Carnero, J. Ishiguro, Y. Sanchez, A. Duran and J. C. Ribas (2005). "The novel fission yeast (1,3)beta-D-glucan synthase catalytic subunit Bgs4p is essential during both cytokinesis and polarized growth." J Cell Sci **118**(Pt 1): 157-174.

Cortes, J. C., J. Ishiguro, A. Duran and J. C. Ribas (2002). "Localization of the (1,3)beta-D-glucan synthase catalytic subunit homologue Bgs1p/Cps1p from fission yeast suggests that it is involved in septation, polarized growth, mating, spore wall formation and spore germination." J Cell Sci **115**(Pt 21): 4081-4096.

Cortes, J. C., M. Konomi, I. M. Martins, J. Munoz, M. B. Moreno, M. Osumi, A. Duran and J. C. Ribas (2007). "The (1,3)beta-D-glucan synthase subunit Bgs1p is responsible for the fission yeast primary septum formation." Mol Microbiol **65**(1): 201-217.

Cox, J., M. Y. Hein, C. A. Luber, I. Paron, N. Nagaraj and M. Mann (2014). "Accurate proteome-wide label-free quantification by delayed normalization and maximal peptide ratio extraction, termed MaxLFQ." Mol Cell Proteomics **13**(9): 2513-2526.

Cox, J. and M. Mann (2008). "MaxQuant enables high peptide identification rates, individualized p.p.b.-range mass accuracies and proteome-wide protein quantification." Nat Biotechnol **26**(12): 1367-1372.

Cox, J., N. Neuhauser, A. Michalski, R. A. Scheltema, J. V. Olsen and M. Mann (2011). "Andromeda: a peptide search engine integrated into the MaxQuant environment." J Proteome Res **10**(4): 1794-1805.

Cull, M. G. and P. J. Schatz (2000). "Biotinylation of proteins in vivo and in vitro using small peptide tags." Methods Enzymol **326**: 430-440.

Ding, D. Q., Y. Tomita, A. Yamamoto, Y. Chikashige, T. Haraguchi and Y. Hiraoka (2000). "Large-scale screening of intracellular protein localization in living fission yeast cells by the use of a GFP-fusion genomic DNA library." Genes Cells **5**(3): 169-190.

Dries, D. R. and G. Yu (2008). "Assembly, maturation, and trafficking of the gamma-secretase complex in Alzheimer's disease." Curr Alzheimer Res **5**(2): 132-146.

Estravis, M., S. Rincon and P. Perez (2012). "Cdc42 regulation of polarized traffic in fission yeast." Commun Integr Biol **5**(4): 370-373.

Estravis, M., S. A. Rincon, B. Santos and P. Perez (2011). "Cdc42 regulates multiple membrane traffic events in fission yeast." Traffic **12**(12): 1744-1758.

Etienne-Manneville, S. (2004). "Cdc42--the centre of polarity." J Cell Sci **117**(Pt 8): 1291-1300.

Fairhead, M. and M. Howarth (2015). "Site-specific biotinylation of purified proteins using BirA." Methods Mol Biol **1266**: 171-184.

Fang, Y., R. Sugiura, Y. Ma, T. Yada-Matsushima, H. Umeno and T. Kuno (2008). "Cation diffusion facilitator Cis4 is implicated in Golgi membrane trafficking via regulating zinc homeostasis in fission yeast." Mol Biol Cell **19**(4): 1295-1303.

Fantes, P. (1979). "Epistatic gene interactions in the control of division in fission yeast." Nature **279**(5712): 428-430.

Feierbach, B. and F. Chang (2001). "Roles of the fission yeast formin for3p in cell polarity, actin cable formation and symmetric cell division." Curr Biol **11**(21): 1656-1665.

Fink, A., N. Sal-Man, D. Gerber and Y. Shai (2012). "Transmembrane domains interactions within the membrane milieu: principles, advances and challenges." Biochim Biophys Acta **1818**(4): 974-983.

Fujita, A., M. Lord, T. Hiroko, F. Hiroko, T. Chen, C. Oka, Y. Misumi and J. Chant (2004). "Rax1, a protein required for the establishment of the bipolar budding pattern in yeast." Gene **327**(2): 161-169.

Fujita, A., C. Oka, Y. Arikawa, T. Katagai, A. Tonouchi, S. Kuhara and Y. Misumi (1994). "A yeast gene necessary for bud-site selection encodes a protein similar to insulin-degrading enzymes." Nature **372**(6506): 567-570.

Goldstein, B. and I. G. Macara (2007). "The PAR proteins: fundamental players in animal cell polarization." Dev Cell **13**(5): 609-622.

Harkins, H. A., N. Page, L. R. Schenkman, C. De Virgilio, S. Shaw, H. Bussey and J. R. Pringle (2001). "Bud8p and Bud9p, proteins that may mark the sites for bipolar budding in yeast." Mol Biol Cell **12**(8): 2497-2518.

Hasegawa, H., N. Sanjo, F. Chen, Y. J. Gu, C. Shier, A. Petit, T. Kawarai, T. Katayama, S. D. Schmidt, P. M. Mathews, G. Schmitt-Ulms, P. E. Fraser and P. St George-Hyslop (2004). "Both the sequence and length of the C terminus of PEN-2 are critical for intermolecular interactions and function of presenilin complexes." J Biol Chem **279**(45): 46455-46463.

Hayles, J. and P. Nurse (2001). "A journey into space." Nat Rev Mol Cell Biol **2**(9): 647-656.

Hayles, J., V. Wood, L. Jeffery, K. L. Hoe, D. U. Kim, H. O. Park, S. Salas-Pino, C. Heichinger and P. Nurse (2013). "A genome-wide resource of cell cycle and cell shape genes of fission yeast." Open Biol **3**(5): 130053.

Hirota, K., K. Tanaka, K. Ohta and M. Yamamoto (2003). "Gef1p and Scd1p, the Two GDP-GTP exchange factors for Cdc42p, form a ring structure that shrinks during cytokinesis in Schizosaccharomyces pombe." Mol Biol Cell **14**(9): 3617-3627.

Hu, C., J. Xu, L. Zeng, T. Li, M. Z. Cui and X. Xu (2017). "Pen-2 and Presenilin are Sufficient to Catalyze Notch Processing." J Alzheimers Dis **56**(4): 1263-1269.

Iwaki, T., Y. Giga-Hama and K. Takegawa (2006). "A survey of all 11 ABC transporters in fission yeast: two novel ABC transporters are required for red pigment accumulation in a Schizosaccharomyces pombe adenine biosynthetic mutant." Microbiology **152**(Pt 8): 2309-2321.

Iwaki, T., H. Iefuji, Y. Hiraga, A. Hosomi, T. Morita, Y. Giga-Hama and K. Takegawa (2008). "Multiple functions of ergosterol in the fission yeast Schizosaccharomyces pombe." Microbiology **154**(Pt 3): 830-841.

Jia, S., P. Dallos and D. Z. He (2007). "Mechanoelectric transduction of adult inner hair cells." J Neurosci **27**(5): 1006-1014.

Kalkhof, S. and A. Sinz (2008). "Chances and pitfalls of chemical cross-linking with amine-reactive N-hydroxysuccinimide esters." Anal Bioanal Chem **392**(1-2): 305-312.

Kang, P. J., E. Angerman, K. Nakashima, J. R. Pringle and H. O. Park (2004). "Interactions among Rax1p, Rax2p, Bud8p, and Bud9p in marking cortical sites for bipolar bud-site selection in yeast." Mol Biol Cell **15**(11): 5145-5157.

Kim, D. U., J. Hayles, D. Kim, V. Wood, H. O. Park, M. Won, H. S. Yoo, T. Duhig, M. Nam, G. Palmer, S. Han, L. Jeffery, S. T. Baek, H. Lee, Y. S. Shim, M. Lee, L. Kim, K. S. Heo, E. J. Noh, A. R. Lee, Y. J. Jang, K. S. Chung, S. J. Choi, J. Y. Park, Y. Park, H. M. Kim, S. K. Park, H. J. Park, E. J. Kang, H. B. Kim, H. S. Kang, H. M. Park, K. Kim, K. Song, K. B. Song, P. Nurse and K. L. Hoe (2010). "Analysis of a genome-wide set of gene deletions in the fission yeast Schizosaccharomyces pombe." Nat Biotechnol **28**(6): 617-623.

Krappmann, A. B., N. Taheri, M. Heinrich and H. U. Mosch (2007). "Distinct domains of yeast cortical tag proteins Bud8p and Bud9p confer polar localization and functionality." Mol Biol Cell **18**(9): 3323-3339.

Kudo, N., N. Matsumori, H. Taoka, D. Fujiwara, E. P. Schreiner, B. Wolff, M. Yoshida and S. Horinouchi (1999). "Leptomycin B inactivates CRM1/exportin 1 by covalent modification at a cysteine residue in the central conserved region." Proc Natl Acad Sci U S A **96**(16): 9112-9117.

Laitinen, O. H., V. P. Hytonen, H. R. Nordlund and M. S. Kulomaa (2006). "Genetically engineered avidins and streptavidins." Cell Mol Life Sci **63**(24): 2992-3017.

Li, R. and G. G. Gundersen (2008). "Beyond polymer polarity: how the cytoskeleton builds a polarized cell." Nat Rev Mol Cell Biol **9**(11): 860-873.

Li, Y. and R. Sousa (2012). "Expression and purification of E. coli BirA biotin ligase for in vitro biotinylation." Protein Expr Purif **82**(1): 162-167.

Makushok, T., P. Alves, S. M. Huisman, A. R. Kijowski and D. Brunner (2016). "Sterol-Rich Membrane Domains Define Fission Yeast Cell Polarity." Cell **165**(5): 1182-1196.

Maley, F., R. B. Trimble, A. L. Tarentino and T. H. Plummer, Jr. (1989). "Characterization of glycoproteins and their associated oligosaccharides through the use of endoglycosidases." Anal Biochem **180**(2): 195-204.

Martin, S. G. and R. A. Arkowitz (2014). "Cell polarization in budding and fission yeasts." FEMS Microbiol Rev **38**(2): 228-253.

Martin, S. G., W. H. McDonald, J. R. Yates, 3rd and F. Chang (2005). "Tea4p links microtubule plus ends with the formin for3p in the establishment of cell polarity." Dev Cell **8**(4): 479-491.

Martin, S. G., S. A. Rincon, R. Basu, P. Perez and F. Chang (2007). "Regulation of the formin for3p by cdc42p and bud6p." Mol Biol Cell **18**(10): 4155-4167.

Martin, V., B. Garcia, E. Carnero, A. Duran and Y. Sanchez (2003). "Bgs3p, a putative 1,3-beta-glucan synthase subunit, is required for cell wall assembly in Schizosaccharomyces pombe." Eukaryot Cell **2**(1): 159-169.

Mata, J. and P. Nurse (1997). "tea1 and the microtubular cytoskeleton are important for generating global spatial order within the fission yeast cell." Cell **89**(6): 939-949.

McDowall, M. D., M. A. Harris, A. Lock, K. Rutherford, D. M. Staines, J. Bahler, P. J. Kersey, S. G. Oliver and V. Wood (2015). "PomBase 2015: updates to the fission yeast database." Nucleic Acids Res **43**(Database issue): D656-661.

Meitinger, F., A. Khmelinskii, S. Morlot, B. Kurtulmus, S. Palani, A. Andres-Pons, B. Hub, M. Knop, G. Charvin and G. Pereira (2014). "A memory system of negative polarity cues prevents replicative aging." Cell **159**(5): 1056-1069.

Miller, P. J. and D. I. Johnson (1994). "Cdc42p GTPase is involved in controlling polarized cell growth in Schizosaccharomyces pombe." Mol Cell Biol **14**(2): 1075-1083.

Mitchison, J. M. and P. Nurse (1985). "Growth in cell length in the fission yeast Schizosaccharomyces pombe." J Cell Sci **75**: 357-376.

Motegi, F., R. Arai and I. Mabuchi (2001). "Identification of two type V myosins in fission yeast, one of which functions in polarized cell growth and moves rapidly in the cell." Mol Biol Cell **12**(5): 1367-1380.

Mullins, R. D. (2010). "Cytoskeletal mechanisms for breaking cellular symmetry." Cold Spring Harb Perspect Biol **2**(1): a003392.

Mutavchiev, D. R., M. Leda and K. E. Sawin (2016). "Remodeling of the Fission Yeast Cdc42 Cell-Polarity Module via the Sty1 p38 Stress-Activated Protein Kinase Pathway." Curr Biol **26**(21): 2921-2928.

Nakano, K., R. Arai and I. Mabuchi (1997). "The small GTP-binding protein Rho1 is a multifunctional protein that regulates actin localization, cell polarity, and septum formation in the fission yeast Schizosaccharomyces pombe." Genes Cells **2**(11): 679-694.

Nakano, K., T. Mutoh and I. Mabuchi (2001). "Characterization of GTPase-activating proteins for the function of the Rho-family small GTPases in the fission yeast Schizosaccharomyces pombe." Genes Cells **6**(12): 1031-1042.

Nakayama, Y., A. Hirata and H. Iida (2014). "Mechanosensitive channels Msy1 and Msy2 are required for maintaining organelle integrity upon hypoosmotic shock in Schizosaccharomyces pombe." FEMS Yeast Res **14**(6): 992-994.

Nance, J. and J. A. Zallen (2011). "Elaborating polarity: PAR proteins and the cytoskeleton." Development **138**(5): 799-809.

Nelson, W. J. (2003). "Adaptation of core mechanisms to generate cell polarity." Nature **422**(6933): 766-774.

Niccoli, T., M. Arellano and P. Nurse (2003). "Role of Tea1p, Tea3p and Pom1p in the determination of cell ends in Schizosaccharomyces pombe." Yeast **20**(16): 1349-1358.

Nourshargh, S. and R. Alon (2014). "Leukocyte migration into inflamed tissues." Immunity **41**(5): 694-707.

Osterberg, M., H. Kim, J. Warringer, K. Melen, A. Blomberg and G. von Heijne (2006). "Phenotypic effects of membrane protein overexpression in Saccharomyces cerevisiae." Proc Natl Acad Sci U S A **103**(30): 11148-11153.

Ozbudak, E. M., A. Becskei and A. van Oudenaarden (2005). "A system of counteracting feedback loops regulates Cdc42p activity during spontaneous cell polarization." Dev Cell **9**(4): 565-571.

Palumbo, R., B. G. Galvez, T. Pusterla, F. De Marchis, G. Cossu, K. B. Marcu and M. E. Bianchi (2007). "Cells migrating to sites of tissue damage in response

to the danger signal HMGB1 require NF-kappaB activation." J Cell Biol **179**(1): 33-40.

Pollarolo, G., J. G. Schulz, S. Munck and C. G. Dotti (2011). "Cytokinesis remnants define first neuronal asymmetry in vivo." Nat Neurosci **14**(12): 1525-1533.

Prentice-Mott, H. V., Y. Meroz, A. Carlson, M. A. Levine, M. W. Davidson, D. Irimia, G. T. Charras, L. Mahadevan and J. V. Shah (2016). "Directional memory arises from long-lived cytoskeletal asymmetries in polarized chemotactic cells." Proc Natl Acad Sci U S A **113**(5): 1267-1272.

Qiu, X. B., Y. M. Shao, S. Miao and L. Wang (2006). "The diversity of the DnaJ/Hsp40 family, the crucial partners for Hsp70 chaperones." Cell Mol Life Sci **63**(22): 2560-2570.

Rappsilber, J., Y. Ishihama and M. Mann (2003). "Stop and go extraction tips for matrix-assisted laser desorption/ionization, nanoelectrospray, and LC/MS sample pretreatment in proteomics." Anal Chem **75**(3): 663-670.

Reynolds, S. M., L. Kall, M. E. Riffle, J. A. Bilmes and W. S. Noble (2008). "Transmembrane topology and signal peptide prediction using dynamic bayesian networks." PLoS Comput Biol **4**(11): e1000213.

Rojas, R., W. G. Ruiz, S. M. Leung, T. S. Jou and G. Apodaca (2001). "Cdc42-dependent modulation of tight junctions and membrane protein traffic in polarized Madin-Darby canine kidney cells." Mol Biol Cell **12**(8): 2257-2274.

Sadok, A. and C. J. Marshall (2014). "Rho GTPases: masters of cell migration." Small GTPases **5**: e29710.

Santos, A., R. Wernersson and L. J. Jensen (2015). "Cyclebase 3.0: a multi-organism database on cell-cycle regulation and phenotypes." Nucleic Acids Res **43**(Database issue): D1140-1144.

Sato, K. and A. Nakano (2007). "Mechanisms of COPII vesicle formation and protein sorting." FEBS Lett **581**(11): 2076-2082.

Schenkman, L. R., C. Caruso, N. Page and J. R. Pringle (2002). "The role of cell cycle-regulated expression in the localization of spatial landmark proteins in yeast." J Cell Biol **156**(5): 829-841.

Skoge, M., H. Yue, M. Erickstad, A. Bae, H. Levine, A. Groisman, W. F. Loomis and W. J. Rappel (2014). "Cellular memory in eukaryotic chemotaxis." Proc Natl Acad Sci U S A **111**(40): 14448-14453.

Snaith, H. A., I. Samejima and K. E. Sawin (2005). "Multistep and multimode cortical anchoring of tea1p at cell tips in fission yeast." EMBO J **24**(21): 3690-3699.

Snaith, H. A. and K. E. Sawin (2003). "Fission yeast mod5p regulates polarized growth through anchoring of tea1p at cell tips." Nature **423**(6940): 647-651.

Snell, V. and P. Nurse (1993). "Investigations into the control of cell form and polarity: the use of morphological mutants in fission yeast." Dev Suppl: 289-299.

Snell, V. and P. Nurse (1994). "Genetic analysis of cell morphogenesis in fission yeast--a role for casein kinase II in the establishment of polarized growth." EMBO J **13**(9): 2066-2074.

Spriestersbach, A., J. Kubicek, F. Schafer, H. Block and B. Maertens (2015). "Purification of His-Tagged Proteins." Methods Enzymol **559**: 1-15.

Tagwerker, C., K. Flick, M. Cui, C. Guerrero, Y. Dou, B. Auer, P. Baldi, L. Huang and P. Kaiser (2006). "A tandem affinity tag for two-step purification under fully denaturing conditions: application in ubiquitin profiling and protein complex identification combined with in vivocross-linking." Mol Cell Proteomics **5**(4): 737-748.

Takano, T., C. Xu, Y. Funahashi, T. Namba and K. Kaibuchi (2015). "Neuronal polarization." Development **142**(12): 2088-2093.

Tassan, J. P. and X. Le Goff (2004). "An overview of the KIN1/PAR-1/MARK kinase family." Biol Cell **96**(3): 193-199.

Tatebe, H., K. Nakano, R. Maximo and K. Shiozaki (2008). "Pom1 DYRK regulates localization of the Rga4 GAP to ensure bipolar activation of Cdc42 in fission yeast." Curr Biol **18**(5): 322-330.

Tatebe, H., K. Shimada, S. Uzawa, S. Morigasaki and K. Shiozaki (2005). "Wsh3/Tea4 is a novel cell-end factor essential for bipolar distribution of Tea1 and protects cell polarity under environmental stress in S. pombe." Curr Biol **15**(11): 1006-1015.

Tay, Y. D., M. Leda, A. B. Goryachev and K. E. Sawin (2018). "Local and global Cdc42 guanine nucleotide exchange factors for fission yeast cell polarity are coordinated by microtubules and the Tea1-Tea4-Pom1 axis." J Cell Sci **131**(14).

Thompson, B. J. (2013). "Cell polarity: models and mechanisms from yeast, worms and flies." Development **140**(1): 13-21.

Tomala, K. and R. Korona (2013). "Evaluating the fitness cost of protein expression in Saccharomyces cerevisiae." Genome Biol Evol **5**(11): 2051-2060.

Toyama, B. H., J. N. Savas, S. K. Park, M. S. Harris, N. T. Ingolia, J. R. Yates, 3rd and M. W. Hetzer (2013). "Identification of long-lived proteins reveals exceptional stability of essential cellular structures." Cell **154**(5): 971-982.

van Werven, F. J. and H. T. Timmers (2006). "The use of biotin tagging in Saccharomyces cerevisiae improves the sensitivity of chromatin immunoprecipitation." Nucleic Acids Res **34**(4): e33.

Verde, F., J. Mata and P. Nurse (1995). "Fission yeast cell morphogenesis: identification of new genes and analysis of their role during the cell cycle." J Cell Biol **131**(6 Pt 1): 1529-1538.

Viklund, H. and A. Elofsson (2008). "OCTOPUS: improving topology prediction by two-track ANN-based preference scores and an extended topological grammar." Bioinformatics **24**(15): 1662-1668.

Vjestica, A., X. Z. Tang and S. Oliferenko (2008). "The actomyosin ring recruits early secretory compartments to the division site in fission yeast." Mol Biol Cell **19**(3): 1125-1138.

Wang, H., X. Tang, J. Liu, S. Trautmann, D. Balasundaram, D. McCollum and M. K. Balasubramanian (2002). "The multiprotein exocyst complex is essential for cell separation in Schizosaccharomyces pombe." Mol Biol Cell **13**(2): 515-529.

Wedlich-Soldner, R. and R. Li (2003). "Spontaneous cell polarization: undermining determinism." Nat Cell Biol **5**(4): 267-270.

Wei, B., B. S. Hercyk, N. Mattson, A. Mohammadi, J. Rich, E. DeBruyne, M. M. Clark and M. Das (2016). "Unique spatiotemporal activation pattern of Cdc42 by Gef1 and Scd1 promotes different events during cytokinesis." Mol Biol Cell **27**(8): 1235-1245.

Wood, I. S. and P. Trayhurn (2003). "Glucose transporters (GLUT and SGLT): expanded families of sugar transport proteins." Br J Nutr **89**(1): 3-9.

Woods, B. and D. J. Lew (2017). "Polarity establishment by Cdc42: Key roles for positive feedback and differential mobility." Small GTPases: 1-8.

Wu, C. F. and D. J. Lew (2013). "Beyond symmetry-breaking: competition and negative feedback in GTPase regulation." Trends Cell Biol **23**(10): 476-483.

Yan, C. and J. Luo (2010). "An analysis of reentrant loops." Protein J **29**(5): 350-354.

Yang, H. W., S. R. Collins and T. Meyer (2016). "Locally excitable Cdc42 signals steer cells during chemotaxis." Nat Cell Biol **18**(2): 191-201.

Zerbino, D. R., P. Achuthan, W. Akanni, M. R. Amode, D. Barrell, J. Bhai, K. Billis, C. Cummins, A. Gall, C. G. Giron, L. Gil, L. Gordon, L. Haggerty, E. Haskell, T. Hourlier, O. G. Izuogu, S. H. Janacek, T. Juettemann, J. K. To, M. R. Laird, I. Lavidas, Z. Liu, J. E. Loveland, T. Maurel, W. McLaren, B. Moore, J. Mudge, D. N. Murphy, V. Newman, M. Nuhn, D. Ogeh, C. K. Ong, A. Parker, M. Patricio, H. S. Riat, H. Schuilenburg, D. Sheppard, H. Sparrow, K. Taylor, A. Thormann, A. Vullo, B. Walts, A. Zadissa, A. Frankish, S. E. Hunt, M. Kostadima, N. Langridge, F. J. Martin, M. Muffato, E. Perry, M. Ruffier, D. M. Staines, S. J. Trevanion, B. L. Aken, F. Cunningham, A. Yates and P. Flicek (2018). "Ensembl 2018." Nucleic Acids Res **46**(D1): D754-D761.

Zhang, D., A. Vjestica and S. Oliferenko (2010). "The cortical ER network limits the permissive zone for actomyosin ring assembly." Curr Biol **20**(11): 1029-1034.

Zhang, D., A. Vjestica and S. Oliferenko (2012). "Plasma membrane tethering of the cortical ER necessitates its finely reticulated architecture." Curr Biol **22**(21): 2048-2052.

Zhang, X., C. J. Yu and S. S. Sisodia (2015). "The topology of pen-2, a gamma-secretase subunit, revisited: evidence for a reentrant loop and a single pass transmembrane domain." Mol Neurodegener **10**: 39.